2021

DESIGN AND IMPLEMENTATION OF AN OXIDATION CATALYST FOR A SPARK IGNITED TWO STROKE SNOWMOBILE ENGINE

Noah Squires
Michigan Technological University, nrsquire@mtu.edu

DESIGN AND IMPLEMENTATION OF AN OXIDATION CATALYST FOR A SPARK IGNITED TWO STROKE SNOWMOBILE ENGINE

By

Noah Squires

A THESIS

Submitted in partial fulfillment of the requirements for the degree of

MASTER OF SCIENCE

In Mechanical Engineering

MICHIGAN TECHNOLOGICAL UNIVERSITY

2021

This thesis has been approved in partial fulfillment of the requirements for the Degree of MASTER OF SCIENCE in Mechanical Engineering.

Department of Mechanical Engineering – Engineering Mechanics

Thesis Advisor:	*Dr. Scott A. Miers*
Committee Member:	*Dr. Jason R. Blough*
Committee Member:	*Dr. Jeremy J. Worm*
Committee Member:	*Brian Eggart*
Committee Member:	*Dr. David Wanless*
Department Chair:	*Dr. William W. Predebon*

Table of Contents

List of Figures v

List of Tables ix

Acknowledgements x

List of abbreviations xi

1 Abstract xii

2 Introduction 1

3 Literature Review 3

3.1 Design Goals 3
3.1.1 Conversion Efficiency 3
3.1.2 Back Pressure 7
3.1.3 Durability 8
3.1.4 Packaging 10

3.2 Design Challenges 11
3.2.1 Two Stroke Operation Review 11
3.2.2 Controlling Catalytic Reactions 16
3.2.3 Minimizing Performance Loss 17

4 Project Details 18

4.1 Test Cell 18
4.1.1 Engine 18
4.1.2 Dyno 23

4.2 Data Collection 24
4.2.1 Engine Data 24
4.2.2 Emissions Data 26
4.2.3 Data Collection Format 27

5 Catalyst Design 29

5.1 Design Considerations 29

5.2 Design Process 29
5.2.1 Developing Design Targets 29
5.2.2 Locating the Catalyst 29
5.2.3 Determining Back Pressure Contributions 30
5.2.4 Selecting Conversion Efficiency Targets 31
5.2.5 Consulting Suppliers 33

6 Testing and Results 35
6.1 Baseline 35
Back Pressure 38
6.2 38
6.2.1 Back pressure Test #1 41
6.2.2 Back Pressure Test #2 46
6.2.3 Finalizing Catalyst Location 51
6.2.4 Uncoated Catalysts 52
6.2.5 Back Pressure Test #3 56
6.2.6 Reaction Phenomenon Investigation 65
6.2.7 Selecting Samples to be Coated 75
6.3 Coated Catalyst Testing 75
6.3.1 Wash-coat Development 76
6.3.2 Conversion Efficiency Testing Setup 82
6.3.3 Catalyst De-Greening Process 84
6.3.4 Conversion Efficiency Testing Results 85
6.3.5 Durability 92
6.4 Model Validation 93
7 Conclusions 98
7.1 Project Outcome Summary 98
7.2 Future Work 100
8 References 104
9 Appendices 107
9.1 Engine Control Charts 107
9.2 XRF and SEM Results 111
9.3 EES Catalytic Reaction Simulation Code 115
9.4 Matlab Hagen Poiseuille Pressure Drop Code 116
9.5 Matlab Catalyst Geometry Calculations Code 117

List of Figures

Figure 3.1 – Flow Distribution Diagram.....5

Figure 3.2 – Turbulent Flow Diagram.....6

Figure 3.3 - Hybrid Substrate Geometry Examples [4].....7

Figure 3.4 - LS and TS Designs [5].....7

Figure 3.5 – Hydraulic Diameter Diagram.....8

Figure 3.6 – Typical Catalyst Cross Section View.....11

Figure 3.7 - Mid-Pipe Diagram.....12

Figure 3.8 - Mid-Pipe Gas Dynamics - Exhaust Port Opening.....13

Figure 3.9 - Mid-Pipe Gas Dynamics – Intake and Transfer Port Opening.....13

Figure 3.10 - Mid-Pipe Gas Dynamics - Both Ports Fully Opened.....14

Figure 3.11 - Mid-Pipe Gas Dynamics - Exhaust Port Closing.....14

Figure 3.12 - Mid-Pipe Tuned Lengths.....15

Figure 4.1 - 600 DSI Exhaust Valve [14].....18

Figure 4.2 – 600 DSI Injector Location and Piston Slot [14].....19

Figure 4.3 – Test Cell Engine Configuration.....20

Figure 4.4 – Engine Drive Shaft.....20

Figure 4.5 – Cooling System.....21

Figure 4.6 – Re-Sol Fuel Cart.....22

Figure 4.7 – Test Cell Dyno Configuration.....24

Figure 4.8 – DAQ Box Front Panel.....25

Figure 4.9 – Baseline Emissions Sampling Location.....27

Figure 6.1 - Baseline Power Sweep Plot.....35

Figure 6.2 - Modified Mid-Pipe for Back Pressure Testing.....39

Figure 6.3 - Completed Orifice Plates 40
Figure 6.4 - Back Pressure Test #1 Setup 41
Figure 6.5 – Global Lambda - Back Pressure Test #1 42
Figure 6.6 - Mid-pipe Pressure - Back Pressure Test #1 43
Figure 6.7 – Mid-pipe Temperatures - Back Pressure Test #1 44
Figure 6.8 - Further Investigation of EV Transition Point....45
Figure 6.9 - Restriction Assembly - Back Pressure Test #2 47
Figure 6.10 – Global Lambda Values - Back Pressure Test #2 48
Figure 6.11 - Mid-pipe Pressure Values - Back Pressure Test #2 49
Figure 6.12 – Mid-pipe Temperature Values - Back Pressure Test #2....50
Figure 6.13 - Disassembled 600 DSI Muffler....52
Figure 6.14 – Uncoated Mantle Samples 53
Figure 6.15 - Cell Width Calculation Graphic 54
Figure 6.16 - Welding Fixture 56
Figure 6.17 - Back Purge Setup 57
Figure 6.18 - Welded Samples....57
Figure 6.19 – Muffler Flanges and Installed Catalyst Sample 58
Figure 6.20 – Instrumented and Installed Muffler 58
Figure 6.21 – Catalyst Inlet Instrumentation 59
Figure 6.22 – Catalyst Outlet Instrumentation....59
Figure 6.23 - Catalyst Pressure Drop - Back Pressure Test #3 60
Figure 6.24 - Delta Temperature Across Catalyst - Back Pressure Test #3 62
Figure 6.25 – Global Lambda - Back Pressure Test #3 63
Figure 6.26 - Mid-pipe Pressure - Back Pressure Test #3 64

Figure 6.27 - Mid-pipe Temperature - Back Pressure Test #3 65
Figure 6.28 - HC Concentration - Reaction Phenomenon Investigation 66
Figure 6.29 - CO Concentration - Reaction Phenomenon Investigation 67
Figure 6.30 - CO2 Concentration - Reaction Phenomenon Investigation 68
Figure 6.31 - Oxygen Concentration - Reaction Phenomenon Investigation 69
Figure 6.32 – Typical Start of Day Test Results.....71
Figure 6.33 - Reaction Rate Visualization Graphic – Coating 1 79
Figure 6.34 - Reaction Rate Visualization Graphic – Coatings 1 & 2.....80
Figure 6.35 - Sample Switching Setup 83
Figure 6.36 - HC Conversion Efficiency Results 86
Figure 6.37 - CO Conversion Efficiency Results 87
Figure 6.38 - Catalyst Pressure Drop - Conversion Efficiency Test.....88
Figure 6.39 – Lambda – Conversion Efficiency Test.....89
Figure 6.40 - Mid-Pipe Temperature – Conversion Efficiency Test 90
Figure 6.41 - Mid-Pipe Pressure – Conversion Efficiency Test 91
Figure 6.42 - EES Model Validation - HC Conversion Efficiency Comparison.....94
Figure 6.43 - EES Model Validation - CO Conversion Efficiency Comparison.....95
Figure 6.44 - Pressure Drop Model Validation.....96
Figure 9.1 – Wide Band Lambda Control Chart.....107
Figure 9.2 – Fuel Flow Control Chart.....108
Figure 9.3 – BSFC Control Chart 108
Figure 9.4 – Intake Manifold and Mid-Pipe Pressures Control Chart 109
Figure 9.5 – Fuel Pressure Control Chart 109
Figure 9.6 – Intake and Coolant Temperatures Control Chart.....110

Figure 9.7 – Exhaust Temperatures Control Chart 110
Figure 9.8 – Non-Active Heraeus Wash Coat XRF Tabulated Data 111
Figure 9.9 – Active Heraeus Wash Coat XRF Tabulated Data 112
Figure 9.10 - Non-Active Heraeus Wash Coat SEM Results 113
Figure 9.11 - Active Heraeus Wash Coat SEM Results 114

List of Tables

Table 4.1 – Engine Specifications 19

Table 4.2 - Discrete 5 Mode Duty Cycle 28

Table 5.1 - EES Model Input Parameters – Typical Mode 1 Data 33

Table 6.1 - 600 DSI Discrete 5 Mode Operating Points 36

Table 6.2 - Baseline Emissions and Engine Data 37

Table 6.3 - Orifice Plate Restriction Data 40

Table 6.4 – Orifice Plate Restriction Data - Back Pressure Test #2 47

Table 6.5 - Uncoated Sample Dimensions 55

Table 6.6 – Typical Start Up Test Sequence 70

Table 6.7 - Catalyst Sample Surface Area Comparison 74

Table 6.8 – Wash-coat Formulation Data 77

Table 6.9 - Durability Requirements 78

Table 6.10 - XRF Results - Heraeus Wash Coat Formula 81

Table 6.11 - Engine Power Loss Data 92

Table 7.1 - Final Emissions Improvement Results 99

Acknowledgements

This project and my personal development as an engineer would not have been possible without the help of many individuals. I would like to take this opportunity to thank those who have been an integral part of this accomplishment in my life. First and foremost, I must thank my friends and family that have seen me through this endeavor. Each of you know who you are and have walked with me through the ups and downs of the project and earning this degree. I appreciate all your encouragement and support through this endeavor.

Specific people I want to thank must begin with Dr. Scott Miers, who not only served as my advisor throughout this project but has also become a close friend whom I will keep for life. Without the resources of his small engine test cell at the APSRC and contacts in the industry I would not have been able to accomplish any part of this project. His efforts to provide the resources necessary to support this unfunded project and encourage me throughout the trials of this process cannot be appreciated enough. I owe him a great deal yet know that he is just the type of person to expect nothing in return. So, thank you Scott, without you I would not be the engineer that I am today, nor would this project have become a reality.

I would also like to thank several individuals in industry who have provided advice, resources, and various services that were integral the project's success. These individuals include Jeff Italiano and John Robinson with Catalytic Combustion Corporation, Hans Hildenbrand and Todd Ballinger with Heraeus, Matt Switalski with Vconverter Active Exhaust Corporation, Cord Christensen and Alex Fuhrman with Arctic Cat, and Ryan Hayes with Polaris. Each of you has generously donated your time and knowledge at various points during this project and I genuinely thank you for investing in my development as an engineer.

Finally, I would like to thank my parents for raising me to be the person I am today. I realize now looking back that undertaking an unfunded masters project with this degree of difficulty takes a specific type of character. A character that I would not possess if it were not for their influence upon my life.

List of abbreviations

API - American Petroleum Institute

CO – carbon monoxide

CPSI – cells per square inch

DSI – dual stage injection

EDS – Energy Dispersive Spectroscopy

EES – engineering equation solver

EGT – exhaust gas temperature

EV – exhaust valve

FID – Flame Ionization Detector

FTIR - Fourier Transform Infrared

GHSV – gas hourly space velocity

HC - hydrocarbons

HSS – Heated Sample System

MAG - magneto

NOx – nitrogen oxides

OEM – original equipment manufacturer

Pd – palladium

PM – precious metal

Pt – platinum

PTO – power takeoff

Rh – rhodium

SEM – Scanning Electron Microscopy

SESAM – System for Emissions Sampling and Measurement

XRF – X-Ray Fluorescence

ZDP - zinc dialkyldithiophosphate

1 Abstract

Spark ignited two stroke engines are under increasing pressure as emissions standards become stricter, making them a perfect candidate for a catalytic aftertreatment system. Yet several significant challenges to catalysis exist. Namely two stroke exhaust systems are very sensitive to back pressure changes and high emissions concentrations can make controlling the temperature of the catalytic reaction difficult. Therefore, it is imperative that a two stroke specific catalyst design process be developed. This project focused on beginning to develop such a design process. Key results of this work include finding a location for the catalyst in the exhaust system that offers significant catalyst sizing freedom as well as exploring methods to estimate catalyst back pressure contributions and approximate conversion efficiency targets. Finally, using this design process, 3 actively coated catalyst samples were tested and showed significant reductions in HC and CO with less than a 2 Hp peak power loss.

2 Introduction

Two stroke engines are still widely used in recreational powersports due to their high power to weight ratio, simple design, and low cost. Production volumes and lifespan of these engines is extremely low in comparison with the automotive industry. However, their emissions contributions are significant and of ever increasing concern. Inherently these engines by design exhibit high concentrations of HC and CO emissions associated with poor fuel economy and low overall engine efficiency across much of their operating range. Still there is not yet a replacement for a two stroke engines power density, simplicity, and low cost in a performance market such as recreational powersports. Therefore, as emissions standards continue to become stricter, without a doubt two stroke engines will soon be phased out if these emissions concerns cannot be addressed. As the automotive industry has proven, catalytic aftertreatment systems are a viable solution and will undoubtable need to be introduced into the two stroke engine market to comply with future emissions standards. Yet as previously alluded to, two stroke engines are inherently different from their spark ignited four stroke and compression ignition counterparts. Due to these differences two stroke engines pose some new and significant challenges to catalysis.

Of primary concern is catalyst durability because two stroke engines have an excess of readily available HC and CO paired with high oxygen concentrations that if left uncontrolled can easily allow catalyst temperatures to become excessively high, accelerating thermal ageing. These high exhaust concentrations are due to the intake and exhaust processes being port controlled paired with the 360° power cycle two stroke engines utilize. These features allow both ports to be open during the gas exchange process causing trapping efficiency to be low over much of the operating range. Yet port controlled gas exchange and a 360° power cycle are the fundamental operating principles that differentiate a two stroke engine from its four stroke counterparts and give it desirable performance characteristics. Therefore, the emissions concerns cannot be alleviated by engine architecture changes. These issues must be addressed through wise catalyst design. The second significant challenge to overcome is the ensuing performance losses associated with the added back pressure of a catalyst within the exhaust system. Two stroke exhaust systems take advantage of gas dynamic properties that are significantly impacted by relatively small changes in exhaust pressure. The addition of a catalyst in the exhaust system has great potential to negatively affect engine performance and output levels if poorly designed. Due to two strokes being utilized largely based on their performance advantages, any drop in performance then becomes of significant concern. Therefore, catalyst location and sizing are also critical to the successful implementation of a catalyst in a two stroke application. These two stroke specific challenges come in addition to the complexities already associated with the design and integration of any catalytic aftertreatment system, making successfully integrating a catalyst into a two stroke application quite difficult.

To begin this project significant time was spent acquiring knowledge from the vast experience the automotive industry has with catalysis and learning how to apply these

concepts to a two stroke application. From this work the beginnings of a design process have emerged. Two stroke catalyst design must be fundamentally different from traditional catalyst design due to the unique challenges two stroke engines pose. This new design process is tailored specifically towards addressing the concerns surrounding controlling the catalyst temperatures as well as minimizing performance losses due to the additional back pressure within the exhaust system. Through the project a greater understanding of how additional back pressure impacts performance was gained as well as how critical catalyst location is to the success of integrating a catalyst into the exhaust system. Additionally, experience was gained in how to leverage catalyst suppliers knowledge to arrive at properly sized samples that target controllable conversion efficiencies. One of the most valuable aspects of this design process was a greater understanding of what information catalyst suppliers require to make design recommendations as well as demystifying some of the methodology utilized to arrive at those solutions. Finally, several interesting phenomena were observed throughout this project that have posed new questions, leaving opportunities for future work in this field of research.

Two stroke catalysis is a relatively new area of research and therefore posed a significant challenge for this project. Yet there is significant value in this work. Continuing to develop a design process for two stroke specific catalysts is one of the most viable solutions to ever increasing emissions concerns surrounding two stroke engines. It is my hope that others will utilize this work and continue to develop it so that two stroke engines can continue to be a part of the recreational powersports market. My passion for this industry and the unforgettable experiences it has provided me has led me to tirelessly pursue this project, and I hope that others will pick up where I have left off and continue to do the same.

3 Literature Review

Prior to beginning this project an extensive literature review of relevant SAE Technical Papers was conducted to review catalyst design methodology, current technology, performance, and common failure modes of catalysts in two-stroke engine applications. Literature is somewhat limited in this area of research, especially specific to snowmobile applications. Due to the lack of literature specific to this application the review expanded to include technical articles from the automotive, marine, and motorize scooter fields. It was assumed that the concepts and research utilized in these fields could be applied to this project.

3.1 Design Goals

All catalyst development projects begin with a specific set of design goals that typically fall into four main categories; conversion efficiency, back pressure, durability, and packaging. In the following sections some of the main design choices required to achieve these targets are summarized.

3.1.1 Conversion Efficiency

Conversion efficiency is the primary measure of how effectively an aftertreatment system is performing and therefore is one of the most important design goals. The catalytic reactions effectiveness at converting harmful engine emissions into nonharmful products is primarily controlled by the substrate surface area, the reactivity of the wash-coat formula, and how well the exhaust flow is distributed to reaction sites.

Substrate surface area, wash-coat reactivity, and flow distribution can be balanced to achieve a given conversion efficiency target. Two methods to determine the proper balance exist; either starting with a given wash-coat and determining the catalyst volume necessary to achieve the desired performance or starting with a substrate volume and adjusting the reactivity of the wash-coat formula [1]. The more traditional approach appears to be experimentally selecting the substrate volume and adjusting the wash-coat formula accordingly. One such method to determine substrate volume is utilizing the gas hourly space velocity (GHSV). The GHSV is defined as the ratio of gas flow rate $\left(\dot{Q}_{Total}\right)$to the volume of the substrate$(V_{Substrate})$, shown below in Equation .

$$GHSV = \frac{\dot{Q}_{Total}}{V_{Substrate}} \tag{3.1}$$

The GHSV simply relates how quickly exhaust gasses flow through the substrate volume or from another perspective correlates to the residence time of the gasses within the

catalyst volume. By targeting a specific GHSV value, exhaust constituents are allowed enough residence time at catalytic sites to react and be converted to non-harmful compounds. In the automotive field a GHSV value of $60{,}000\ hr^{-1}$has been widely accepted whereas in performance applications, where substrate area is sized based on maximum flow conditions, a value of $120{,}000\ hr^{-1}$ is generally accepted [2]. It has also become apparent that when working with performance two stroke applications an even higher GHSV constant of $200{,}000\ hr^{-1}$ is typically used because exhaust emissions concentrations are much higher.

Wash-coat formulation design choices include which precious metals (PM) to include, what ratio of PM's to utilize, how densely to load the substrate, and if any doping agents should be added to produce desirable performance characteristics. There are three PM's commonly used in catalysts including platinum (Pt), palladium (Pd), and rhodium (Rh). These PM's are mixed to a specific ratio based on the exhaust composition and conversion efficiency targets. Typically, only Rh and Pt are used in two-stroke applications because Pd leads to large formations of CO under the fuel rich conditions within two-stroke exhaust gasses [3]. Wash-coat slurries which carry the PM typically fall into two categories; alumina or ceria/zirconia. Most often ceria is utilized because it promotes water-gas shift and steam reforming reactions which are the main mechanisms for catalysis in two-stroke applications [3]. These reactions relate the dissociation of CO and HC in the exhaust into CO_2, CO, and H_2. These reactions are based upon temperature dependent chemical equilibrium between the production and removal of exhaust components. If these chemical equilibrium reaction rates are approached significant conversion of exhaust components will ensue. The water gas shift and steam reforming reactions are shown below in Equation 3.2 and 3.3 respectively.

$$CO + H_2O \leftrightarrow CO_2 + H_2 \tag{3.2}$$

$$C_nH_m + nH_2O \rightarrow CO + \left(n + {}^{m}/_{2}\right)H_2 \tag{3.3}$$

Additionally, ceria has oxygen storage properties that promote a more stable conversion rate during fuel rich operating conditions. The final consideration in wash-coat formulation is if any doping agents should be added to produce favorable performance characteristics. Doping agents are often used to resist the effects of thermal ageing, which is a significant concern in two-stroke applications. Doping agents for alumina slurries can include alkaline and rare earth metals, where ceria is often paired with zirconia. These doping agents counteract the loss of micro porosity, particle growth, and decreases in PM dispersion that thermal ageing causes. The last step will then be applying the coating to the substrate, which involves selecting the desired loading. Loading is most often measured in mass per unit area, but conceptually can be thought of as thickness of the wash-coat layer on the substrate. Substrates can be loaded to higher levels to improve their lifespan, but this comes at increased cost and has an impact on back pressure

contributions from the substrate. Additionally, several different wash-coats can be applied to create a layered reactive coating, where each layer has specific characteristics or targets specific exhaust constituents.

The final consideration that must be made to achieve a conversion efficiency target is that the exhaust gas flow is both evenly distributed across the substrate cells and that the flow remains turbulent. A simple representation of good and poor flow distributions is shown below in Figure 3.1.

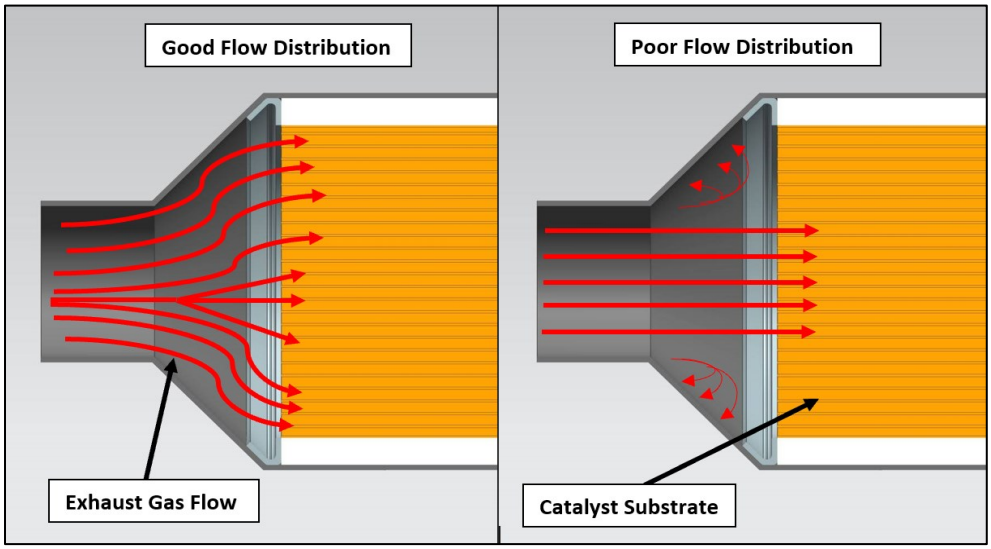

Figure 3.1 – Flow Distribution Diagram

As shown in the right half of Figure 3.1, poor flow distribution only utilizes a portion of the catalyst substrate, effectively reducing the size of the catalyst, which can increase back pressure contributions as well as decrease conversion efficiency performance. Achieving even flow distribution is accomplished primarily through the package that houses the substrate. Catalyst shells are typically optimized to promote even flow distribution using CFD analysis software. Equally as important as flow distribution is that the flow remains turbulent within the substrate cells. Turbulent flow promotes good mixing of exhaust gasses, improving the likelihood that exhaust constituents reach reactive sites. Flow entering the substrate is almost always turbulent, but if substrate length is too great, within the cells, the flow can become laminar. If the substrate volume cannot be decreased by shortening the substrate, substrates can be split into two sections and packaged with a small gap between sections, which allows flow to become turbulent again. Below in Figure 3.2 the left portion of the diagram shows a traditional substrate and a detail of how flow transitions from turbulent to laminar within the substrate cells. The right portion shows the split substrate design and how it can re-introduce turbulent flow.

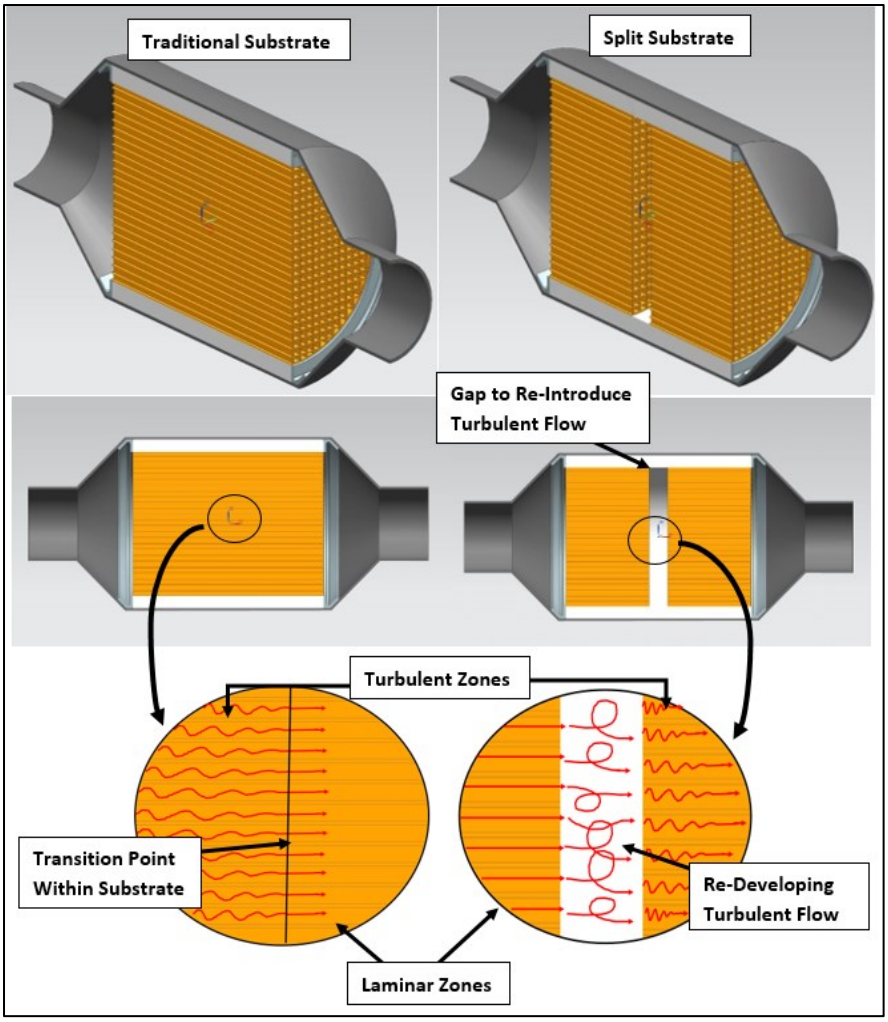

Figure 3.2 – Turbulent Flow Diagram

A relatively new method to promote turbulent flow involves what are categorized as hybrid substrate geometries. These substrates implement lateral features and or features in the radial layers that allow gasses to mix between cells at various locations along the substrate length. Several examples are shown below in Figure 3.3 as well as two trademarked products named the LS-Design™ (Longitudinal Structure) and TS-Design™ (Transverse Structure) in Figure 3.4.

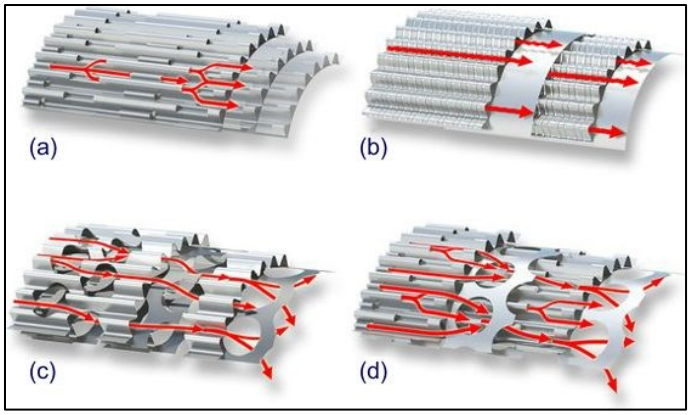

Figure 3.3 - Hybrid Substrate Geometry Examples [4]

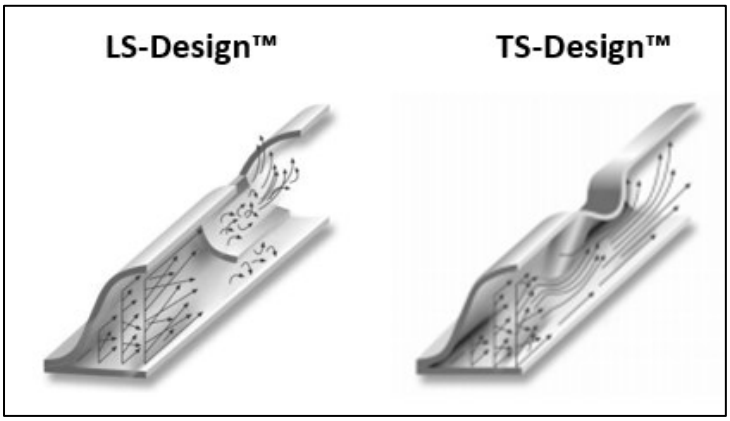

Figure 3.4 - LS and TS Designs [5]

These hybrid substrate geometries have produced promising improvements in conversion efficiency over standard substrates of equivalent surface area with minimal increases to back pressure [6]. If utilized, hybrid geometries could reduce the loading required to achieve the desired conversion efficiency target.

3.1.2 Back Pressure

The addition of a catalyst to any exhaust system will undoubtable add a measurable amount of back pressure, which can negatively affect engine performance. Two-stroke engines and in particular their exhaust systems are incredibly sensitive to back pressure. Therefore, minimizing back pressure contributions from the catalyst is a high design priority. The back pressure created by a catalyst is controlled by the substrate geometry and more specifically the open frontal area and length of the substrate.

The open frontal area is defined as the cross-sectional area that exhaust gasses can flow through on the leading face of the substrate. The open frontal area is defined by substrate diameter, cell density, and wall thickness. Based on extensive research part diameter has

been found to have the largest impact on back pressure, followed by length, and cell density. Based on a fixed substrate volume back pressure is fourth order dependent upon substrate diameter, followed by length which has a second order effect, and cell density with a first order effect [7]. These relationships originate from the Hagen Poiseuille Equation shown below in Equation 3.4, which is commonly used to predict the pressure drop across substrates. Variables include total volume flow rate $(\dot{Q}_{Total})$, dynamic viscosity (μ), substrate volume $(V_{Substrate})$, substrate outer diameter (D_{Part}), cell density (N), cell wall thickness (T), and cell width (L).

$$\Delta P = C(\dot{Q}_T \mu)\left(\frac{V_{Substrate}}{{D_{Part}}^4}\right)\left(\frac{N}{\left[1-\left({}^{T}/_{L}\right)\right]^4}\right) \quad 3.4$$

With a fixed substrate, i.e. diameter and length, the pressure drop can be influenced by wall thickness and hydraulic diameter of the cells. The main influence on wall thickness comes from substrate material selection, which is either ceramic or metallic. Metallic substrates are almost exclusively used in applications requiring minimal back pressure because much smaller wall thicknesses are achievable. The hydraulic diameter of the cells can also be changed primarily with changes to cell density. However, some relatively new hex shaped cell structures, which have larger hydraulic diameters than square cells of the same cell density, show lower pressure drops as well as increased surface area [8]. Figure 3.5 below shows how the hydraulic diameter of each cell type is measured.

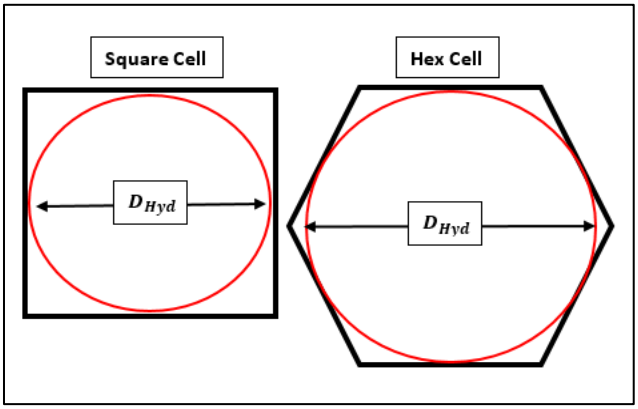

Figure 3.5 – Hydraulic Diameter Diagram

3.1.3 Durability

Durability of aftertreatment systems is always of great importance to ensure conversion efficiency degrades as little as possible over the lifespan of the catalyst. There are three main failure modes catalysts must manage to achieve acceptable durability. These include thermal ageing, poisoning, and fatigue.

Thermal ageing is often the highest threat to catalyst durability. Once the catalyst bed reaches its light off temperature the exothermic catalytic reactions begin and further elevate the exhaust gas temperatures as flow travels along the length of the substrate. This elevated temperature is the driving factor of thermal ageing, which induces changes to the wash-coat and in extreme cases the substrate material. These changes manifest themselves in several ways. Relative to the wash-coat, thermal ageing is characterized by localized melting of the wash-coat which can cause loss of porosity, agglomeration, and crystallization, all of which lower the conversion efficiency. This phenomenon occurs at an upper temperature threshold which is highly dependent upon the application, however temperatures on the order of $800 - 900℃$ are generally accepted as an upper temperature bound. [2] [3] A loss of porosity involves migration of the wash-coat that effectively smooths the roughness of the wash coat surface, reducing the surface area where agglomeration involves the same migration mechanism, but reactive sites collect into large bunches, lowering the dispersion level of reactive sites. Aluminum oxide-based formulas are less resilient to the effects of thermal ageing than ceria/zirconia-based coatings due to their smaller microstructures, which can be more easily damaged. Crystallization is a little different in that crystal growth occurs at the elevated temperature, which blocks reactive sites, and this seems to be more closely related to the slurry utilized in the coating process. Preventing crystallization is often the driving factor for the use of doping agents. In extreme cases where the bed temperature is left uncontrolled the substrate material can lose its structural stability, causing collapse of the cell structures and rendering the catalyst completely ineffective. While the temperature substrate melting occurs at is dependent upon the material used, for metallic substrates temperatures on the order of $1100\ ℃$ are generally accepted as detrimental to substrate materials. Keeping these concerns in mind, it is important to realize that thermal ageing is an inevitable process in any catalyst. Managing the rate at which it occurs is therefore key. The rate can be controlled if catalyst bed temperatures are effectively managed through wise design choices.

Poisoning, sometimes referred to as masking depending on the nature of the process, can be a significant concern in a two-stroke catalyst application. Poisoning can fall into two categories, one being the physical covering of catalytic reaction sites by buildup of particulate matter or crystalline growth, which are both referred to as masking, and deactivation occurring through constituents reacting with or completely destroying reactive sites. Masking is common in most catalyst applications, where over time particulate matter can build up on the substrate surface and block exhaust gasses from reaction sites. In a two-stroke application this becomes important because of the presence of unburned oil originating from the total loss lubrication systems two-stroke engines employ. The rate at which unburned oil builds up on a substrate or how compounds from the oil interact with exhaust gasses to form crystalline growth are areas of research yet to be explored. However, it is believed that ash content will be a significant factor in masking rates. Poisoning of the catalyst due to constituents originating from the oil does have significant research in the automotive field which can likely be used to guide future work in the two-stroke field. Phosphorous is one of the most widely known chemicals to form both crystalline growth and interact with reaction sites to lower conversion

efficiency [9]. Phosphorous originates from a common engine oil additive called zinc dialkyldithiophosphate (ZDP) which serves to provide wear protection but decomposes into various phosphorous species. As a result of the discovery that phosphorous species deactivate catalyst reaction sites the American Petroleum Institute (API) specified lower concentrations of phosphorus in four stroke engine oils [10]. Most market two stroke oils do not contain phosphorus or ZDP, so this form of poisoning is of less concern to this project.

The final main failure mode is from fatigue due to thermal stresses and or vibration. Thermal stresses are induced longitudinally on the catalyst substrate due to the temperature gradient from the exothermic reactions taking place. However, lateral and radial stresses are often of greater concern because the strength of the substrate in these directions is significantly lower. Lateral and radial stresses primarily occur from uneven flow distribution across the cells of the substrate. This is another scenario in which flow optimization using CFD analysis becomes important. It should be noted that some longitudinal and radial stresses are placed on the substrate by design to hold it in place. Longitudinally the part is often retained by a geometrical feature in the center section of the catalyst shell. Traditionally substrates are also wrapped with a fiberglass or similar material blanket to insulate them from the outer walls and isolate some vibration. This substrate and blanket package is inserted into the main body of the catalyst and the pressure the metal mantle exerts on the substrate is referred to as canning pressure. Canning pressure must be sufficient to hold the substrate in place and isolate it from vibration but is limited by the structural strength of the substrate.

3.1.4 Packaging

Packaging of the catalyst is a relatively simple step after having designed the substrate and wash-coat formula. However, there is some overlap in design considerations because flow distribution is controlled by how the substrate is packaged. Typically, the inlet and outlet exhaust tubing are of significantly smaller diameter than that of the substrate diameter, therefore cones are often used to achieve the diameter transition in a gradual manner. The taper of these cones can have a large influence on flow distribution. Typically, the most gradual cone taper angle the design space allows is ideal for good flow distribution. Additionally, the inside diameter of the center section of straight tubing that houses the substrate and blanket controls canning pressure. Within the center section one of two methods are used to retain the substrate in its position. Most commonly the ends of the center section are necked to a smaller diameter on either side of the substrate. The second method utilizes welded in rings on either end to constrain the substrate. Finally, integrating the catalyst into the exhaust system involves selecting a mounting system. Common options are bolted flanges and v band clamp flanges. Typically, most catalyst packaging materials are steel, either stainless or low carbon with a corrosion resistant coating, to prevent rusting. A typical catalyst cross section view is shown below in Figure 3.6.

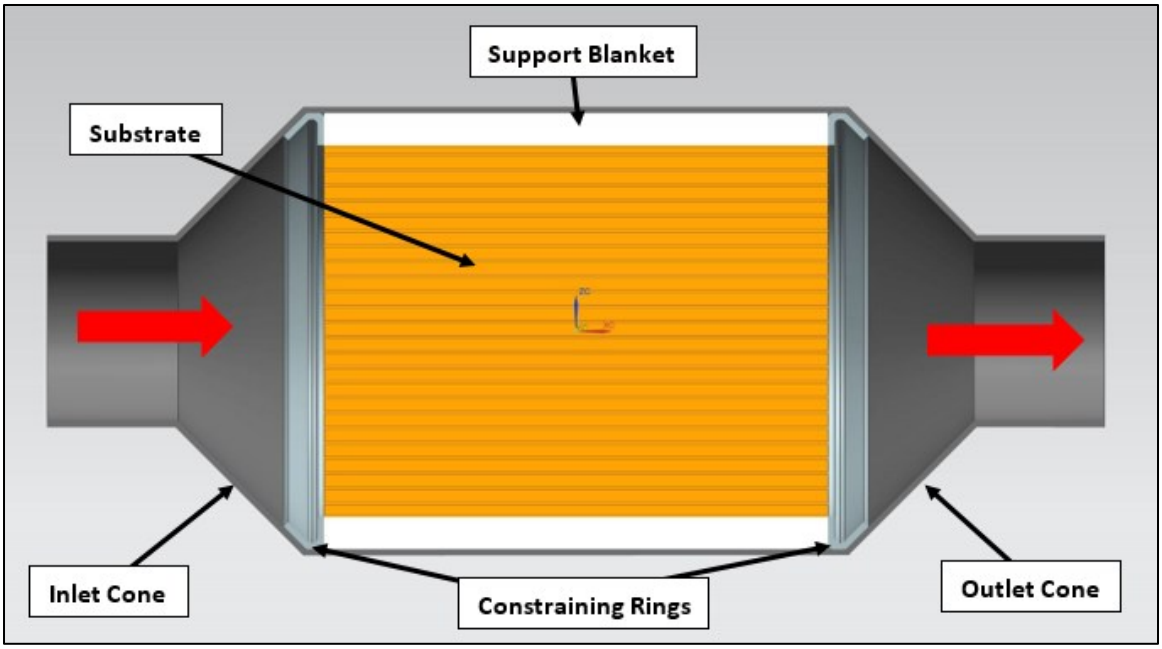

Figure 3.6 – Typical Catalyst Cross Section View

3.2 Design Challenges

Now that the typical design considerations for catalyst development have been covered it is important to understand the unique challenges posed by implementing a catalyst on a two-stroke engine. The most significant challenges are controlling the catalytic reaction and minimizing performance changes due to increased back pressure in the exhaust system. Possessing a working understanding of fundamental two-stroke engine design and operation, specifically the scavenging process and how it is assisted by the mid-pipe design is necessary to appreciate these design challenges.

3.2.1 Two Stroke Operation Review

This section reviews the two stroke engine scavenging process and some high level exhaust system design considerations. Understanding the gas dynamics within the exhaust system is advantageous because these concepts will help to support several key decisions throughout this project. It is assumed that the reader conceptually understands the two stroke gas exchange process within the cylinder and how it differs from a four stroke engine. Heywood's Internal Combustion Engine Fundamentals [11], Blair's Design and Simulation of Two-Stroke Engines [12], and Jennings Two-stroke Tuners Handbook [13] are excellent resources to fill in any gaps in understanding.

It is well understood that two stroke engines have high HC and oxygen concentration within their exhaust systems due to how the intake and exhaust processes are port controlled and overlap with each other during the gas exchange process. This inevitably allows a portion of the fresh fuel and air mixture to escape the cylinder during the blow down process. Scavenging is an important process in all engines. When properly executed exhaust gas evacuation from the cylinder is promoted and more fresh charge can fill the cylinder for the subsequent cycle. In two stroke engines this process is complicated by the port controlled gas exchange process because over scavenging is a valid concern. Therefore, retention of the fresh charge within the cylinder, which is referred to as trapping efficiency, is also an important consideration.

Below in Figure 3.7 is a simple diagram containing a sectioned view of a mid-pipe and the relevant design terminology. Exhaust gasses flow from the exhaust port into the manifold, through the pipe to the right and exit the stinger into the muffler.

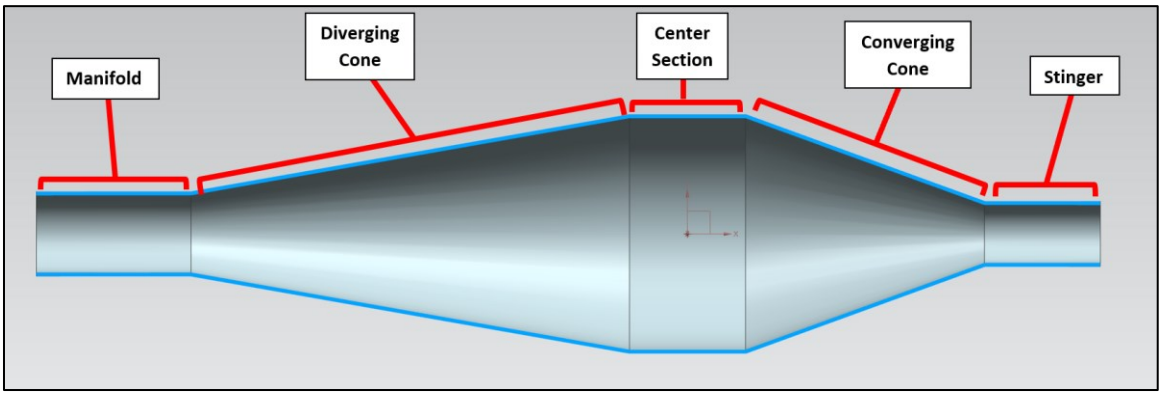

Figure 3.7 - Mid-Pipe Diagram

Beginning with the moment the piston begins to open the exhaust port two things occur, first the exhaust gasses begin to flow out of the cylinder and into the exhaust system and second, because of the high pressure and flow present, a positive sonic wave is also produced. The wave is considered positive because it causes a local high pressure zone in the exhaust stream, which moves exhaust particles in the same direction as the wave itself is travelling. This process is illustrated below in Figure 3.8. The green arrows denote the pistons direction of motion in cylinder.

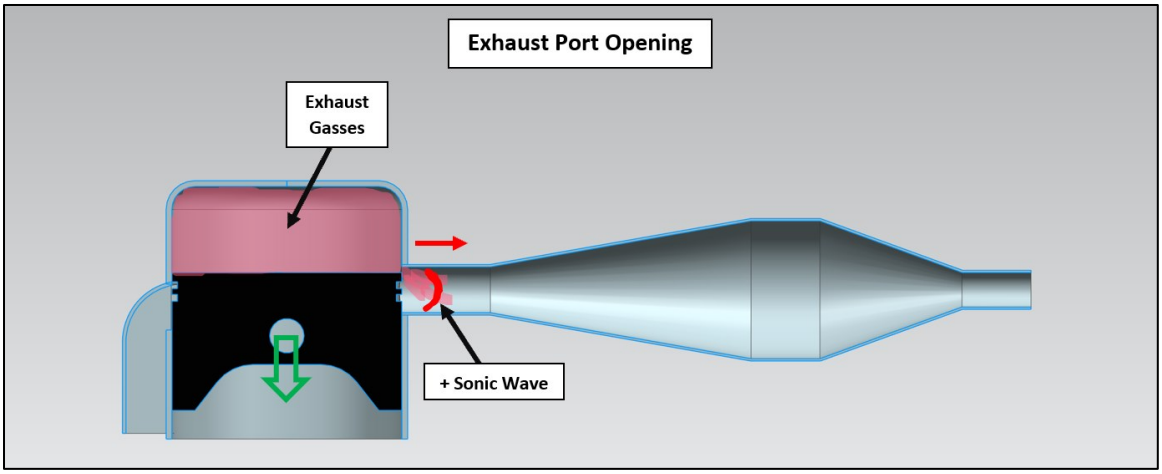

Figure 3.8 - Mid-Pipe Gas Dynamics - Exhaust Port Opening

The blowdown process continues as the piston descends within the cylinder, ultimately uncovering the intake port(s) and starting the gas exchange process. Meanwhile the positive sonic wave initially produced by the start of the blowdown process reaches the diverging cone within the mid-pipe. The diverging walls of this cone produce a reflection wave that is opposite in both sign and direction to the positive sonic wave. This translates to a local low pressure zone in the exhaust stream that moves particles in the opposite direction of the waves direction of travel. As this negative sonic wave travels back to the exhaust port it assists in the gas exchange process, mainly in drawing out the remaining exhaust gasses. This process is illustrated below in Figure 3.9.

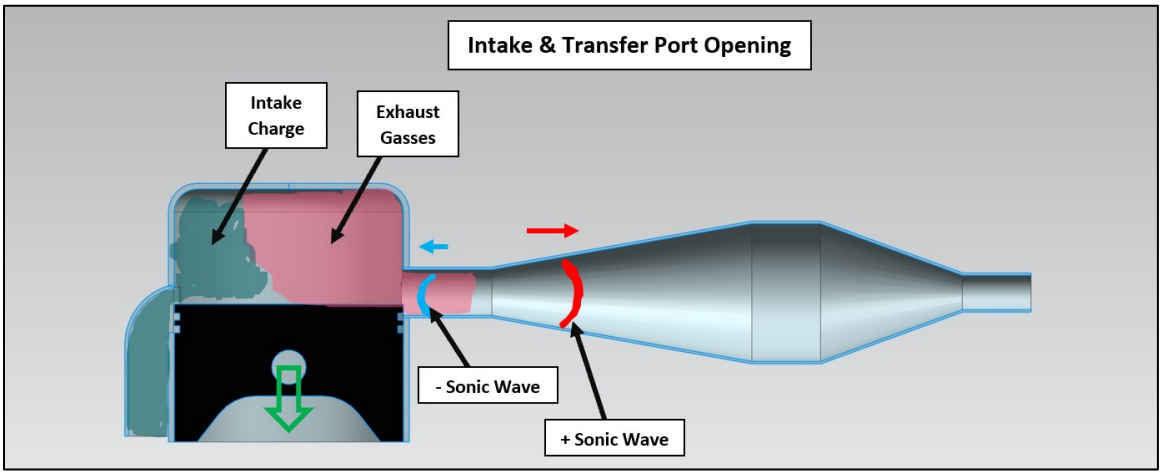

Figure 3.9 - Mid-Pipe Gas Dynamics – Intake and Transfer Port Opening

Continuing to follow the initial positive sonic wave, it eventually reaches the converging cone near the end of the mid-pipe. The converging walls reflect the positive wave, changing its direction but not its sign. So now the wave travels back toward the exhaust

port, moving particles in the same direction as the wave itself. This is illustrated below in Figure 3.10.

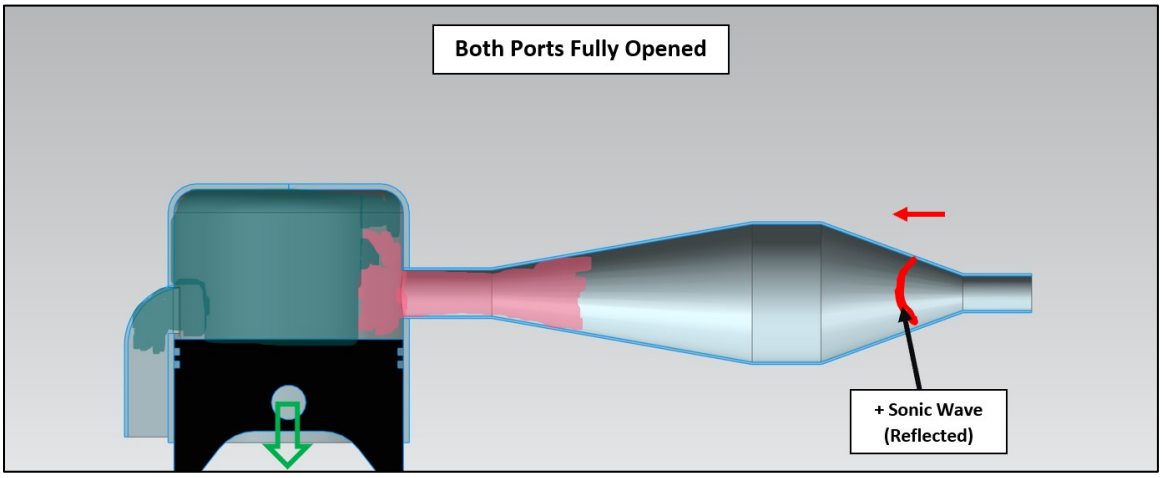

Figure 3.10 - Mid-Pipe Gas Dynamics - Both Ports Fully Opened

Upon reaching the exhaust port, if properly timed, the piston will be very close to closing the exhaust port. The reflected positive wave then serves to drive fresh fuel and air particles that escaped during gas exchange process back into the cylinder before the port closes. This is illustrated below in Figure 3.11.

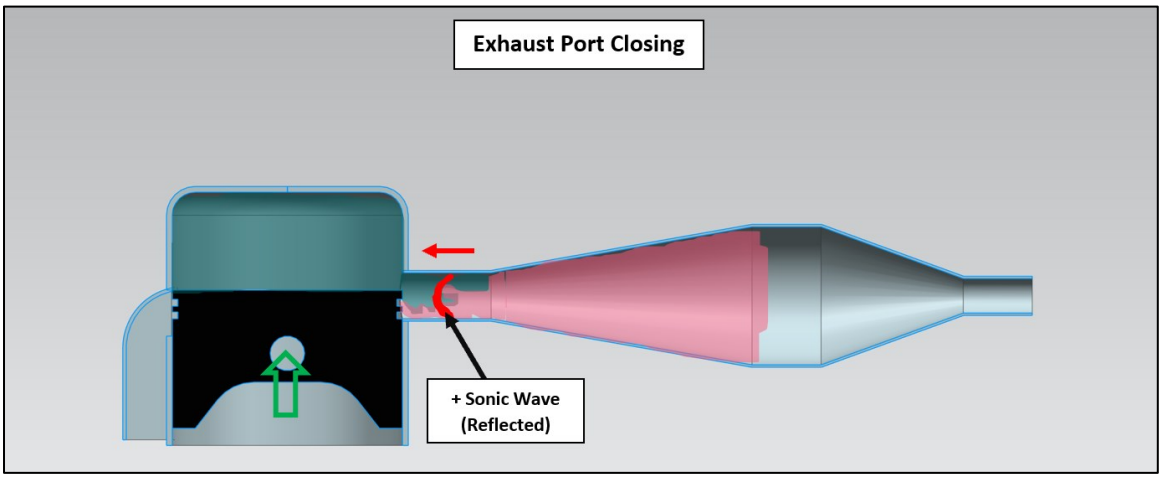

Figure 3.11 - Mid-Pipe Gas Dynamics - Exhaust Port Closing

It must be noted that the time at which the negative wave assisting in the scavenging process and the reflected positive wave assisting in retention of the fresh charge arrive at the exhaust port in relation to the piston position within the exhaust port are critical to scavenging and trapping efficiency. This is where the tuned length of the pipe comes into play. Matching up the distance of the diverging and converging cones from the exhaust port with the port timing allow the peak scavenging efficiency to be aligned with a specific engine speed target. These tuned lengths are depicted below in Figure 3.12. It is

standard practice to measure tuned lengths from the manifold inlet to the center of the cone, as shown by the yellow dashed lines. The center point is determined by the overall length of the full cones. The full cone profiles are projected by the black dashed lines in the figure.

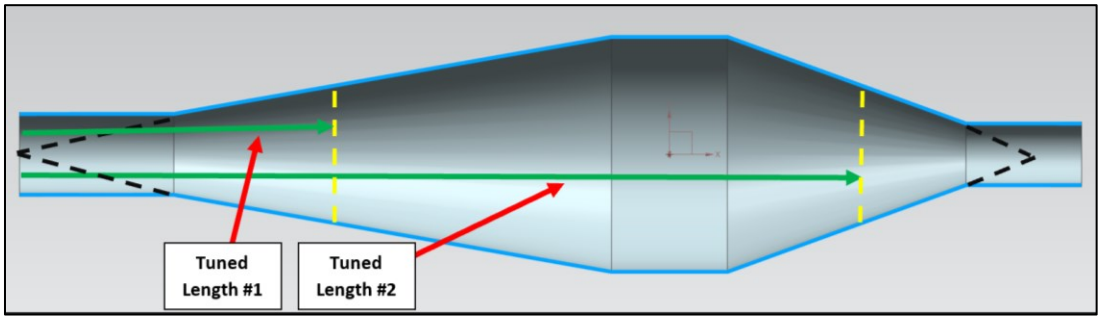

Figure 3.12 - Mid-Pipe Tuned Lengths

Figure 3.12 shows that Tuned Length #1 primarily controls the negative pressure wave that assists in scavenging, whereas Tuned Length #2 controls the positive pressure wave that assists in fresh charge retention. Finally, through changes to the converging and diverging cone angles, as well as manifold and center section length, the strength and duration of the pressure zones created by the sonic wave can be altered. However, these alterations and their associated effects are beyond the scope of this project.

One relevant addition to this exhaust system is an exhaust valve, which is now found on most modern performance two stroke engines. The exhaust valve effectively varies the exhaust port height at various engine speed load cases which offers two benefits. The first is improved trapping efficiency at low engine speed load cases. In these engine operating states, the exhaust valve remains in the closed position, making the port height the shortest it can be. This decreases the time which the exhaust port is open, allowing less of the fresh charge to escape during the gas exchange process. The second benefit comes at higher speed load cases in which the mid pipe gas dynamics start to benefit performance. At these states the exhaust valve is opened, making the port height as high as it can be. This increases the time that the port remains open during each cycle. An open exhaust valve allows more time for scavenging to take place as well as more time for the reflected sonic waves to push unburned fuel and air back into the cylinder to be combusted. So, in summary a properly controlled exhaust valve can improve trapping efficiency at low speed load cases, and both strengthen and broaden the power curve in high speed load cases.

Alignment of sonic waves with port timing at a target engine speed is complex, however, the situation is further complicated by the sensitivity of the speed of sound to the pressure and temperature of the medium through which it travels. Small changes in pipe temperature or pressure speed up or slow down the speed at which sonic waves travel, shifting the carefully aligned timing, ultimately moving the peak scavenging and trapping efficiency point above or below the designed engine speed target. With the use of closed

loop fueling systems using pipe temperature as a feedback parameter this problem can be alleviated though engine calibration. Most if not all fuel injected two stroke engines with a closed loop system do not contain pipe pressure feedback systems. This is largely because pipe pressure does not vary as significantly as pipe temperature as operating conditions change. The diameter of the stinger on the outlet of the mid-pipe is selected in such a way as to achieve a desired pipe pressure which is relatively consistent under most operating conditions. Essentially the stinger is a pressure bleed off resistor that is quite resilient to changes in ambient conditions. This is very significant to a two stroke catalyst project because as previously discussed, a catalyst will undoubtably add back pressure to the exhaust system. Seeing as there is no pressure feedback sensor in the system, the OEM calibration has no way to compensate for this change and both engine and emissions performance can suffer is the catalyst is poorly integrated into the exhaust system.

3.2.2 Controlling Catalytic Reactions

Due to the inefficiencies of port-controlled intake and exhaust processes in conjunction with the 360 degree cycle that causes overlap of intake and exhaust port opening during the scavenging process, fresh charge is inevitably lost out of the exhaust port. This causes two-stroke engines to have much higher HC and CO levels than their four-stroke counterparts. This is also significant because exhaust oxygen concentrations are also elevated in the two-stroke engines, reaching levels in excess of 10% by volume [3]. With high concentrations of HC and CO combined with plenty of available oxygen for oxidation the catalyst bed temperature can quickly surpass safe levels if not controlled. While this may not be a concern under all operating points it is significant in terms of durability.

There are a few current approaches to address this challenge, including secondary air injection and the use of Hot Tubes™. Secondary air injection dilutes the exhaust gas mixture using fresh ambient air. This air is injected pre-catalyst using an engine driven auxiliary pump. Dilution of the exhaust stream has a cooling effect which helps to keep bed temperatures in check. The volume of air injected must be controlled based on the emissions concentrations in the catalyst and the catalyst bed temperature. Several drawbacks to this approach include the power loss associated with running an engine driven secondary air injection pump and more significantly dilution lowers the probability that exhaust constituents will reach a reactive site and be converted to non-harmful components. The second approach to better controlling the catalyst bed temperature is a technology called Hot Tubes™ developed in India and commonly used in smaller two and three wheeled motorcycles. This technology is essentially a tube treated with the wash-coat and located before the substrate. This tube reacts with some of the emission constituents before they enter the substrate, spreading out the thermal load of the exothermic reaction. It can be compared to close coupled catalyst systems which have become standard in the automotive industry. The advantage a Hot Tube™ provides beyond a close coupled catalyst architecture is very minimal back pressure contributions due to a large hydraulic diameter. This solution can only provide minimal conversion

efficiency benefits because its surface area is small in comparison to a traditional substrate and depending on its size can also make packaging more difficult.

3.2.3 Minimizing Performance Loss

The second most important challenge to a two-stroke catalyst is overcoming the impact it will inevitably have upon performance. One of the primary means by which scavenging and trapping efficiencies are improved is through the gas dynamics created by the mid-pipe. The two-stroke mid-pipe generates and directs sonic waves in the exhaust stream that are synchronized with port timing. These sonic waves induce gas flows that when properly synchronized with the exhaust port opening and closing assist the scavenging process and promote trapping of the fresh charge. From a performance perspective this translates to increased peak power and improvements in emissions levels. The physics at work within the mid-pipe are highly dependent upon the speed of sound within the exhaust system, which changes with temperature and pressure. Very minute changes in either pressure or temperature can easily cause the sonic waves in the mid-pipe and the port timing to no longer be synchronized. This causes the engine speed at which the exhaust system is most efficient to be different than the engine speed at which the calibration was designed around to leverage the benefits of the mid-pipe. When these points no longer align, performance losses ensue unless there is closed loop feedback in place to compensate based on pipe pressure and temperature. As previously discussed a catalyst will add a measurable amount of back pressure and to some degree change the temperature within the mid-pipe, both of which will negatively affect engine performance. There appears to be two main approaches to implementing a catalyst in spark ignited two stroke engines. The first, which this project explores, aims at wisely selecting catalyst geometry, location in the exhaust, and conversion efficiency targets to integrate the catalyst as seamlessly as possible into the stock configuration. Any advances in lowering the back pressure introduced by the catalyst will be helpful when using this approach. The second approach requires access to more development resources and has the potential to be much more complex of a design process. Rather than trying to seamlessly integrate a catalyst into the stock configuration the engine and exhaust systems would be specifically designed and calibrated with catalyst integration in mind from the start. Using this approach has several benefits, namely the added back pressure of the catalyst can be compensated for in either the mid-pipe design or the engine calibration. This would allow more freedom in catalyst geometry choices and even the location of the catalyst within the exhaust system. It is also likely that this approach could allow for more precise control of the catalytic reaction, mainly through engine calibration. It is likely this second approach will become more widely used when OEM's begin to integrate catalysts into performance spark ignited two stroke engines.

4 Project Details

4.1 Test Cell

The testing conducted for this project was completed at Michigan Technological Universities Advanced Power Systems Research Center (APSRC) Lab in the small engine groups research facility. The following section outlines the equipment and software used to complete this research.

4.1.1 Engine

The engine package selected to complete this project was a 2016 Arctic Cat Dual Stage Injection (DSI) 600 which is a relatively common snowmobile engine. This engine is a semi direct injected twin cylinder two stroke with electronically controlled exhaust valves. A cutaway image of an exhaust valve (EV) is shown below in Figure 4.1.

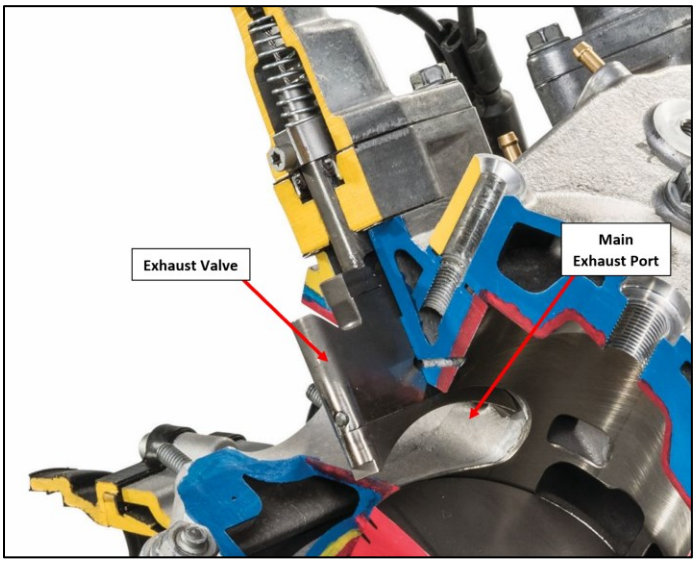

Figure 4.1 - 600 DSI Exhaust Valve [14]

The DSI system is unique in that the injectors are located high in the transfer ports and in conjunction with slotted piston skirts, can direct fuel above or below the piston dome depending on fuel delivery timing relative to the pistons location in its stroke, see Figure 4.2 below. A list of relevant engine specifications is also shown below in Table 4.1.

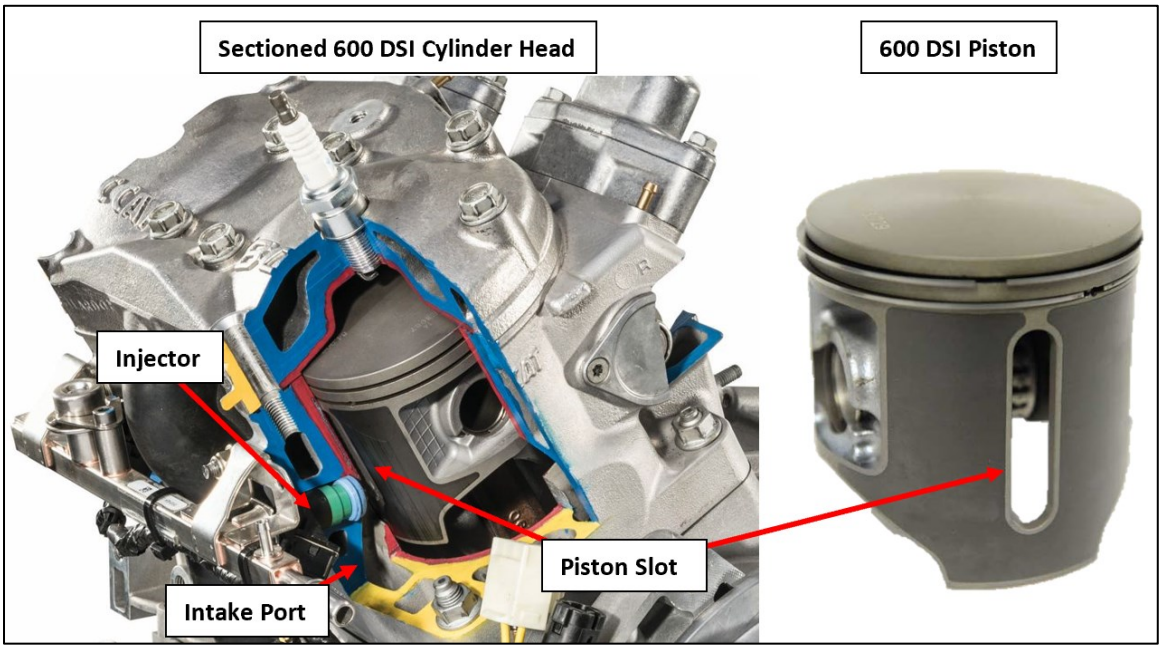

Figure 4.2 – 600 DSI Injector Location and Piston Slot [14]

Table 4.1 – Engine Specifications

Engine Specifications	
Displacement	600 cc
Bore x Stroke	73.8 x 70.0 mm
Peak Power	123 Hp
Peak Engine Speed	8100-8300 RPM
Cooling System	Water Cooled
Induction System	Crankcase Reed Valve
Exhaust Valve System	Self-Cleaning Guillotine Valve
Fuel Delivery System	Semi-Direct Transfer Port Injection

The engine is solid mounted to a billet cradle which is then fastened to a plate connected to the bed plate by three rubber isolated, height adjustable feet. The engine is directly

coupled to the dynamometer through a drive shaft with universal joints on either end, a slip joint in the middle section with an integrated rubber element that compensates for the difference in inertia between the engine and dyno. The torsional stiffness of the drive shaft is 5500 Nm/rad. This shaft attaches to a billet steel disc which is fit onto the tapered engine output shaft. The billet components were designed to be equivalent to the drive clutch in mass and inertia. See Figure 4.3 and Figure *4.4* for pictures of the engine configuration and dyno shaft with the billet disc and adaptor used to simulate the drive clutch.

Figure 4.3 – Test Cell Engine Configuration

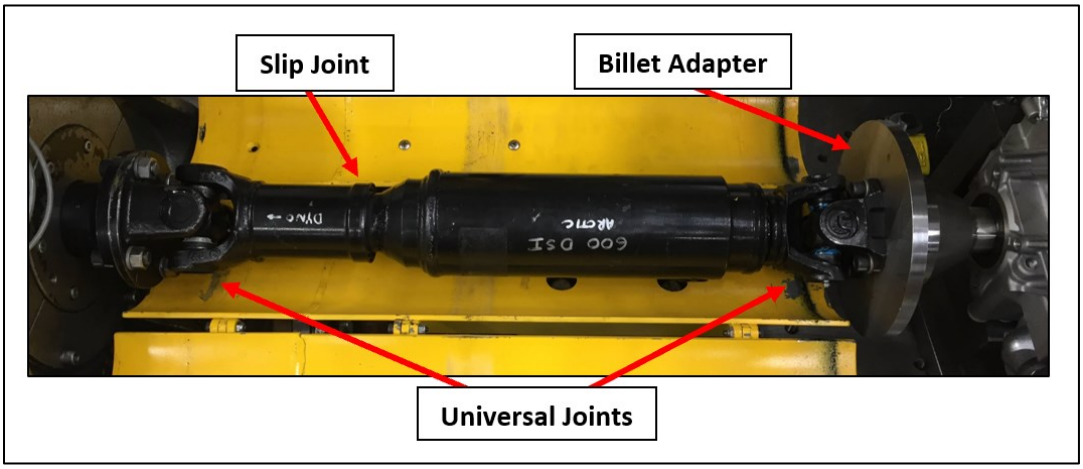

Figure 4.4 *– Engine Drive Shaft*

The cooling system is managed by a PID controlled Belimo valve. Engine coolant is routed through a heat exchanger, where engine coolant inlet and outlet temperature are measured. The Belimo valve controls flow of building supply water through the heat exchanger based on the engine coolant outlet temperature. A target temperature of 43.3℃ was utilized for all testing. The cooling system is shown below in Figure *4.5*.

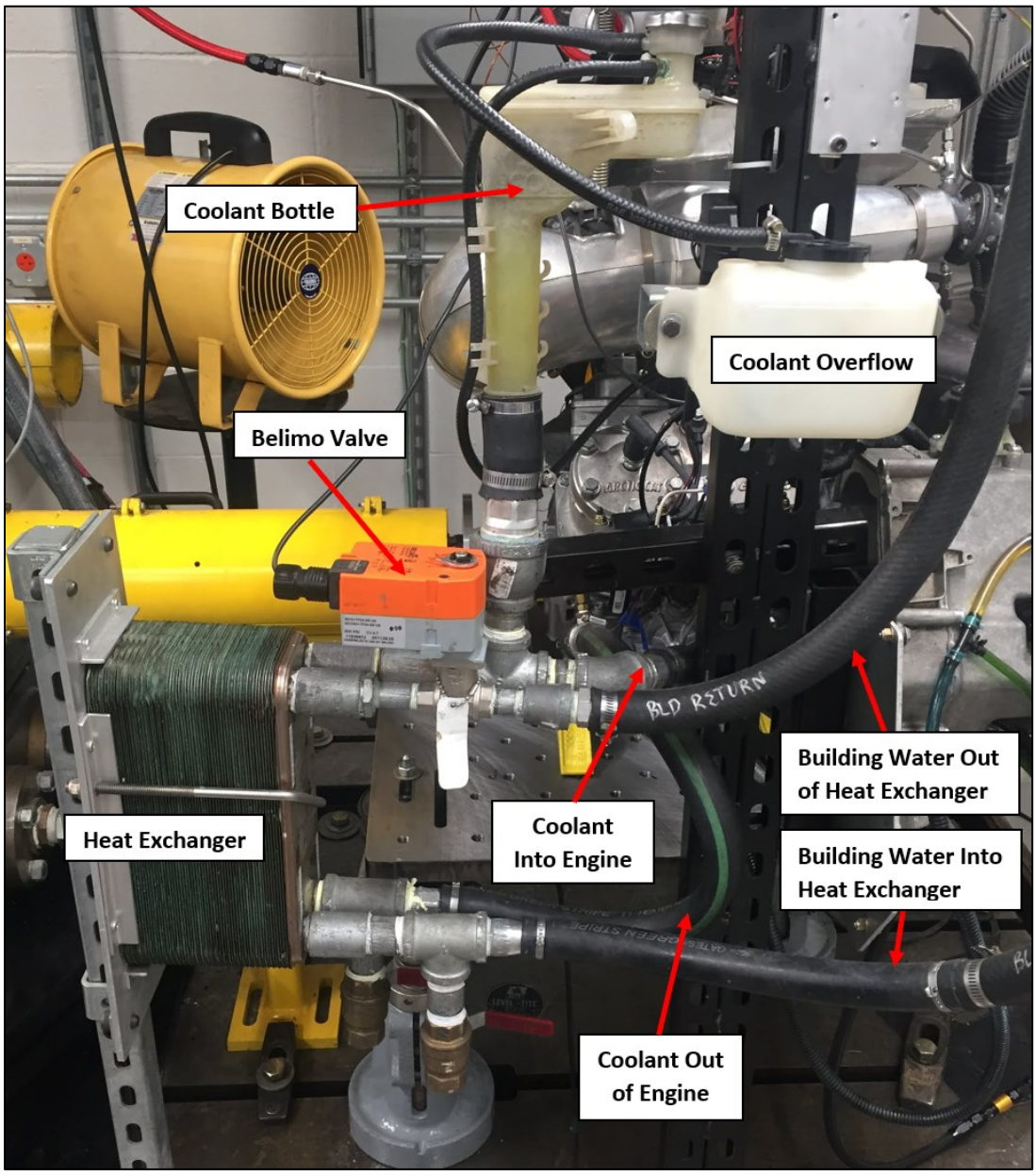

Figure 4.5 – *Cooling System*

The fuel is supplied by a returnless fuel cart manufactured by Re-Sol. This system regulates outlet pressure to the fuel rail to 60 psi_g at idle per the OEM instructions. It should be noted that the fuel pressure consistently drops by approximately 2 psi_g at mode 1, however, this is considered normal for this engine. Fuel temperature and pressure are both logged during testing. Fuel flow is measured through a Coriolis style flow meter located directly before the outlet line of the fuel cart. Standard 91E0 fuel form a local fuel station and Arctic Cat C-Tec2 injection oil were used for all testing. The stock injection oil reservoir and oil injection pump were utilized for all testing. The fuel delivery system is shown below in Figure 4.6.

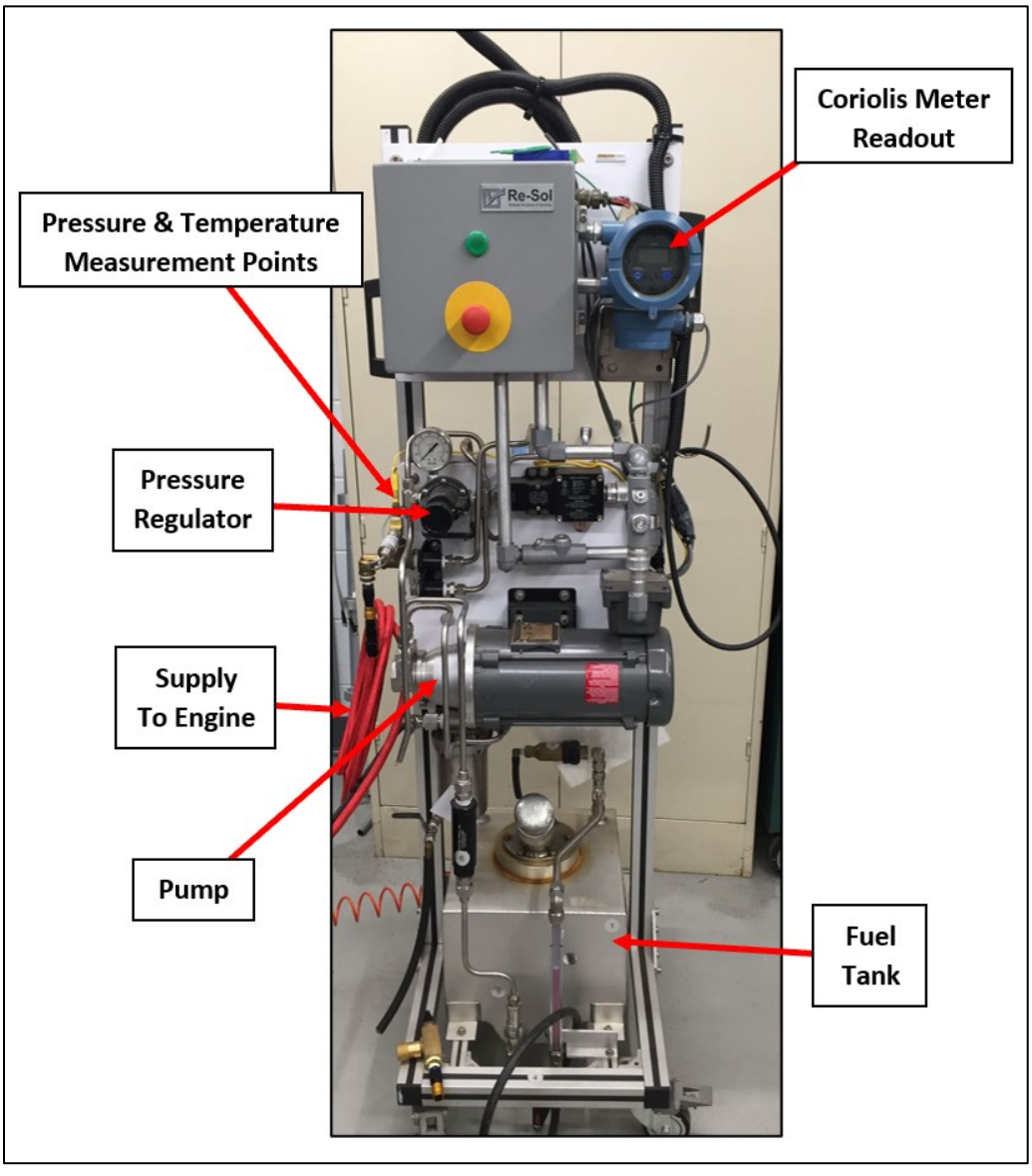

Figure 4.6 – Re-Sol Fuel Cart

The test cell ventilation system controls the exchange of outside air to a target temperature of 21.0 ℃. The inlet temperature of the engine is monitored separately, as radiant heat from the engine increases the inlet air temperature exceeds 21.0℃ under some test conditions. Exhaust gasses are vented out of the building though ducting beginning at the muffler outlet pipe. There is not a direct connection between the muffler outlet and exhaust gas ducting to prevent creating a vacuum on the exhaust system.

Finally, throttle position is controlled by a servo throttle actuator connected directly to the throttle cable. Throttle position can then be remotely adjusted in increments as fine as 0.1% of full scale.

4.1.2 Dyno

The test cell utilizes a Froude & Hofmann AG150HS low inertia eddy current absorber for a dynamometer. This system is controlled using a DYNOmite Eddy-Current Power Supply Controller Module. Additionally, on the side of the dyno opposite the engine a remote starting system has been added. This consists of a ring gear coupled to the dyno shaft which is rotated by a standard automotive starter motor. The dyno was calibrated before beginning testing using a calibrated arm and weight set. A three-point calibration was utilized with load points corresponding to low, mid, and high points within the advertised torque range of the 600 DSI engine. Finally, the dyno bearing and loss plate temperatures during operation were monitored, and the bearings greased regularly. See Figure 4.7 below for a picture of the dyno configuration.

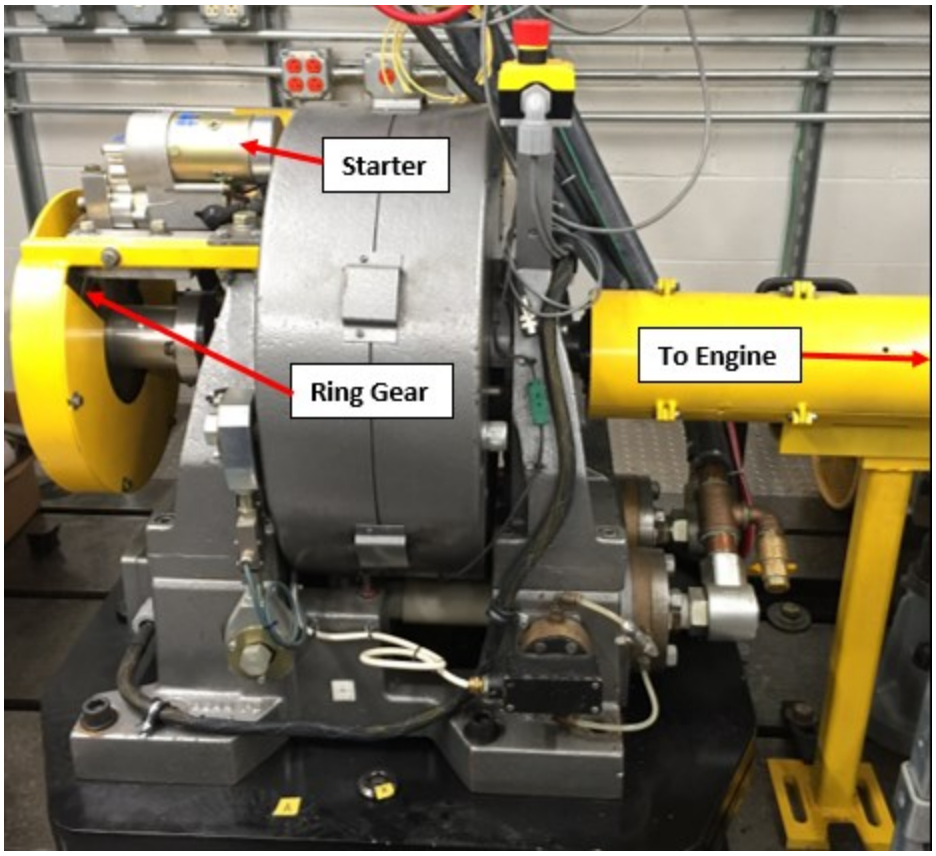

Figure 4.7 – Test Cell Dyno Configuration

4.2 Data Collection

4.2.1 Engine Data

Engine data is collected with Land & Sea DYNOmax software. Four Land & Sea data acquisition boards are utilized to collect data from the engine, dyno, and test cell. The test cell utilizes a DAQ box complete with k-type thermocouple inputs, piezoresistive pressure transducer inputs, analog voltage input and outputs, and DC voltage outputs. The front panel of the DAQ box is shown below in Figure 4.8. Additionally, an Ecotrons wideband O2 sensor is utilized to measure oxygen levels in the center section of the mid-pipe.

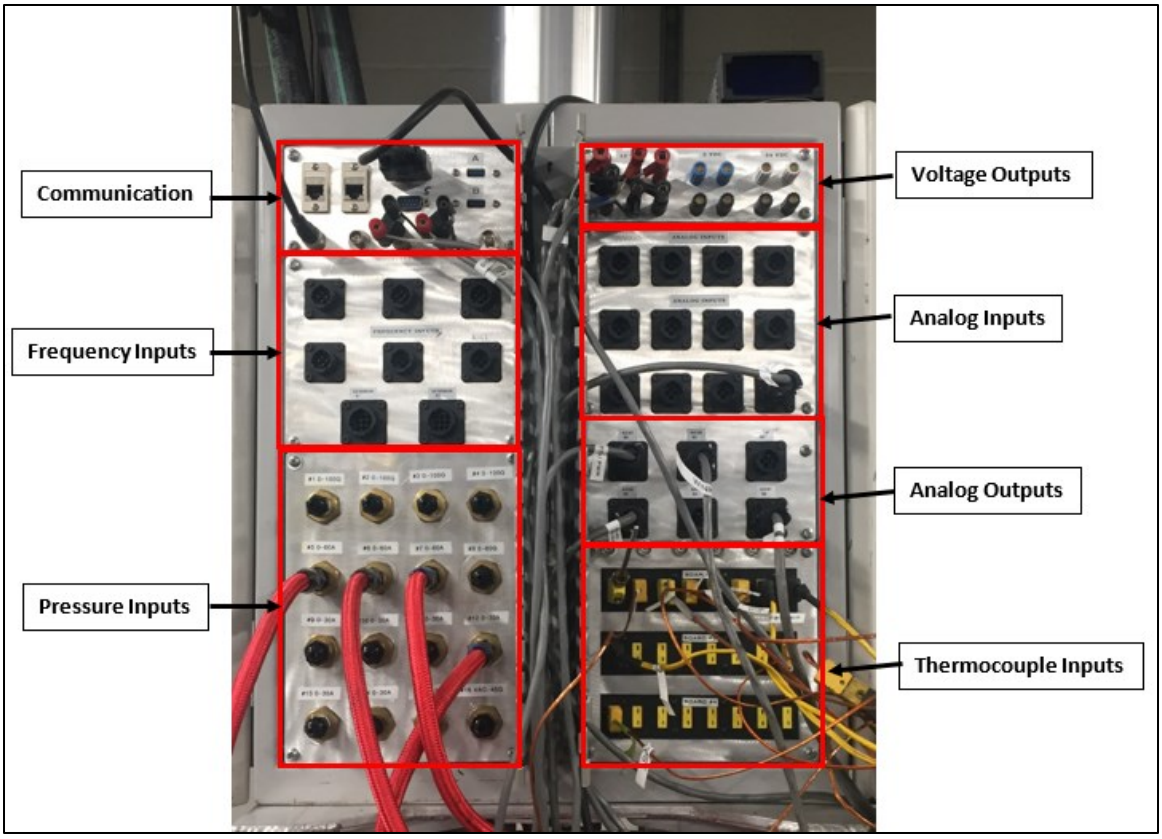

Figure 4.8 – DAQ Box Front Panel

Additionally, a control point was established for this project and data logged at this point prior to the start of testing each day. This data was then plotted on a series of control charts to ensure consistent results were being attained during each testing date. The control point was set to an engine speed of 6200 RPM and a brake torque of 35 Nm because very stable torque was observed at this operating point. Control charts included global lambda, fuel flow, BSFC, intake manifold and mid-pipe pressure, as well as coolant in, coolant out, intake manifold, EGT, mid-pipe, and muffler outlet temperatures. These charts can be found at the end of this document in Appendix 9.1. It should be noted that fuel pressure was increased from 58 psi_g to 60 psi_g after configuring the test cell and giving the engine a shakedown per the manufacturers recommendation. Additionally, the intake air temperature and coolant in temperature can vary significantly based on the ambient outdoor air temperature and building supply water temperature. Finally, during catalyst testing control points were still collected despite the addition of a catalyst and its associated effects on engine performance. The operator can factor these variables in when consulting the control chart for the consistency of these measurements.

In addition to the control charts, daily engine health checks were performed. The engine, dyno, measurement equipment, and all associated fluid levels were inspected at the start of each testing date. Additionally, more in depth engine health checks were performed periodically as time allowed. These checks included compression checks on each

cylinder, visually inspecting the pistons through the ports, visually inspecting the intake reeds, and inspection of the exhaust valves for carbon buildup.

4.2.2 Emissions Data

Emissions measurements for this project were made using an AVL System for Emissions Sampling and Measurement (SESAM) emissions bench with an AVL Heated Sample System (HSS) pre filter cart. This bench includes an MKS 2030 Multigas Fourier Transform Infrared (FTIR) Analyzer , a Flame Ionization Detector (FID) for total hydrocarbon measurement, a paramagnetic detector (PMD) for oxygen measurement, as well as a nitrogen generator to continually purge the FTIR. Temperature of the sample stream was regulated to a set point of $191℃$ for all testing. At the beginning of each day a specific operating procedure was used to prepare the instrument for measurement. This included conducting a leak check, recording a new FTIR background, zeroing and spanning the FID and oxygen measurements, span checking the FTIR, setting the purge and backflush parameters, and conducting a HC hang up test. Leak rate results remained below $2.78\ hPa/min$ for all leak checks. The FTIR background check results were recorded and monitored for significant deviation. H20 and CO2 percentages of less than 2% in the background were considered acceptable. The FID and oxygen analyzers were both zero calibrated using a nitrogen purge. The FID was then spanned with 1.8% propane span gas and the Oxygen analyzer with HC free air certified to contain 20.9% oxygen. To span check the FTIR, 15.09% CO2 was utilized and the resulting correction factor was recorded. Correction factors reached a maximum of 1.044 during testing. The purge and backflush settings were utilized to purge measurement devices when switching from measure to standby mode and back flushing dislodges any PM build up in the HSS filter. The purge and backflush are set to occur each time the bench is switched from measure mode to stand by. Finally, with the sample line open to ambient air, the bench is set to measure mode and the FID HC reading in ppm recorded. This data is logged and monitored to understand when the sample line needs to be cleaned. HC hang up values reached a maximum of $128\ ppm$ during testing and averaged approximately $73\ ppm$.

Emissions were sampled using a flexible Teflon heated sampling line manufactured by Unique Heated Products. The emissions sampling ports utilize ¼" stainless steel line, cut at a $45°$angle on the tip, and inserted to mid-stream in the sampling location cross section. Baseline emissions were sampled in the upper most chamber of the muffler. The sampling location is shown below in Figure 4.9.

It should also be noted that HC measurements are reported on a C1 basis throughout testing. Additionally, the FID measurement saturates at approximately $57{,}000\ ppm$ in mode 5. Based on historical data from Arctic Cat the 600 DSI engine HC level in mode 5 is in the vicinity of $120{,}000\ ppm$. It will be assumed that HC concentrations at idle follow this historical data throughout this project. Finally, this emissions bench is not configured to sample multiple streams simultaneously, this is of greater importance later when measuring catalyst conversion efficiency.

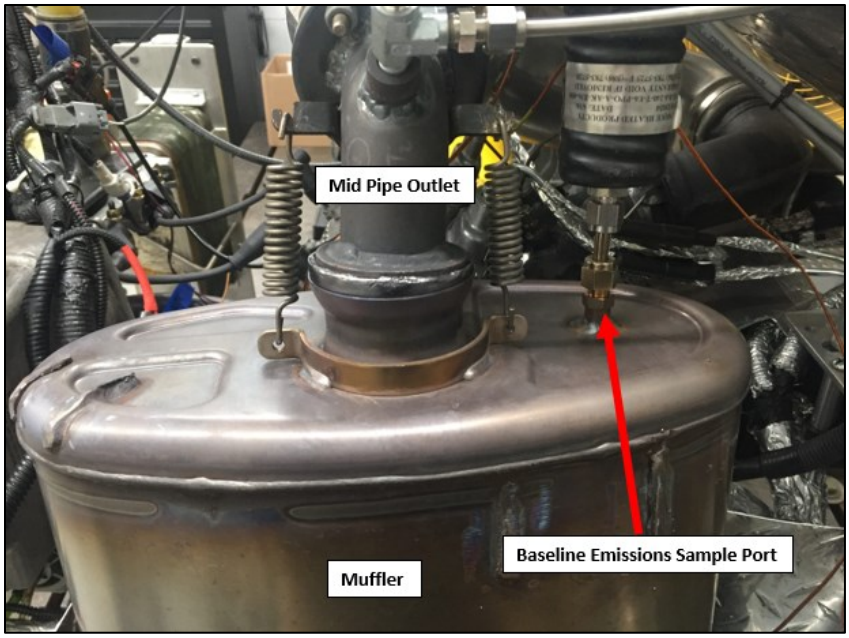

Figure 4.9 – Baseline Emissions Sampling Location

4.2.3 Data Collection Format

Snowmobile emissions testing for EPA certification is conducted using a standardized 5 mode test procedure [15]. There are two variations, the discrete and the ramped modal tests for snowmobile certification. For this project the discrete mode testing method was utilized to select engine operating points and collect data. The only exception to the standards guidelines is that an average emissions level was not calculated for the entire cycle, instead the modal data was reported individually for each mode as it was more valuable to the project in this format. The standards discrete 5 mode duty cycle parameters are shown below in Table 4.2.

Table 4.2 - Discrete 5 Mode Duty Cycle

Mode	Engine Speed (%)	Brake Torque (%)	Minimum Time in Mode (minutes)
1	100	100	3.0
2	85	51	3.0
3	75	33	3.0
4	65	19	3.0
5	Idle	0	3.0

It should also be noted that the engine was sufficiently warmed up to a stable coolant out temperature of 42 ℃ to 44 ℃ before beginning any testing and ambient temperatures were kept within the standards limitations of between 20 ℃ and 30 ℃. Finally, the standard procedure for collecting modal data for this project included starting at mode 5 and working up to mode 1, allowing 3 minutes minimum at each mode and collecting data for the final minute of the mode being tested. Between each mode the engine was returned to idle. The stability of the measurements is then verified graphically before averaging the measurements for each mode.

5 Catalyst Design

5.1 Design Considerations

Previously, in the literature review section, conversion efficiency, back pressure, and durability were introduced as primary catalyst design criteria. The considerations that make up these criteria were discussed in detail to give an understanding of the key goals at hand when developing a catalyst. Goals included achieving a considerable conversion efficiency while maintaining safe catalyst bed temperatures, minimizing engine performance losses due to added back pressure in the exhaust system and achieving both these goals with an acceptable level of durability to ensure the catalyst performs reliably throughout the vehicles lifespan. Using the information from the literature review, a design process was developed to provide a starting point for future catalyst development projects. This process is tailored towards a two stroke application, prioritizing maintaining control of catalyst bed temperatures, minimizing back pressure effects, and giving ample consideration to durability. The testing and results section will further outline how key aspects of the process were tested and validated.

5.2 Design Process

When developing this design process it was assumed that catalyst design is relatively new to the designers and therefore catalyst suppliers knowledge and expertise will be significantly relied upon in certain stages of design. In subsequent projects, after gaining knowledge regarding catalytic converters in two stroke applications, designers can begin to be more independent from the suppliers and the process will change accordingly. For the time being this process serves to provide a good starting point.

5.2.1 Developing Design Targets

The main responsibilities of the designer include selecting target conversion efficiencies for each emissions constituent to be converted, quantifying an acceptable level of performance loss, and defining the location as well as space claim for the catalyst.

5.2.2 Locating the Catalyst

Seeing as two stroke engines are incredibly sensitive to changes in back pressure within the exhaust system, understanding catalyst back pressure contributions seemed to be the most logical starting point for design. However, to measure the back pressure and correlate it to a performance loss, the approximate location of the catalyst must first be selected. Initially this location was thought to be somewhat arbitrary in that if the tuned length of the mid-pipe and its cone angles remained unaltered the scavenging process would remain unaffected. Using this thinking the stinger was selected as a favorable location for two reasons; integration of the catalyst would be relatively easy, and it was

assumed this location would not significantly affect the gas dynamics within the mid-pipe. This location was selected before fully understanding the stingers role in maintaining mid-pipe pressure. Through initial back pressure testing it was discovered that altering the length and diameter of the stinger would not be a viable solution. The ensuing performance losses were obvious and significant. Results of this testing are discussed later in Section 6.2.1. After learning more about two stroke gas dynamics and the stingers role in maintaining pipe pressure it was determined that if the stinger remained the most restrictive point in the exhaust system mid-pipe function would remain relatively unaltered. Subsequent back pressure testing validated this theory, constraining the catalyst location to be within the muffler. This is not to say that a mid-pipe could not be designed to incorporate a catalyst in place of the stinger The catalyst could potentially replace the stinger, acting as the pressure bleed off resistor. It would simply have to be designed with that intent in mind from the beginning and the engine calibration adjusted accordingly.

5.2.3 Determining Back Pressure Contributions

With the location of the catalyst loosely defined, attention was now directed to understanding what an acceptable level of back pressure was and what substrate dimensions would correlate with this measurement. For this project in particular a percent loss in peak power output was set as the performance loss limit. The 600 DSI engine produces an advertised 91.7 kW or 123 hp at an engine speed of 8250 RPM. The acceptable loss was set to 4 hp or roughly 3.25% power loss for this project. As previously mentioned, back pressure testing was conducted to assist in locating the catalyst, but also served to better understand the level of pressure increase the 600 DSI engine could handle without significant performance losses. This testing is covered in greater detail in Section 6.2, but basically involved inserting various diameter restriction plates into the exhaust system to simulate the presence of a substrate. These restriction plates were first inserted into the stinger, and upon realizing this was not a favorable location, were subsequently redesigned to be located between the stinger and muffler. Utilizing the results and observations of this testing, suppliers sent several uncoated catalyst samples to be tested in a similar manner to the restriction plates. These samples were non-actively coated to simplify the testing process, speed up part lead times, and decrease the cost of experimentally narrowing the catalyst testing field.

Although during back pressure testing the pressure drop across the test restrictions was measured it seemed advantageous to explore methods of modelling the pressure drop across a substrate. If able to model the pressure contributions of catalyst substrates the substrate selection process could be greatly expedited. It was determined that validating the accuracy of the Hagen Poiseuille equations ability to model this pressure drop may allow it to become a useful design tool in future catalyst development. As a result, a Matlab script was constructed using Equations 5.1 through 5.6 listed below. Equation 5.1 is Sutherlands law relating dynamic viscosity and the absolute temperature of an ideal gas. The dynamic viscosity $\left(1.716 * 10^{-5}\left[\frac{kg}{ms}\right]\right)$ and temperature $(110.4\ [K])$ of air were

used as reference values to approximate the dynamic viscosity of exhaust at a given EGT. The ideal gas law, Equation 5.2, was used to approximate the density of the exhaust gas. Next Equation 5.3 is utilized to determine the exhaust mass flow rate by using fuel mass flow ($\dot{m_{Fuel}}$), lambda (λ), and a stoichiometric AFR of 14.7. Finally, the mass flow rate of the exhaust is converted back to a volume flow rate $(\dot{Q_T})$ using Equation 5.4 for use in the Hagen-Poiseuilli equation (5.6). The volume of the substrate is calculated using Equation 5.5, which is the quotient of the volume flow rate of exhaust over the GHSV which was set to $200{,}000\ hr^{-1}$ as previously discussed.

$$\mu_{Exh} = 1.716 * 10^{-5} * \left(\frac{T_{Exh}}{273.15}\right)^{\frac{3}{2}} * \left(\frac{273.15 + 110.4}{T_{Exh} + 273.15 + 110.4}\right) \quad 5.1$$

$$\rho = \frac{P}{R * T} \quad 5.2$$

$$\dot{m}_{Exh} = AFR_s * \lambda * \dot{m_{Fuel}} + \dot{m_{Fuel}} \quad 5.3$$

$$\dot{Q}_{Exh} = \dot{Q}_T = \frac{\dot{m}_{Exh}}{\rho_{Exh}} \quad 5.4$$

$$V_{Substrate} = \frac{\dot{Q}_{Exh}}{GHSV} \quad 5.5$$

$$\Delta P = C(\dot{Q}_T \mu)\left(\frac{V_{Substrate}}{D_{Part}^{\ 4}}\right)\left(\frac{N}{\left[1 - \left({}^{T}/_{L}\right)\right]^4}\right) \quad 5.6$$

This models ability to accurately predict the pressure drop across a substrate is evaluated in Section 6.4 using the results of testing the back pressure contributions of the non-actively coated catalyst samples.

5.2.4 Selecting Conversion Efficiency Targets

Selecting conversion efficiency targets in most catalyst applications simply means maximizing the efficiency at an acceptable level of performance loss. However, in a two stroke application, careful consideration must be given to this design parameter as it is the primary means of controlling the exothermic reaction and ultimately managing catalyst bed temperatures. As stated before, elevated bed temperatures accelerate thermal ageing effects and in extreme cases can completely melt the catalyst substrate rendering it ineffective.

To approximate a safe conversion efficiency target, an EES script was created modelling the conversion of HC and CO into CO_2 and H_2O as a simple combustion reaction.

Baseline emissions data and exhaust temperatures were used as inputs for the model and the upper temperature limit of the outlet gasses were set to 950 ℃ based on information from the literature reviews. The script utilized this data to converge upon a singular conversion efficiency target for HC and CO that would reach a maximum outlet temperature of 950 ℃ under adiabatic conditions. This was thought to be the worst case scenario and a sufficient starting point for a conversion efficiency target. The governing equations used in the model are outlined below in Equation 5.7 through 5.9. Equation 5.7 is the combustion reaction in which the reactants are the inlet constituents to the catalyst and the products are the outlet constituents. The fast and slow variables represent fast and slow burning HC components. When developing the EES model, how to represent the HC without any data on HC speciation was a challenge. However, Gamma Technologies offered a method to approximate the actual HC within the exhaust stream utilizing fast, partially oxidized, and large slow burning HC's in a ratio in the range of 4:1 to 5.6:1 respectively on a molar basis [16]. For this model propylene (C_3H_6) and propane (C_3H_8) were utilized as the fast and slow burning HC's respectively at a 4:1 ratio. Less than a 0.1% increase in conversion efficiency was produced between the 4:1 and 5.6:1 ratio. Therefore, the more conservative ratio of 4:1 was utilized in the model. Equations 5.8 and 5.9 represent the enthalpy of the reactants and products respectively. The fast and slow terms in each equation represent the fractional amount of fast and slow HC's based on the previously mentioned 4:1 ratio. These two equations are set equal to create adiabatic conditions, allowing the model to converge on a conversion efficiency. The enthalpy of the reactant was calculated at catalyst inlet temperatures based on baseline EGT data measured just prior to the muffler inlet and the products enthalpy calculated at the upper temperature limit previously mentioned.

$$aCO_2 + bCO + cH_2O + dO_2 + e(fast * C_3H_8 + slow * C_3H_8) + fN_2 \rightarrow gCO_2 + hCO + cH_2O + iO_2 + j(fast * C_3H_8 + slow * C_3H_8) + fN_2 \quad 5.7$$

$$H_R = aH_{CO_2} + bH_{CO} + cH_{H_2O} + dH_{O_2} + e\left(fast * H_{C_3H_6} + slow * H_{C_3H_8}\right) + fH_{N_2} \quad 5.8$$

$$H_P = gH_{CO_2} + hH_{CO} + cH_{H_2O} + iH_{O_2} + j\left(fast * H_{C_3H_6} + slow * H_{C_3H_8}\right) + fH_{N_2} \quad 5.9$$

Using the parameters outlined below Table 5.1, which are typical mode 1 data the model produced a conversion efficiency target of approximately 24% for both HC and CO. Knowing that from a catalyst bed temperature standpoint this is a worst case approximation a conversion efficiency of 25-30% was deemed acceptable to move forward with.

Table 5.1 - EES Model Input Parameters – Typical Mode 1 Data

Parameter	Value	Parameter	Value
T_{Inlet}	600 ℃	CO	4.2 %
T_{Outlet}	950 ℃	H_2O	11 %
$Fast\ (C_3H_6)$	0.80	O_2	4.2 %
$Slow\ (C_3H_8)$	0.20	HC	3.6 %
CO_2	6.5 %	N_2	70.5 %

At this point in the design process, it was necessary to rely upon the supplier's experience with wash-coat formulation and PM loading to achieve the conversion efficiency targets with the samples that met the performance loss criteria.

5.2.5 Consulting Suppliers

The suppliers, Catalytic Combustion Corporation and Heraeus, were provided the data necessary to recommend wash coat formulas. This section will cover the general information provided to suppliers and summarize the discussions leading to selection of a wash-coat formula. Later in Section 6.3.1 the specific details of the data provided for this project and the selected wash-coat formulas will be covered.

There are several key considerations to be addressed when beginning to design the wash-coat formulas. These considerations centralize around the exhaust composition, conversion efficiency targets, and durability requirements. These three considerations aim to provide the supplier with enough information to define the operating states the catalyst will experience so that they can select a wash-coat formula that will meet the set conversion efficiency and durability targets. The catalyst operating conditions are defined by the inlet temperature, exhaust flow rate, and emissions concentrations. But to define what engine operating state these temperature and concentration measurements originate from the durability requirements must first be defined. Defining the durability demands of a catalyst is like other powertrain related components in that designers have an expected lifespan paired with some sort of histogram that reflects what conditions the component will be subject to over that lifespan. In the case of a catalyst, it must last the lifespan of the engine and the conditions it is subject to are directly linked to the engine operating history. The approach for this project was to utilize historical throttle position sensor (TPS) histogram data typical of a snowmobile paired with the typical engine lifespan of a snowmobile engine. Based on the TPS histogram the engine lifespan can be broken down into a duration of engine runtime at each TPS bin. These TPS bins can then be correlated to an approximate engine RPM range. Finally, these RPM ranges can be mapped to the discrete modal test modes previously introduced. The result gives a good

approximation of the time the catalyst will be subjected to relative to each mode of the 5 mode test. Then baseline 5 mode testing data can be used to define the inlet temperatures, exhaust flow rate, and concentrations that comprise the catalyst inlet conditions.

There are several things to note regarding the inlet condition measurements. First the inlet conditions should be measured as close as possible to the proposed catalyst inlet location to best reflect the actual inlet conditions the catalyst will experience. Second, the emissions concentration data must include concentrations for the constituents that will be converted by the catalyst as well as any other constituents that will participate in the reaction. Typically, this will include HC, CO, CO2, NOx, oxygen, and sometimes H2O depending on the application. Third, exhaust flow rate is difficult to measure directly without affecting the exhaust system, therefore approximating the exhaust flow rate is an appealing option. There are many methods to approximate this measurement. The method selected for this project utilized fuel flow data in conjunction with a derivation of the AFR equation to compute intake air flow. Both the air and fuel flow rates can then be added to approximate the exhaust mass flow rate. Fourth, AFR or lambda is often a requested parameter in the design process. This parameter can cause confusion in a two stroke application based upon where the measurement is collected. An in depth explanation of various AFR measurement types in a two stroke engine is not within the scope of this project. However, note that the differences between trapped AFR in the cylinder and the global AFR in the exhaust are significant and which measurement is being utilized should be explicitly communicated. Roy Douglas published an SAE Technical paper outlining a method of computing trapped AFR using emissions data that is particularly useful in understanding the differences in trapped and global AFR. [17] Finally, being a research based project, the wash-coat formulation discussions excluded conversations about part cost. This is a significant consideration when implementing a catalyst in a production setting and will undoubtably affect the design process, especially during the wash-coat formulation process.

6 Testing and Results

The following section outlines all testing and results performed related to this project. This includes gathering baseline data, several back pressure tests, and testing actively coated catalyst samples to measure their conversion efficiency performances.

6.1 Baseline

Testing began with collecting baseline emissions and engine performance data for the 600 DSI engine in the stock configuration. The first step was performing three power sweeps and averaging the peak brake torque to establish the 5 mode test points previously outlined in Section 4.2.3. Prior to testing the engine was warmed up and then heat soaked in mode 4. The sweep rate was set to $30\ \frac{RPM}{sec}$ from an engine speed of 5000 RPM up to 8250 RPM at WOT. The power sweeps are shown below in Figure 6.1.

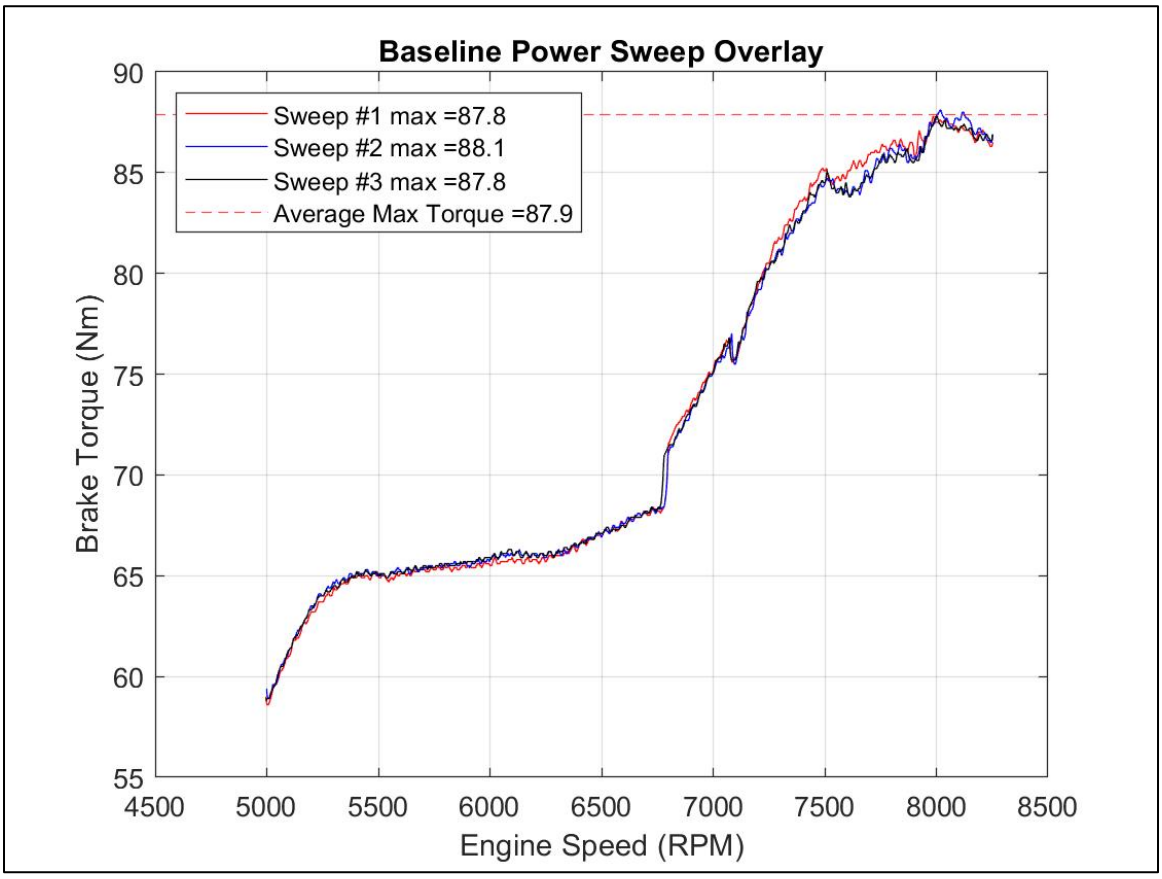

Figure 6.1 - Baseline Power Sweep Plot

The average peak torque from the three sweeps was 87.9 Nm. This average peak brake torque value was then utilized to establish the 5 mode test operating points outlined below in Table 6.1

Table 6.1 - 600 DSI Discrete 5 Mode Operating Points

Mode	Engine Speed (RPM)	Brake Torque (Nm)
1	8250	87.9
2	7013	44.3
3	6188	28.7
4	5363	16.5
5	Idle (~1750)	0.0

After establishing the modal test points for the 600 DSI a baseline 5 mode test was conducted with engine performance and emissions measurements. The relevant baseline data is tabulated below in Table 6.2.

Table 6.2 - Baseline Emissions and Engine Data

Parameter (units)	Mode 5	Mode 4	Mode 3	Mode 2	Mode 1
$CO\ (ppm)$	33142	8167	14152	39261	59521
$CO_2\ (ppm)$	29288	92011	92921	61289	51430
$O_2\ (ppm)$	113929	49058	36699	55690	46617
$H_2O\ (ppm)$	67332	114618	121553	106679	108467
$HC\ (ppm)$[1]	[2]120000	24027	21046	42795	32560
[3]$Lambda$	0.99	1.02	0.94	0.88	0.80
[4]EGT (°C)	200	564	674	661	621
$Mid\ Pipe$ (°C)	157	419	543	614	655
$Muffler\ Exit$ (°C)	68	273	399	504	592
$Coolant\ Out$ (°C)	41.5	43.0	42.8	42.6	47.7
$Intake\ Air$ (°C)	22.3	23.0	25.1	28.4	31.7
$Mid\ Pipe\ Pressure\ (psi_a)$	14.7	14.2	14.3	14.9	17.3
$Intake\ Manifold\ Pressure\ (psi_a)$	14.4	14.1	14.1	14.1	13.9
$BSFC\ \left(g/_{kWhr}\right)$	4277	425.3	345.9	463.3	415.7
$Brake\ Torque\ (Nm)$	2.08	16.6	28.5	43.9	86.5
$Engine\ Speed\ (RPM)$	1748	5361	6190	7010	8250

[1] HC concentrations are measured on a C1 basis
[2] Measurement saturates FID at 57,000 ppm, based on historical data measurement should be approximately 120,000 ppm
[3] Measured by Ecotron Wideband Sensor in the mid-pipe center section
[4] Average EGT between PTO and MAG sides of manifold

6.2 Back Pressure

Back pressure testing was conducted initially to determine the 600 DSI engine's ability to handle the pressure contributions of a catalyst in the exhaust system. When reviewing literature, it was noted that the open frontal area has a dominating impact on substrate pressure contributions in comparison to the length of the cell structure. Keeping this in mind, the frontal area of the substrate can be thought of as a simple orifice plate. If the open cross sectional area of the orifice matches the open frontal area of the substrate, pressure contributions were assumed to be similar. Thus, to simulate catalyst back pressure without sample parts a series of orifice plates were designed to be inserted into the exhaust system and mimic the effects of a substrate in the exhaust flow path. As previously mentioned the initial catalyst location was determined to be in the stinger section of the mid-pipe for convenience and to avoid alterations to the gas dynamics within the mid-pipe. To prepare for back pressure testing, the stinger was cut and two four bolt flanges welded in as well as both pre and post restriction pressure and temperature taps installed. The completed mid-pipe can be seen below in Figure 6.2.

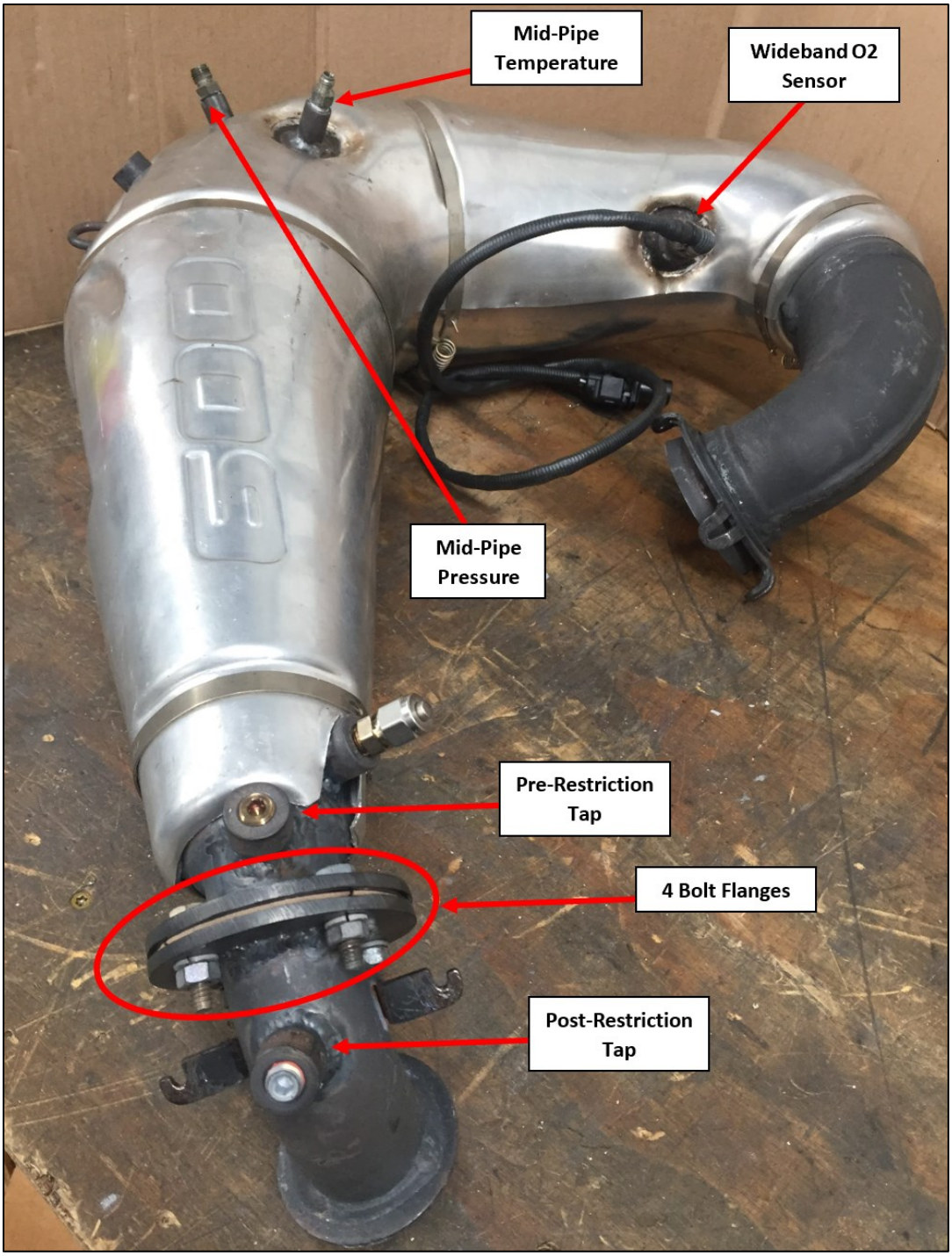

Figure 6.2 - Modified Mid-Pipe for Back Pressure Testing

Finally, several orifice plates with matching bolt hole locations were manufactured to fit into the modified mid-pipes 4 bolt flanges. The sizing of the orifices was arbitrary but spaced out to cover a broad range of restriction levels. The completed orifice plates and paper gaskets used to seal the flanges are shown below in Figure 6.3 followed by Table

6.3 where the percent of cross sectional area restricted by the plates within the 38 mm diameter stinger are given.

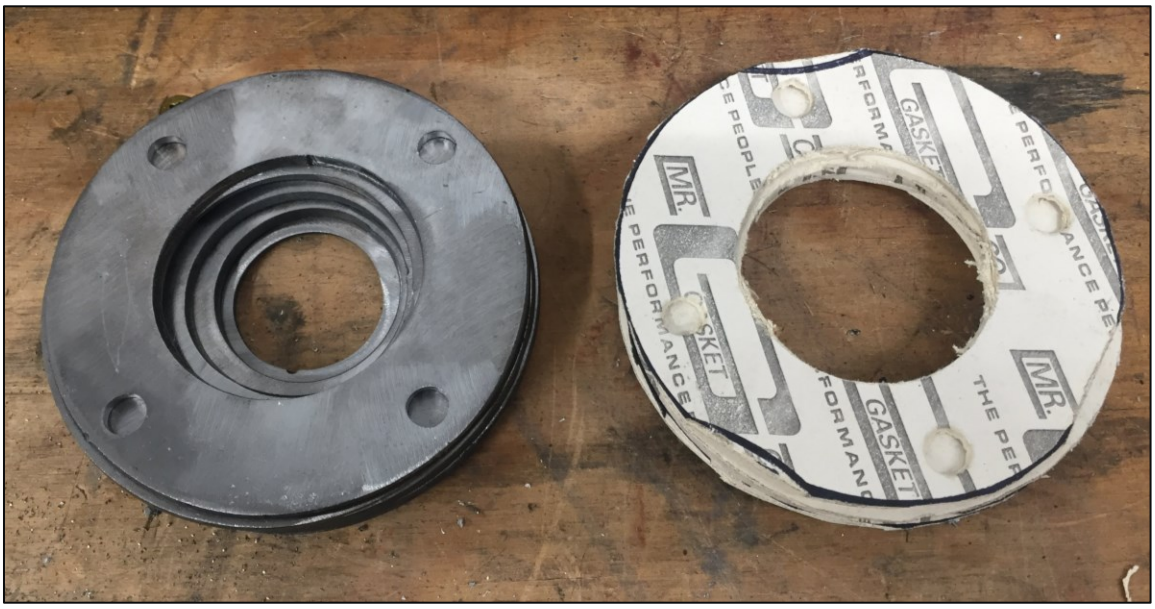

Figure 6.3 - Completed Orifice Plates

Table 6.3 - Orifice Plate Restriction Data

Orifice Diameter	Restricted Area of Stinger
36.5 mm	7.75 %
30.5 mm	35.6%
24 mm	60.1%
17.5 mm	78.8%

The final testing setup is shown below in Figure 6.4.

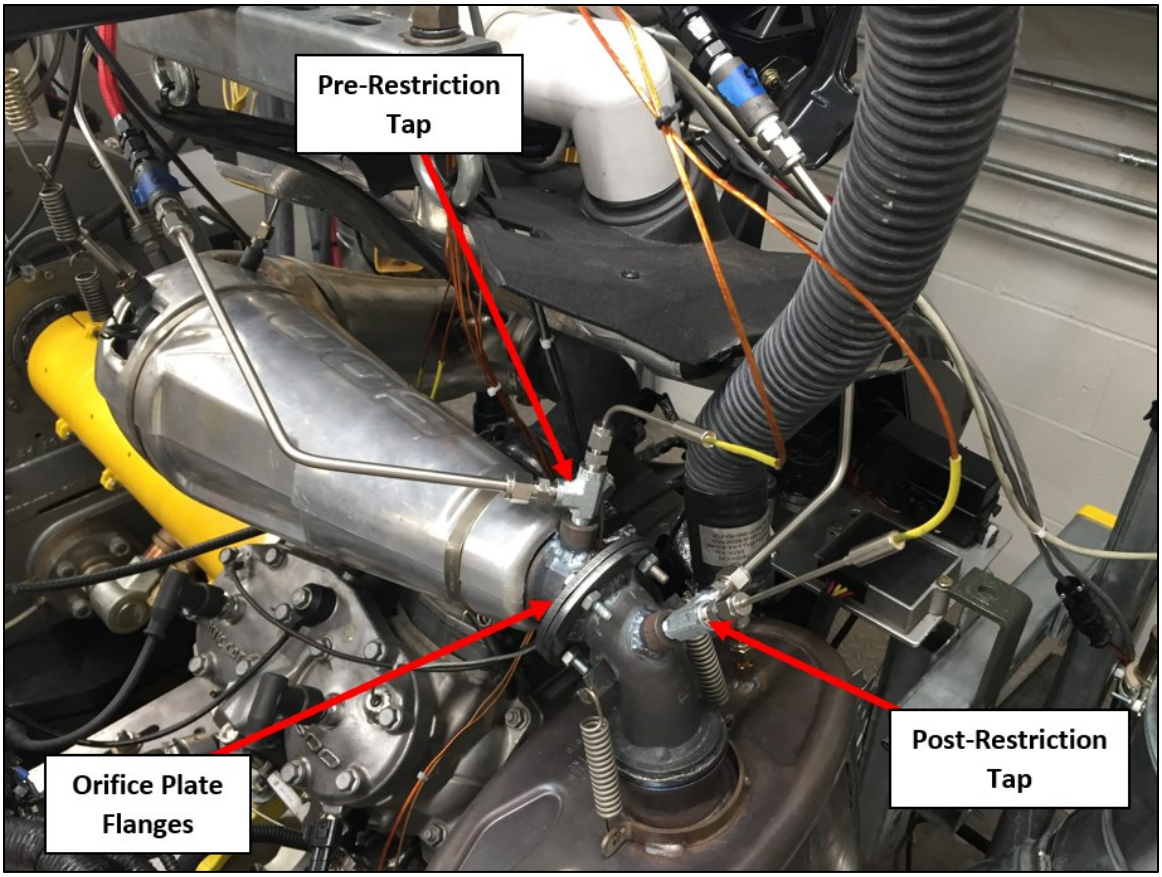

Figure 6.4 - Back Pressure Test #1 Setup

6.2.1 Back pressure Test #1

Testing was conducted using the standard discrete 5 mode test format starting with the least restrictive plate and moving toward the most restrictive. It quickly became apparent that the elevated restriction was having significant adverse effects on engine performance. The effects started to become very clear when unable to reach mode 1 with the 30.5 mm restriction installed and got progressively worse as restriction increased. With the 24 mm restriction installed both mode 1 and 2 could not be achieved. The 17.5 mm restriction was not tested due to this trend in performance loss. Engine operation was erratic surrounding changes in the exhaust valve position, which changes from low to mid at approximately 6900 RPM and mid to high near 7300 RPM. When undergoing the EV position change brake torque dropped followed by engine speed. Backing down the load allowed the engine to recover to normal operation, but the erratic behavior continued with each subsequent attempt to cross the EV transition points. When comparing data to baseline values the main differences with the elevated restriction were

lower lambda and mid-pipe temperature readings as well as higher mid-pipe pressures. Results showing these changes can be seen below in Figure 6.5 through Figure 6.7.

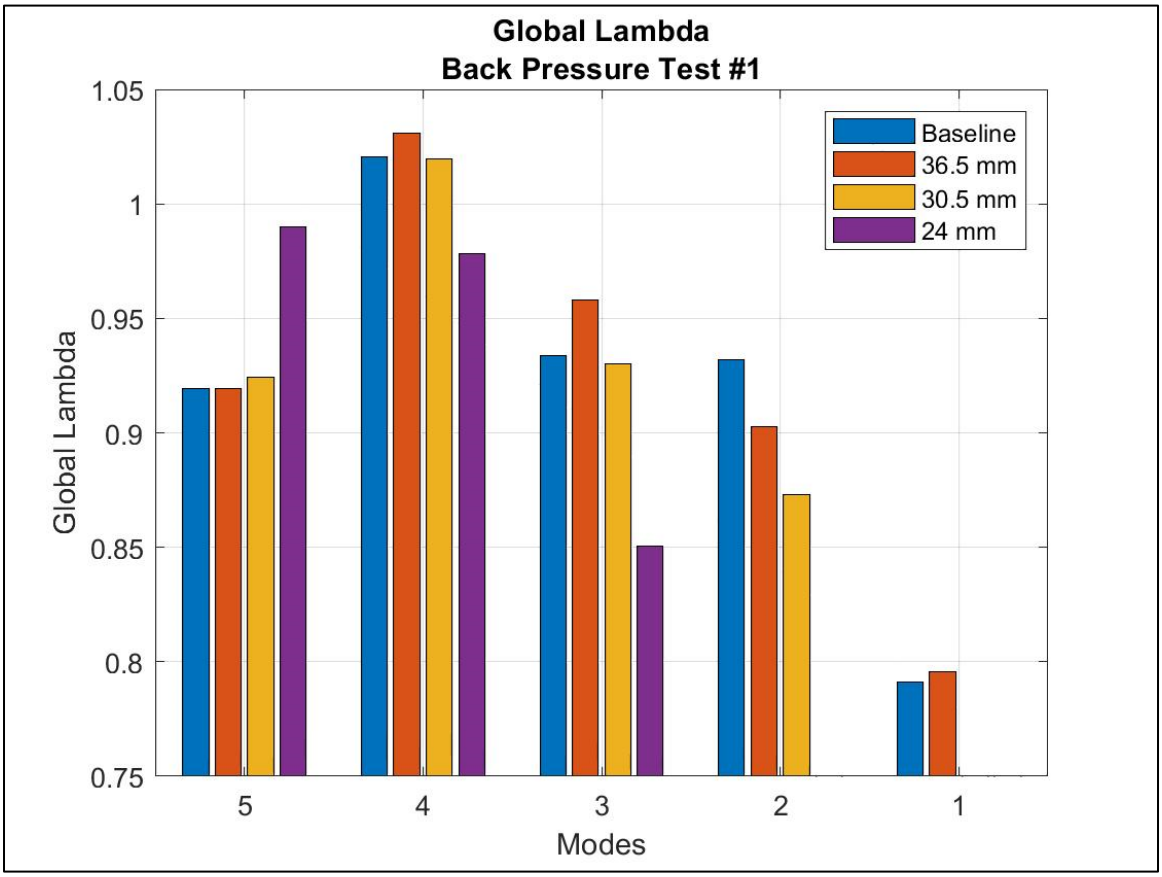

Figure 6.5 – Global Lambda - Back Pressure Test #1

Figure 6.5 shows that as the restriction diameter decreased global lambda observed a general trend of becoming more fuel rich except for in mode 5. The general decrease in lambda became more significant as the restriction diameter decreased. For example, the 30.5 mm restriction began to have an effect in mode 2, whereas the 24 mm restriction started affecting lambda values all the way back in mode 4.

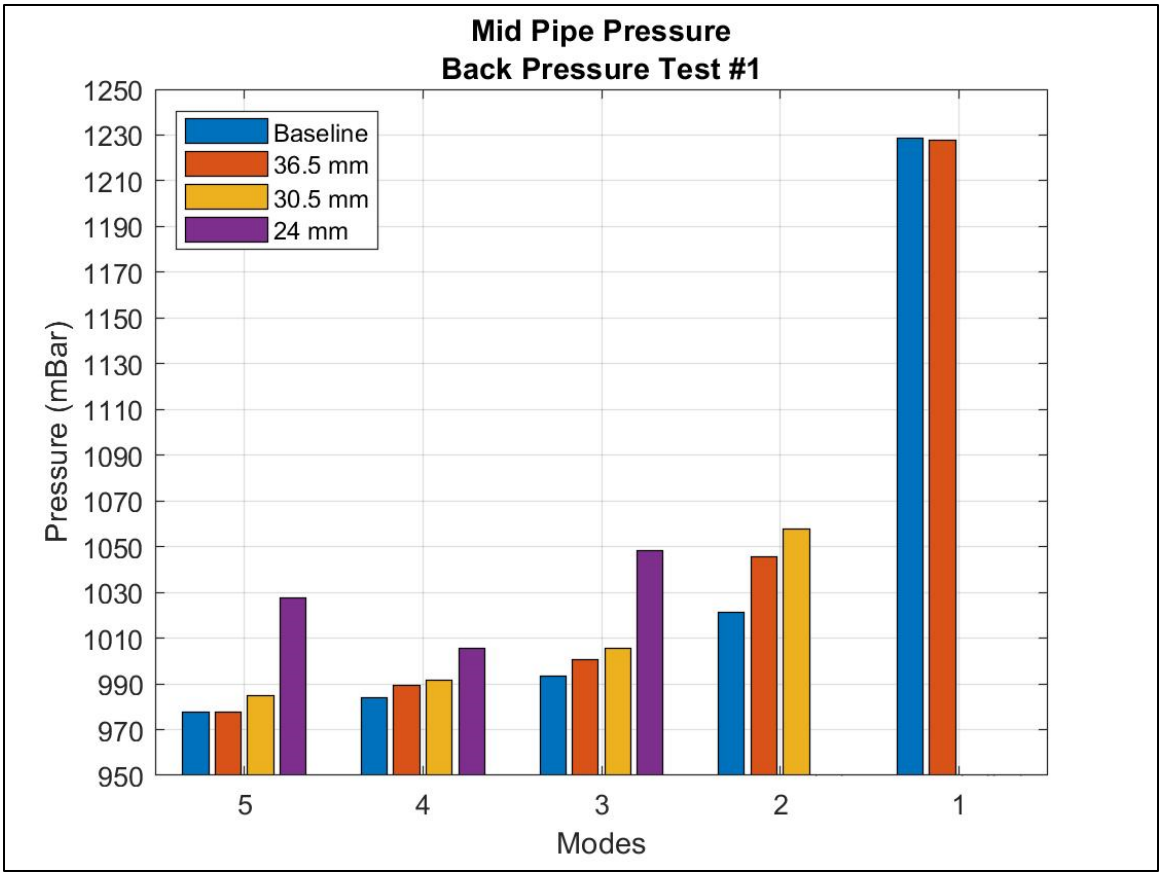

Figure 6.6 - Mid-pipe Pressure - Back Pressure Test #1

The mid-pipe pressure observed a steady increase as restriction diameter decreased with a very significant increase occurring with the 24 mm restriction installed. At this time in the project, it was learned that increases in mid-pipe pressure on the order of 20 $mBar$ are considered significant. This corelates nicely with the observations of back pressure test #1, as mid-pipe pressure increases of greater than 20 $mBar$ were associated with erratic engine behavior around attempted EV transitions.

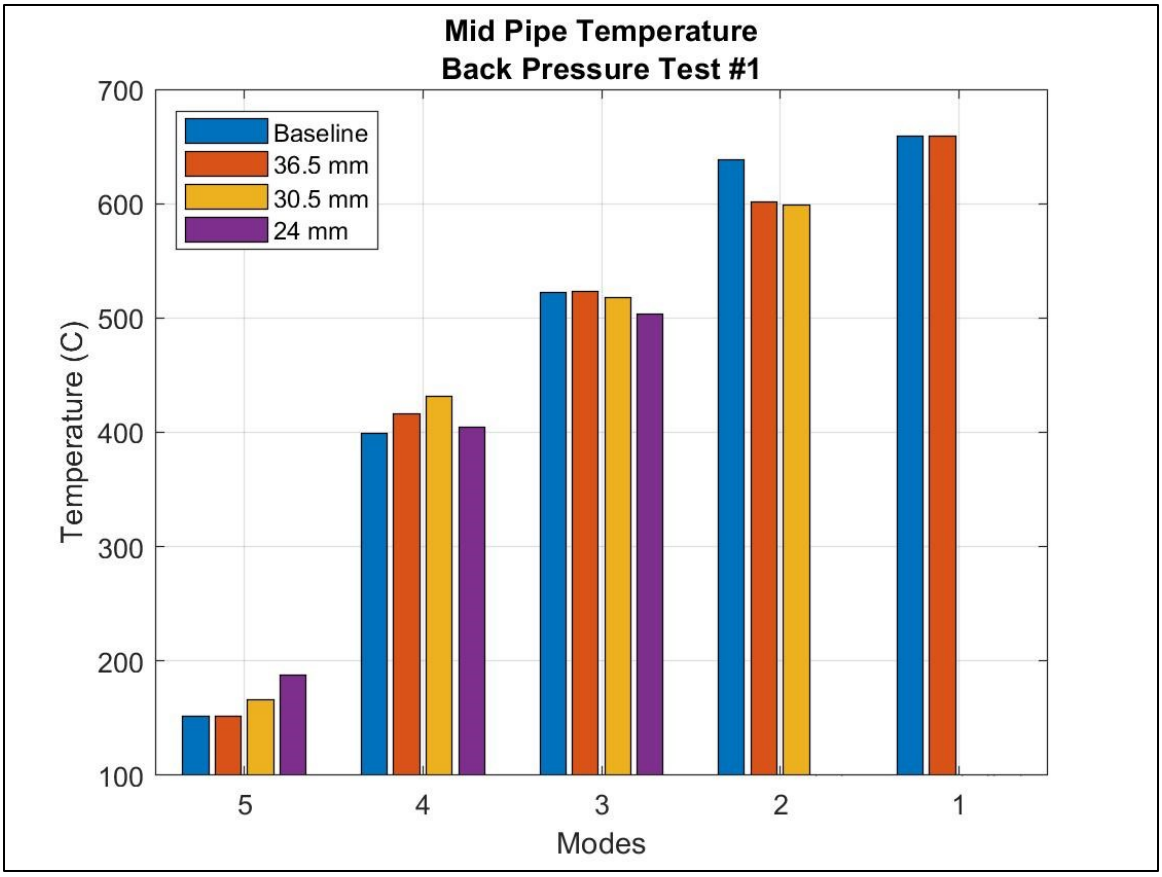

Figure 6.7 – Mid-pipe Temperatures - Back Pressure Test #1

In general exhaust gas temperatures throughout the exhaust system decreased as restriction diameter decreased. This general trend is captured in the mid-pipe temperature data shown in Figure 6.7.This is most likely due to the decrease in lambda and the cooling effect caused by increased unburned HC concentrations in the exhaust.

Further investigation of engine performance around EV transition points was conducted by sweeping engine speed at WOT from 5000 RPM up through the EV mid to open transition at 7300 RPM with the 30.5 mm restriction plate installed. The results of engine speed and torque vs EV position are plotted below in Figure 6.8. Please note EV closed is represented by a sensor voltage of 2.8 volts, mid at 2 volts, and open at 1.2 volts.

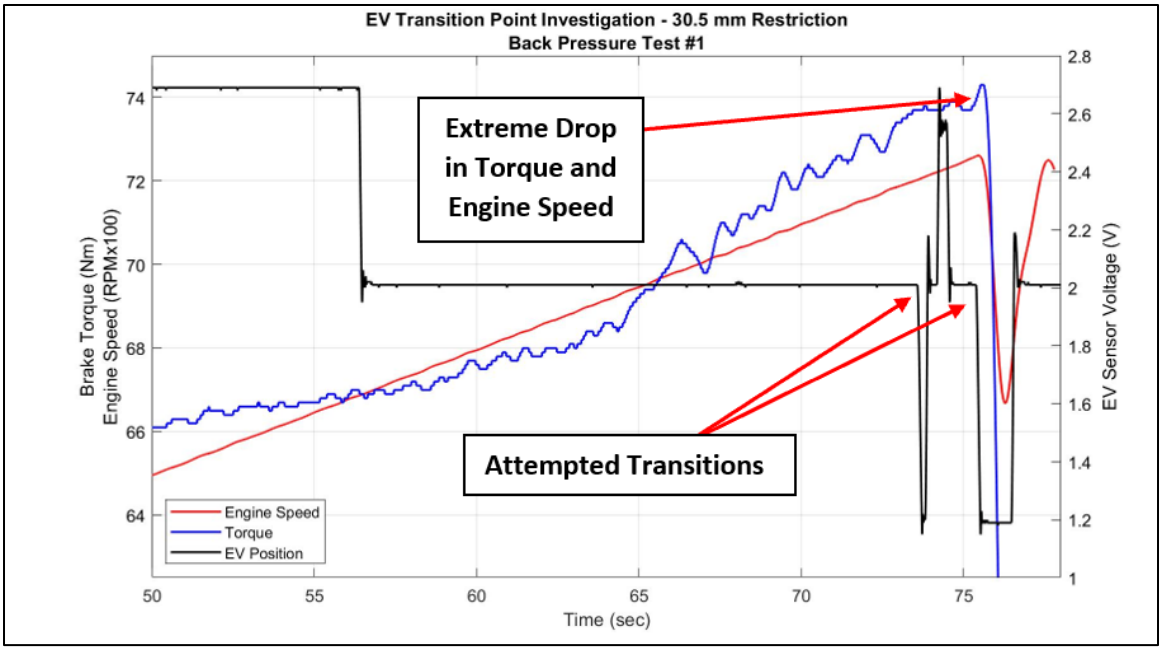

Figure 6.8 - Further Investigation of EV Transition Point

In Figure 6.8 at approximately 73 seconds the EV makes a transition from mid to open position. Immediately it returns to mid then all the way closed, this is followed by another attempt to hold the open position at approximately 76 seconds, which causes the extreme drop in torque noted during testing.

This additional testing, as well as a review of mid-pipe gas dynamics, concluded elevating the pressure within the mid-pipe had several effects. The most notable of which is slowing the speed of sound within the pipe. Slowing the speed of sound has two main effects on the mid-pipe performance; wave timing is altered relative to port timing and the mass flow rate of exhaust particles is altered, negatively impacting scavenging efficiency. Recall that mid-pipe tuned length is dependent not only upon geometry of the mid-pipe but also pressure and temperature of the exhaust gasses, both of which changed due to the added restriction. Also, in the study of gas dynamics it is understood that expansion waves move faster whereas compression waves move slower as the pressure of the medium through which they travel increases[5]. In the mid-pipe this translates to a stronger positive pressure wave inducing faster flow of exhaust gasses out of the cylinder during blowdown and a weaker negative pressure wave resulting in slower flow of fuel and air particles back into the cylinder prior to the exhaust port closing. The misalignment of pressure waves and port timing due to changes in the effective tuned length of the pipe and changes in wave strength could both easily lead to more fuel rich lambda readings. Without more sophisticated measurement equipment, it is difficult to

[5] *Design and Simulation of Two Stroke Engines* by Gordon Blair was extremely helpful in understanding these concepts.

determine which effect is dominant and to what degree the engine performance is affected by each potential change to the gas dynamics. It is possible that with mid-pipe design alterations as well as EV calibration changes the engine could have minimal performance losses with a catalyst located in the stinger. However, this is beyond the scope of this project.

6.2.2 Back Pressure Test #2

A second back pressure test was conducted using the knowledge gained from back pressure test #1. Based on the first test and better understanding of the stingers role in maintaining mid-pipe pressure it was speculated that if the catalyst was located after the stinger and remained less restrictive than the stinger mid-pipe operation and ultimately engine performance would be minimally affected. Furthermore, the location of the catalyst was not so critical if it was located after the stinger in the flow path. To validate this hypothesis back pressure test #2 involved placing the restriction in between the stinger outlet and muffler. To achieve this larger diameter restriction plates were manufactured to be integrated into the larger $55\ mm$ tube diameter used in the muffler inlet. To use the same flange mounting system lengths of tube were installed on either side of the restriction, between the stinger outlet and muffler inlet. The length of this additional assembly was simply selected to resemble the length of one of the perforated tubing sections in the muffler. This assembly was mounted between the mid-pipe and muffler using springs and the stock exhaust doughnut used to seal the stinger to the muffler. The completed assembly installed in the exhaust system can be seen below in Figure 6.9. This is followed by Table 6.4 which outlines the restriction diameters and restricted area values.

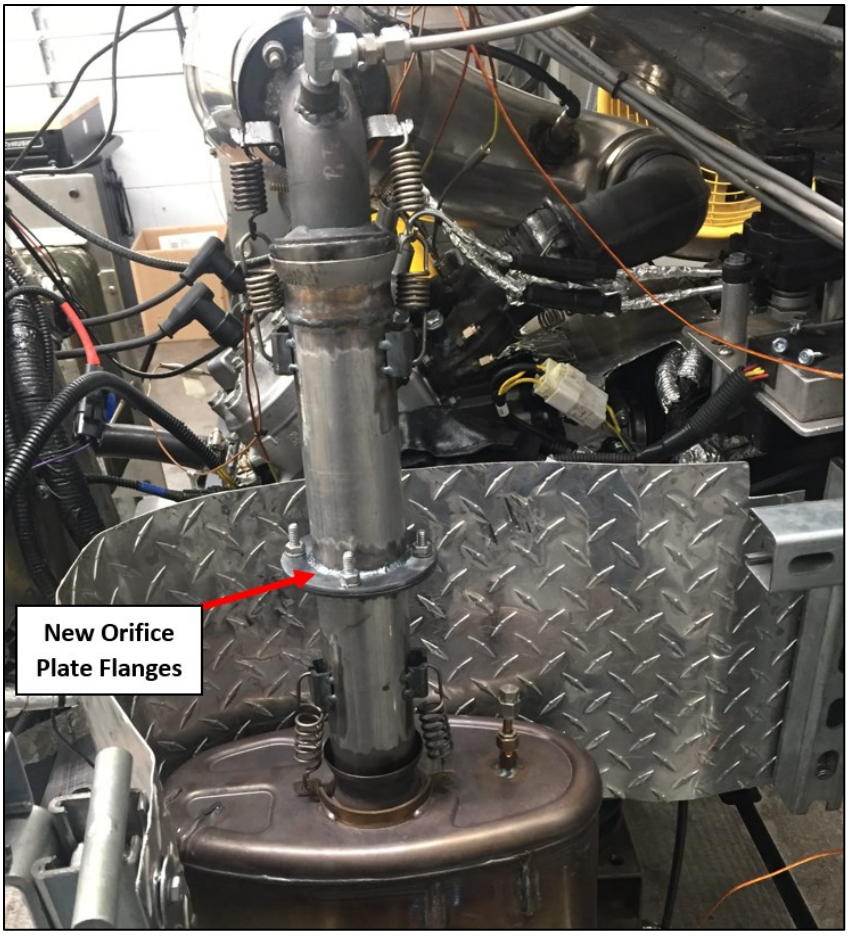

Figure 6.9 - Restriction Assembly - Back Pressure Test #2

Table 6.4 – Orifice Plate Restriction Data - Back Pressure Test #2

Orifice Diameter	Restricted Area of Tube
51 *mm*	14.0 %
50 *mm*	17.4 %
44 *mm*	36.0 %
37 *mm*	54.7 %
31 *mm*	68.2 %

It should also be noted that there were no pressure and temperature taps installed in this restriction assembly. Based on the first test, mid-pipe pressure, mid-pipe temperature, and global lambda were sufficient to investigate any significant effects on performance.

Back pressure test #2 was conducted in the same manner as back pressure test #1, using the discrete 5 mode format and starting with the least restrictive plate and moving to the most restrictive. All but the 31 mm restriction plate were able to complete the 5 mode test. With the 31 mm restriction installed a significant drop in torque was again observed at the EV transition point. Similar bar charts to back pressure test #1 are shown below in Figure 6.10 through Figure 6.12 showing test #2's results.

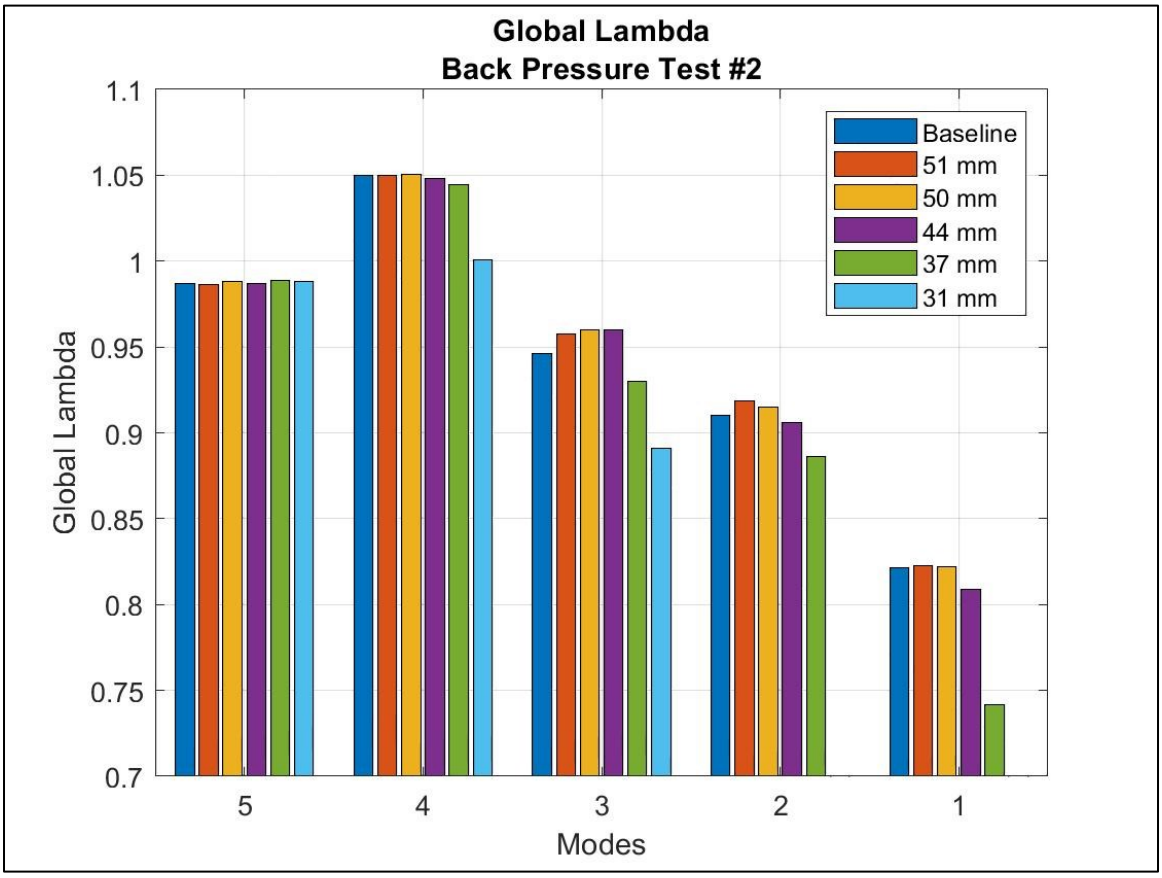

Figure 6.10 – Global Lambda Values - Back Pressure Test #2

Figure 6.10 shows that global lambda values were stable when the restriction diameter was greater than the stinger diameter. When restriction diameter becomes less than the stinger diameter significant drops in global lambda occur at modes 1 through 4. The 44 mm restriction did lower global lambda values in modes 1 and 2 but the drop was relatively low compared to the 37 mm and 31 mm restrictions effects.

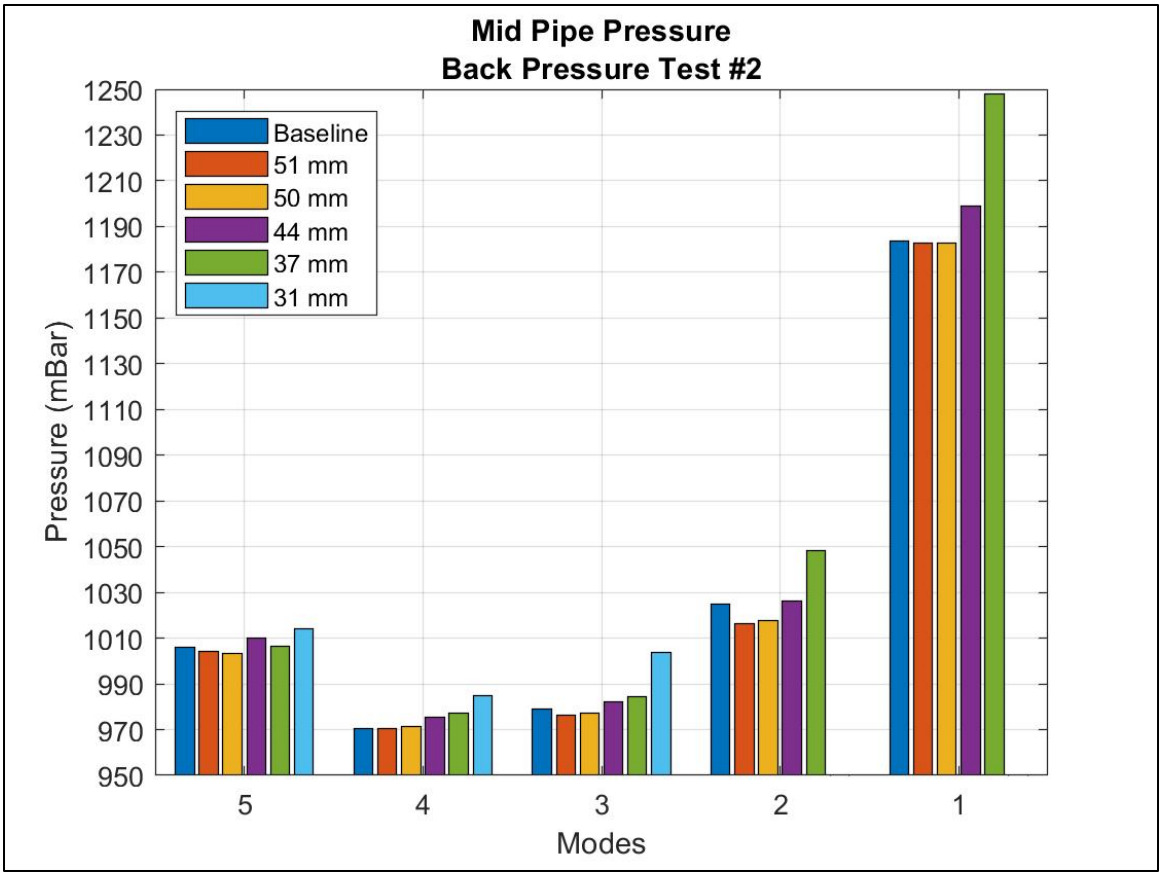

Figure 6.11 - Mid-pipe Pressure Values - Back Pressure Test #2

Figure 6.11 tells a similar story to the lambda measurements, where mid-pipe pressure increased most notably when restriction diameter became less than the stinger diameter. This is especially apparent at mode 1 where mid-pipe pressure is at its highest.

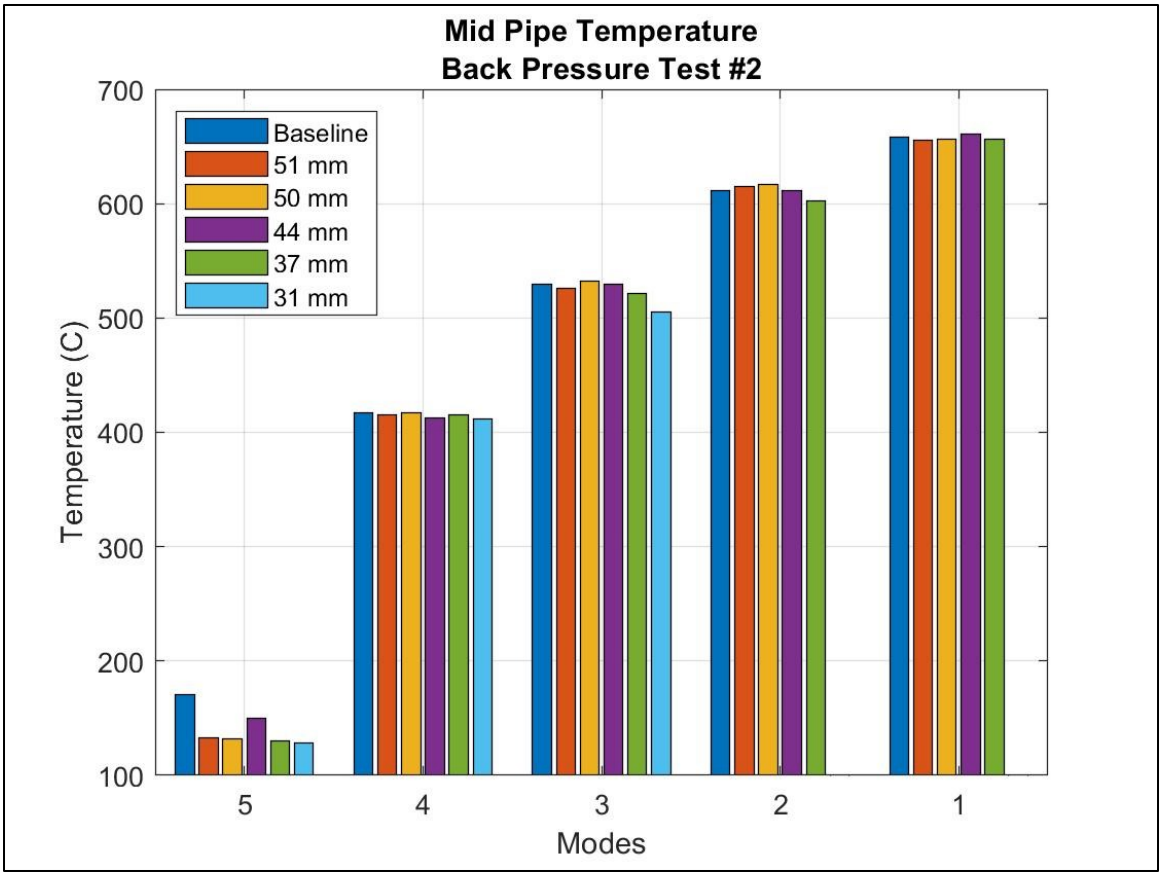

Figure 6.12 – Mid-pipe Temperature Values - Back Pressure Test #2

Finally, in Figure 6.12, the affect to mid-pipe temperature was minimal until the 37 mm and 31 mm restrictions were installed. Just like the effect on global lambda, these two smallest restrictions caused a significant drop in mid-pipe temperature from mode 3 up to mode 1.

As the plots show, global lambda, mid-pipe pressure, and mid-pipe temperature for the first two restriction plates are very consistent with the baseline results. With the 44 mm restriction results started to deviate around mode 3 and up to mode 1. A significant increase in pipe pressure occurred in modes 1 and 2 with the 37 mm plate, but the engine was still able to overcome this 64 $mBar$ increase in pressure and complete the 5 mode test. The most restrictive plate elevated pipe pressure beyond what the engine could handle, leading to the same dramatic drop in torque when EV position attempted to change when entering mode 2.

These results are consistent with the hypothesis previously stated in that engine operation is minimally affected until any restriction after the stinger becomes more restrictive than the stinger itself. In this case the 37 mm restriction started to impact performance with only a 1 mm smaller inside diameter than the 38 mm stinger and a 7 mm smaller diameter was too much to overcome. The results of back pressure test #2 are significant

for two reasons; first the location of the catalyst is narrowed to being after the stinger, and second the open frontal area of the substrate is now constrained to be no less than the stinger cross sectional area. Meeting these two criteria will ensure that the addition of a catalyst will have minimal impact on engine performance.

6.2.3 Finalizing Catalyst Location

Knowing that the catalyst must come after the stinger leaves 3 location options including; between the stinger and muffler, inside the muffler, or after the muffler outlet. It was decided that locating the catalyst between the stinger and muffler or after the muffler outlet would make packaging in the chassis difficult. This is especially a concern with the muffler outlet because the Code of Federal Regulations requires the sample port be a minimum of 12 inches or 10 pipe diameters upstream of the outlet, whichever is greater. [18] To locate a catalyst after the muffler would then require a significant length of tube follow the catalyst to ensure quality sampling results. Finally, temperature was taken into consideration. Locating a catalyst between the stinger and muffler would expose the catalyst to the highest inlet temperatures, making achieving sufficient thermal durability more difficult. Conversely, the muffler outlet location may experience too low of exhaust temperatures at some operating points, making catalyst activation a concern. With all these considerations in mind, packaging the catalyst within the muffler was the most favorable location.

The 600 DSI utilizes an absorption type muffler, including 3 sections of perforated tubing surrounded by a fiberglass packing material. To begin integrating a catalyst with the stock 600 DSI muffler an old muffler was cut apart to inspect the interior and select a mounting location. The muffler with its outer shell and fiberglass packing removed is shown below in Figure 6.13. The exhaust flow path has been added to the figure.

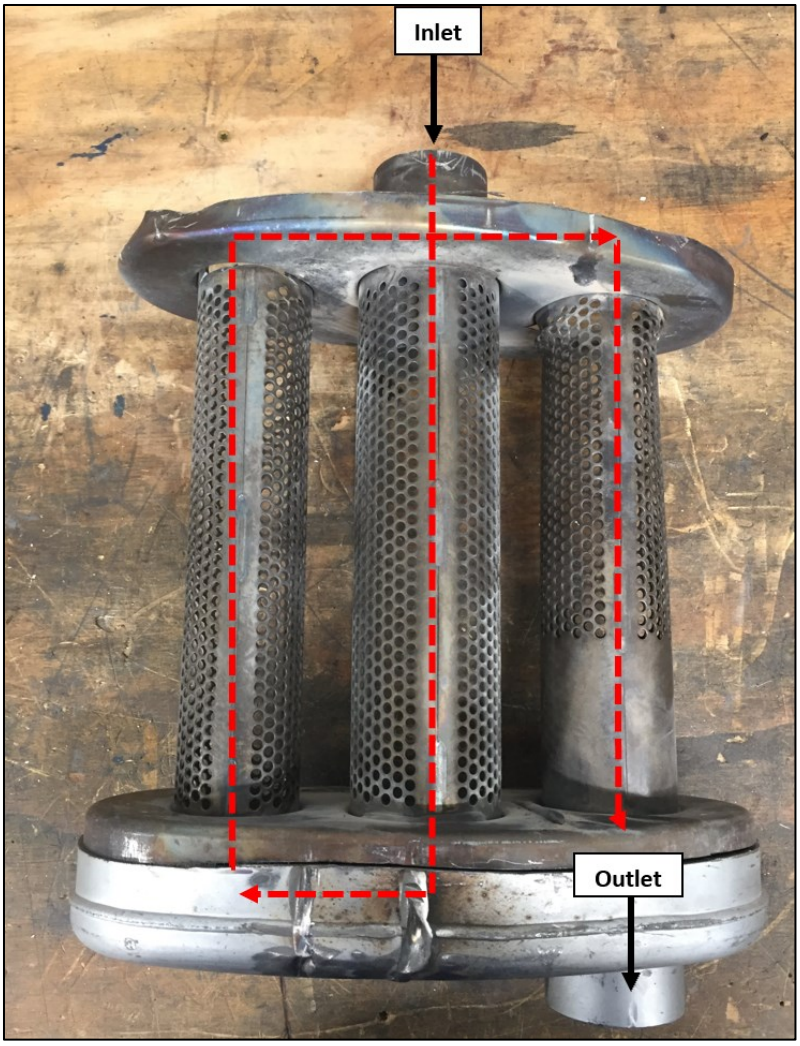

Figure 6.13 - Disassembled 600 DSI Muffler

With the internals of the muffler accessible it was determined that the left most section of perforated tube in Figure 6.13 would be a favorable location to integrate the catalyst. This location met the emissions sampling port location requirements without the need to add tube length to the muffler outlet and would experience slightly cooler exhaust gas temperatures than the center perforated tube section. Knowing the location of the catalyst now allowed a space claim to be defined, constraining the maximum diameter and length of the catalyst and its mounting systems to be roughly 80 mm and 240 mm respectively.

6.2.4 Uncoated Catalysts

With baseline data collected, catalyst location defined, and constraints on open frontal area, diameter, and length established, suppliers were contacted for catalyst samples. Samples with non-active coatings were requested to keep the cost low while testing a large group of samples. Non-active coatings refers to a wash-coat containing no PM

materials, so no catalytic reaction will take place. It was determined that having samples coated with a wash coat was important to get an accurate cell wall thickness, seeing as the wash-coat adds a non-negligible thickness to the substrate wall thickness. Although sample availability was somewhat limited, 8 samples were acquired, 5 from Heraeus and 3 from CCC. These substrate samples with stainless steel mantles are shown below in Figure 6.14.

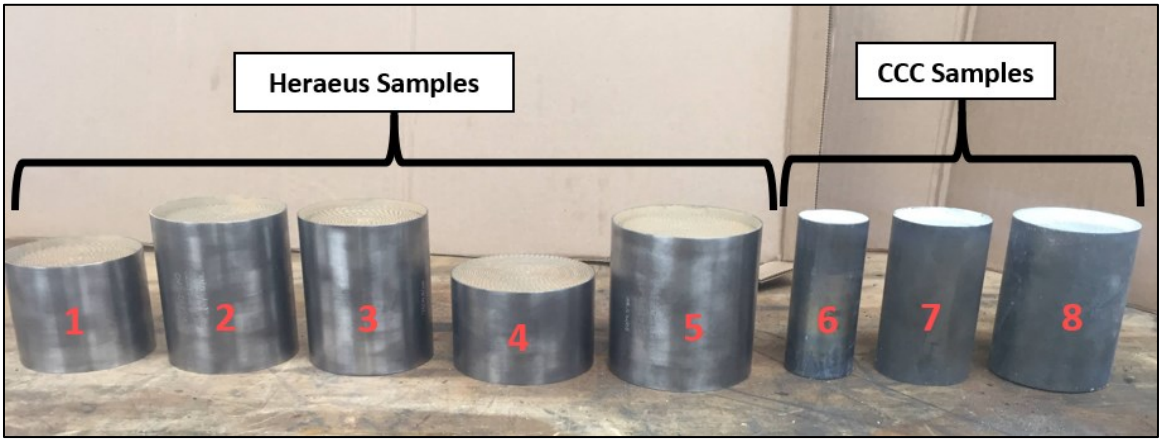

Figure 6.14 – Uncoated Mantle Samples

The open frontal area was calculated using Equation 6.1 through Equation 6.4 so that it could be compared to the cross sectional area of the stinger. Equation 6.1 is simply the cross sectional area of the catalyst, this is used with Equation 6.2 to determine the number of cells within the catalyst. Figure 6.15 was created to help visualize how Equation 6.3 was derived. In this simple example a 1 in^2 portion of the substrate is considered and has a CPSI (N) of 16. To find the dimensions of an individual cell within the area being analyzed the square root of the CPSI is taken, which equates to 4 in this example. Next the open length along one side of the cell matrix must be computed. There is $\sqrt{N+1}$ walls of a known thickness (T) on any given side of the matrix. Therefore, by subtracting the product of the number of walls and the wall thickness from the overall side length $(1\ in)$ the open length on each side of the matrix is computed. This is then divided by the dimension of the cell matrix (4) to obtain the open cell width (L). Finally, using Equation 6.4, the cell width is squared to calculate the cross sectional area of one cell and multiplied by the number of cells in the catalyst. The Matlab code used for this calculation is located in Appendix 9.5.

$$A_P = \left(\frac{\pi}{4}\right)^2 * D_P^2 \quad 6.1$$

$$n_{cells} = A_P * N \quad 6.2$$

$$L = \frac{\left(1 - \sqrt{N+1} * T\right)}{\sqrt{N}} \quad 6.3$$

$$A_{Open} = n_{cells} * L^2 \quad 6.4$$

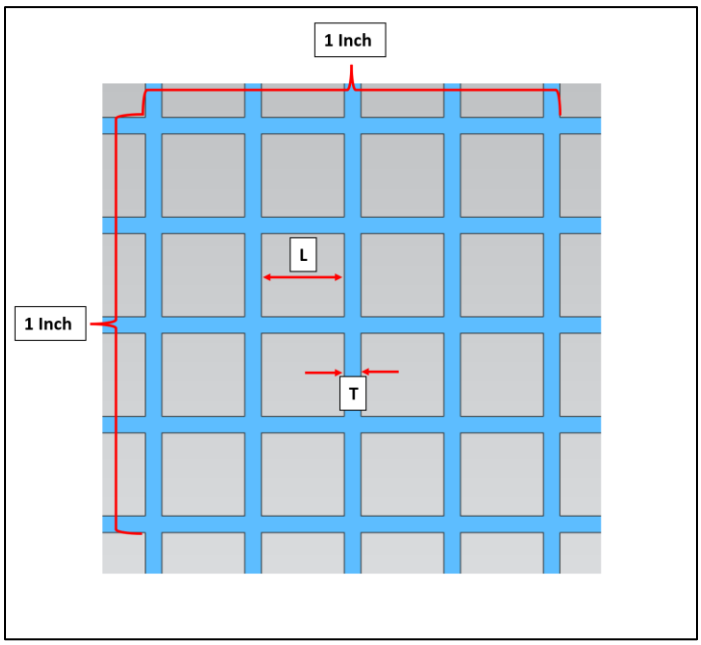

Figure 6.15 - Cell Width Calculation Graphic

Table 6.5 below outlines the physical part dimensions for all the samples as well as relevant stinger dimensions. Please note the naming convention column as this is how the samples will be referred to throughout the remainder of the document.

Table 6.5 - Uncoated Sample Dimensions

Sample Number	Naming Convention	Supplier	Diameter[6] $[mm]$	Length[7] $[mm]$	Cell Density $[CPSI]$	Open Frontal Area[8] $[mm^2]$
stinger	stinger	NA	38	NA	NA	1134
1	H-70x50-300	Heraeus	70	50	300	3734
2	H-74.5x50-200	Heraeus	70	74.5	200	3755
3	70x74.5-300	Heraeus	70	74.5	300	3734
4	H-80x50-300	Heraeus	80	50	300	4877
5	H-80x74.5-300	Heraeus	80	74.5	300	4877
6	CCC-36-75-150	CCC	36	75	150	996
7	CCC-48-75-200	CCC	48	75	200	1765
8	CCC-60-75-200	CCC	60	75	200	2758

Because this was a research based project, samples were selected so that a wide range of geometries could be tested. The H-70x50-300 and H-70x74.5-300, as well as the H-80x50-300 and H-80x74.5-300 samples vary only in length. Where the H-74.5x50-200 and H-70x74.5-300 samples vary in cell density. Finally, the H-70x74.5-300 and H-80x74.5-300, as well as the CCC-48-75-200 and CCC-60-75-200 samples vary in diameter. This offers the ability to observe any effects due to each major defining feature of the substrate geometry individually. Additionally, the CCC-36-75-150 sample was selected because its open frontal area is slightly less than the stingers cross sectional area. Which offers another data point to validate that the stinger must remain the most restrictive point in the exhaust system.

[6] Diameter of the substrate itself, excluding mantle
[7] Length of the substrate itself, excluding the mantle
[8] Open Frontal Area approximated using a bare wall thickness of 0.022 mm

6.2.5 Back Pressure Test #3

Back pressure test #3 focused on narrowing the substrate geometry to a few substrate samples to have actively coated. This was completed by testing all eight samples, installed in the proposed catalyst location, using the same test format as the previous back pressure tests. To expedite the testing process and ensure repeatable results the muffler was modified to allow the catalysts to be swapped out between tests. Inlet and outlet cones were designed for each sample using a 25° taper. Small sections of tube matching the diameter of the perforated tube that was removed were welded onto the cones along with v-band style flanges. To ensure each sample fit into the design space a welding fixture was manufactured to control the flange to flange spacing. All welding was completed using a back purge of pure Argon gas to avoid granulation on the back side of the welded surfaces. The welding fixture, back purge setup, and completed samples can be seen below in Figure 6.16 through Figure 6.18.

Figure 6.16 - Welding Fixture

Figure 6.17 - Back Purge Setup

Figure 6.18 - Welded Samples

Upon completion of the catalyst samples the stock 600 DSI muffler was modified to accept the catalysts. This involved removing the section of perforated tubing where the catalysts would be mounted and installing a set of v-band flanges for mounting the catalyst samples. A section of the muffler shell was removed to enable catalysts to be changed between test relatively easily. The section was sealed with a high temperature graphite based exhaust gasket and a sheet metal plate which was riveted in place. It should also be noted the stock fiberglass blanket material was reinstalled around the remaining perforated tubes when reassembling the muffler. Lastly, the muffler was fitted with bungs to measure both inlet and outlet pressure, temperature, and emissions in the top and bottom chambers of the muffler immediately before and after the catalyst. Several pictures of this reassembly process and the instrumentation can be seen below in Figure 6.19 through Figure *6.22*.

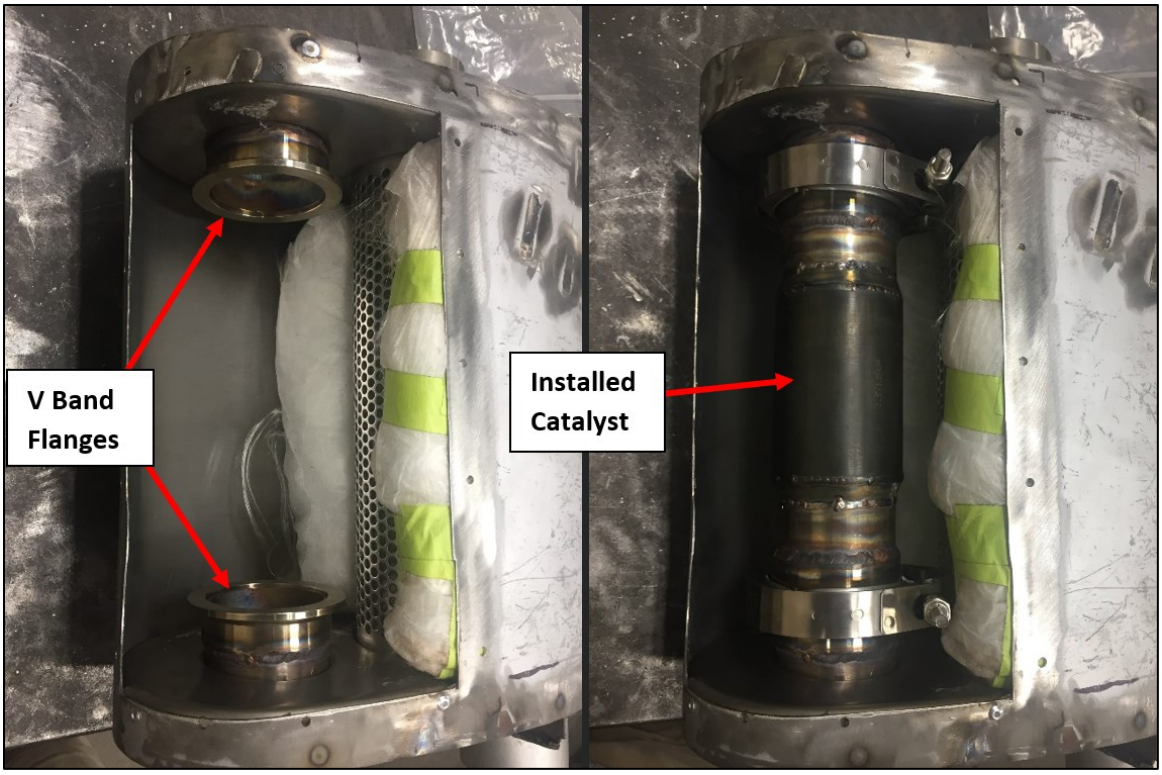

Figure 6.19 – Muffler Flanges and Installed Catalyst Sample

Figure 6.20 – Instrumented and Installed Muffler

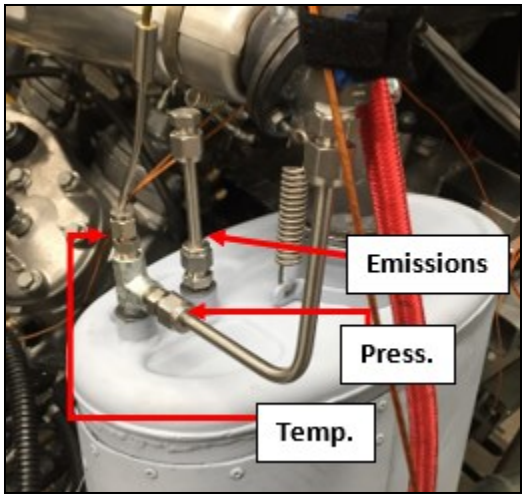

Figure 6.21 – Catalyst Inlet Instrumentation

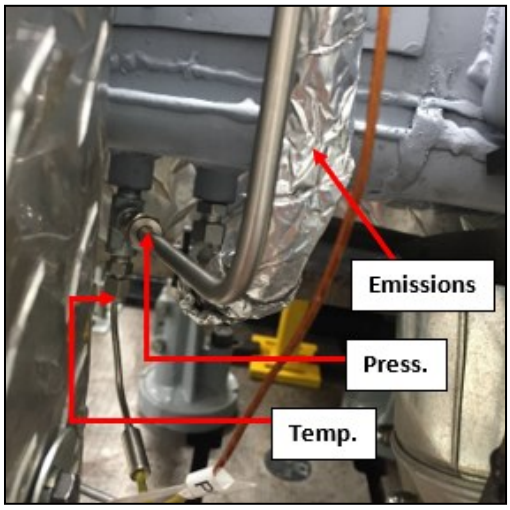

Figure 6.22 *– Catalyst Outlet Instrumentation*

Since back pressure test #3 significantly changed the location of the added restriction associated with the catalyst and modified the muffler it was determined a new baseline 5 mode test should be established to accurately measure effects due to the addition of each catalyst sample. The baseline aimed to simulate no catalyst being installed, but still capture and changes due to the alterations to the muffler. To achieve this a straight section of 58 mm tubing was fitted with v band flanges and installed in the muffler in the same place as the catalyst samples would be tested. A standard 5 mode test was then conducted. All results from back pressure test #3 were then compared to this new baseline.

Back pressure test #3 was conducted in the same manner as tests #1 and #2, using the discrete 5 mode format and starting with the sample that had the highest open frontal area and moving towards the sample with the lowest open frontal area. Key measurements for

this testing to characterize the catalyst performance included the pressure drop and the temperature differential across the catalyst. Catalyst pressure drop was calculated as the inlet pressure minus the outlet pressure, whereas the temperature differential was calculated as the outlet temperature minus the inlet temperature. Additional measurements of interest to understand the effects on engine performance included global lambda, mid-pipe pressure, and mid-pipe temperature. These results are shown and discussed in greater detail below in Figure 6.23 through Figure 6.25.

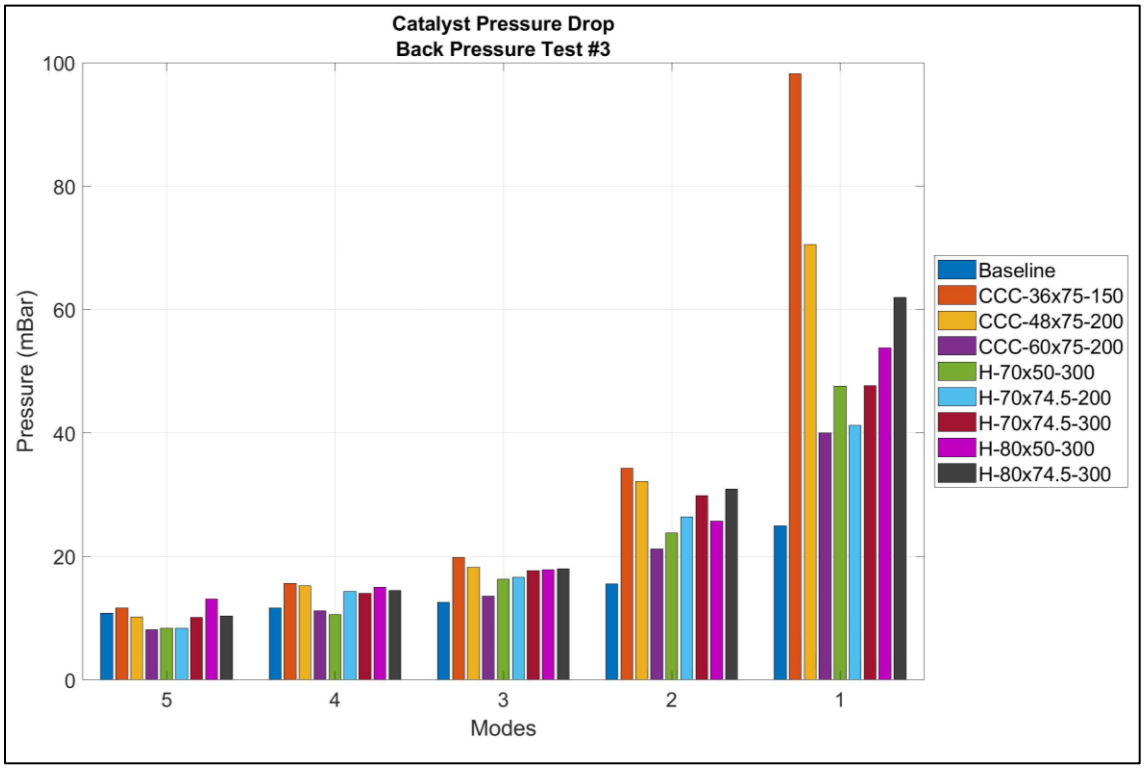

Figure 6.23 - Catalyst Pressure Drop - Back Pressure Test #3

As you can see in Figure 6.23 all samples had significant pressure drops at modes 1 and 2. Looking at mode 1 there are three distinct groups to this data. Group one can be classified as a high pressure drop at greater than $50\ mBar$ and includes the CCC-36-75-150 and CCC-48-75-200 samples. Group two is a moderate pressure drop at greater than $20\ mBar$ and includes the H-80x74.5-300, H-80x50-300, H-70x74.5-300, and H-70x50-300 samples. Finally, group three can be classified as a low pressure drop at less than $20\ mBar$ and includes H-74.5x50-200 and $60x75 - 200$ samples. It is somewhat surprising that the samples with the largest open frontal area are not the lowest in pressure drop. Potentially the flow distribution was not good on the larger diameter samples. This would likely cause higher than expected pressure drops as seen in the $80\ mm$ diameter samples. The $70\ mm$ diameter samples behaved closer to initial expectations, where the highest open frontal area sample had the lowest pressure drop. It appears that cell density has a large effect on pressure drop because the H-74.5x50-200 sample has a much lower pressure drop than the H-70x74.5-300 sample. The three CCC

samples followed this same behavior, where the highest open frontal area sample offered the lowest pressure drop. It should be noted that the 36-75-150 sample provided yet another validation point that once catalyst open frontal area is less than the stinger cross section significant back pressure will be added to the exhaust system. If the poor flow distribution hypothesis is entertained the pressure drop results begin make more sense. The $80\ mm$ samples offer the largest diameter change between the exhaust tubing and catalyst diameter making flow distribution concerns valid. Poor flow distribution equates to only a portion of the substate is being utilized by the exhaust gas flow, effectively rendering the catalyst to have a smaller volume and lower open frontal area. When transitioning to the $70\ mm$ diameter parts the flow distribution likely improves because less of a diameter transition between exhaust tubing and catalyst diameter is required causing lower pressure drops. Furthermore, the decreased cell density of the H-74.5x50-200 sample further decreased the pressure drop because of the increased open frontal area and larger hydraulic diameter of the cells. Like the $70\ mm$ samples the CCC-60-75-200 sample offers a very small diameter transition, meaning flow distribution is likely good. However, once the catalyst diameter becomes significantly less than the exhaust tubing diameter pressure drops increase rapidly as observed in the CCC-48-75-200 and CCC-36-75-150 samples. This is to be expected because the catalyst is now more restrictive than the inlet and outlet exhaust tubing.

To summarize, assuming flow distribution in the large open frontal area samples was poor, good flow distribution is critical to low pressure drops, cell density and diameter have significant impacts on pressure drop, and if the catalyst diameter is less than the exhaust tubing diameter pressure drop will increase significantly. Recall that these conclusions are consistent with the literature review material surrounding catalyst pressure contributions and how catalyst geometry is related to back pressure.

Figure 6.24 shows the temperature differential across each sample. The temperature difference across the catalyst is where results started to become interesting and unexpected.

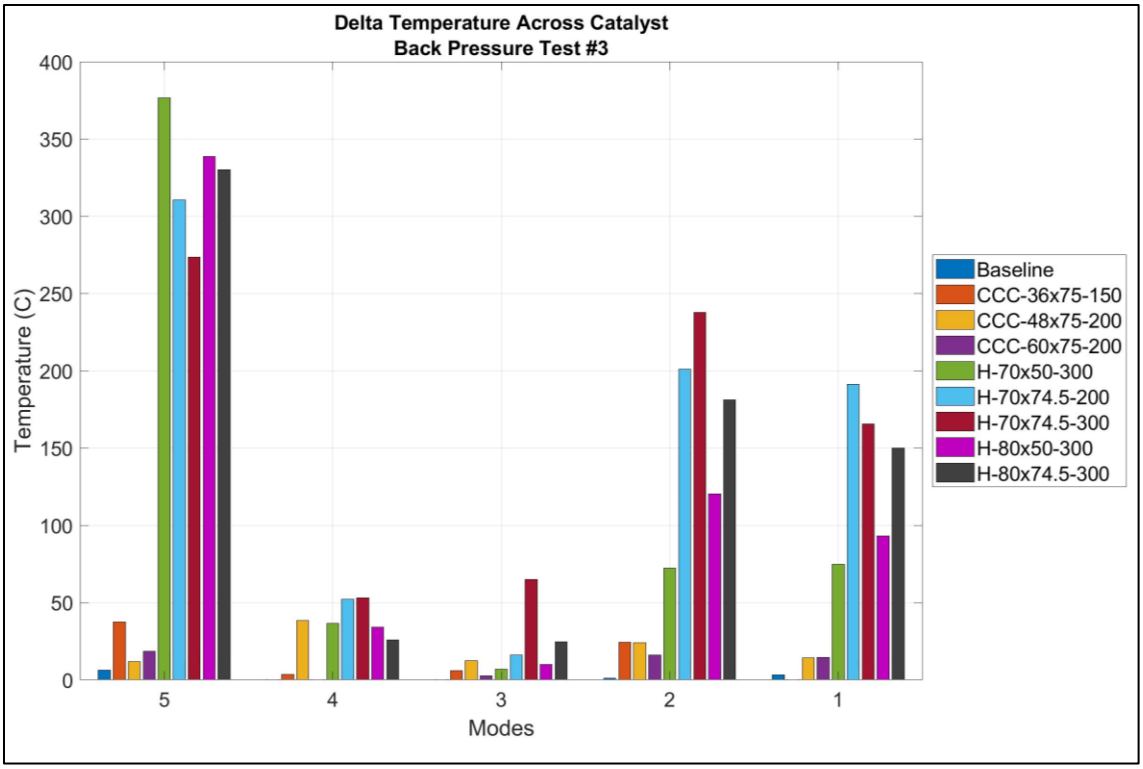

Figure 6.24 - Delta Temperature Across Catalyst - Back Pressure Test #3

As you can see in Figure 6.24 the Heraeus samples exhibited an extreme temperature difference from inlet to outlet at modes 5, 2, and 1. Because the samples tested in back pressure test #3 were non-actively coated it was expected that the temperature difference across the catalyst would be minimal. The reason for this extreme temperature difference was determined to be related to the oxygen storage characteristics of the high ceria content wash coat paired with the thermal mass of the catalyst retaining heat energy and causing exhaust constituents to be oxidized through a non-catalytic reaction. The investigation process and conclusions are covered in greater detail in section 6.2.6 following back pressure test #3 results.

Key engine performance indicators were also reviewed as a part of back pressure test #3. These again included mid-pipe pressure, mid-pipe temperature, and global lambda. Results are shown below in Figure 6.25 through Figure 6.27Figure 6.26 respectively.

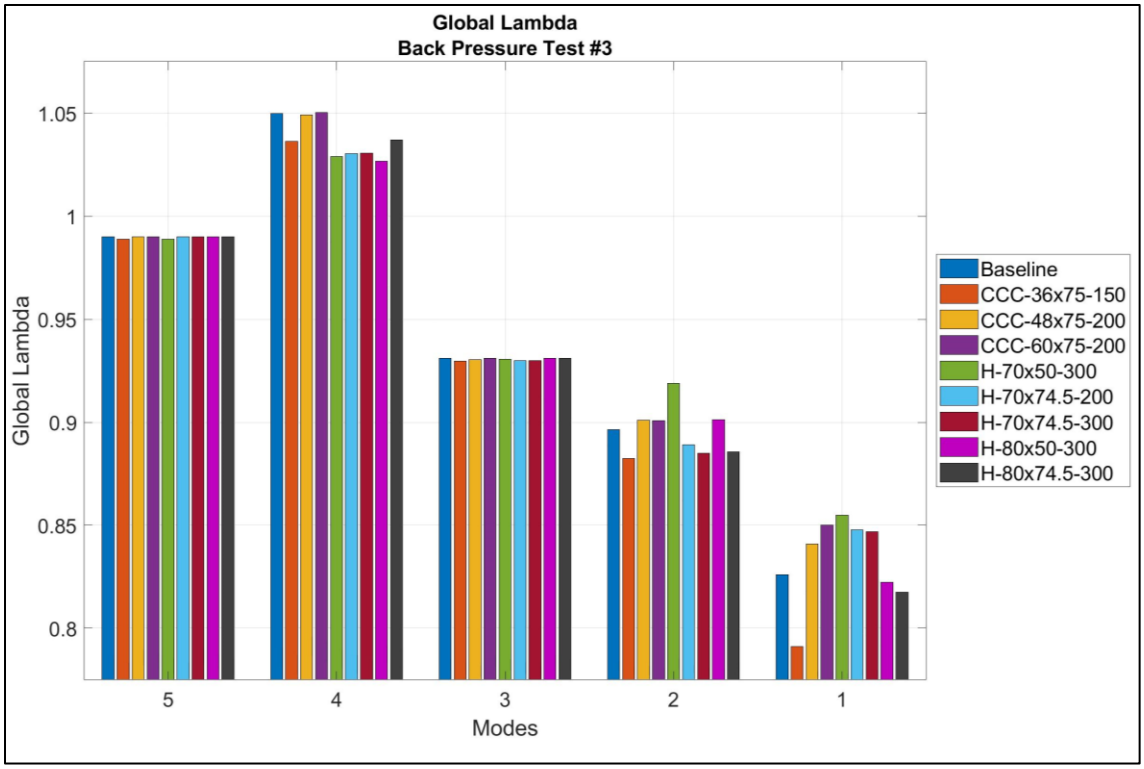

Figure 6.25 – Global Lambda - Back Pressure Test #3

Figure 6.25 shows similar global lambda trends to those observed in previous back pressure tests, in that as restriction increases lambda begins to decrease. This is especially apparent at mode 1 for the CCC-36-75-150, H-80x50-300, and H-80x74.5-300 samples. Why the global lambda increased above the baseline test results at modes 1 and 2 and tended to decrease below the baseline at mode 3 is not apparent. It is possible that torque stability at these modes could have an impact. Modes 5 and 3 are very stable operating points relative to holding the torque target, whereas in the remaining 3 modes torque oscillates slightly around the target. This is only one possible reason for the differences observed in global lambda measurements compared to the baseline data.

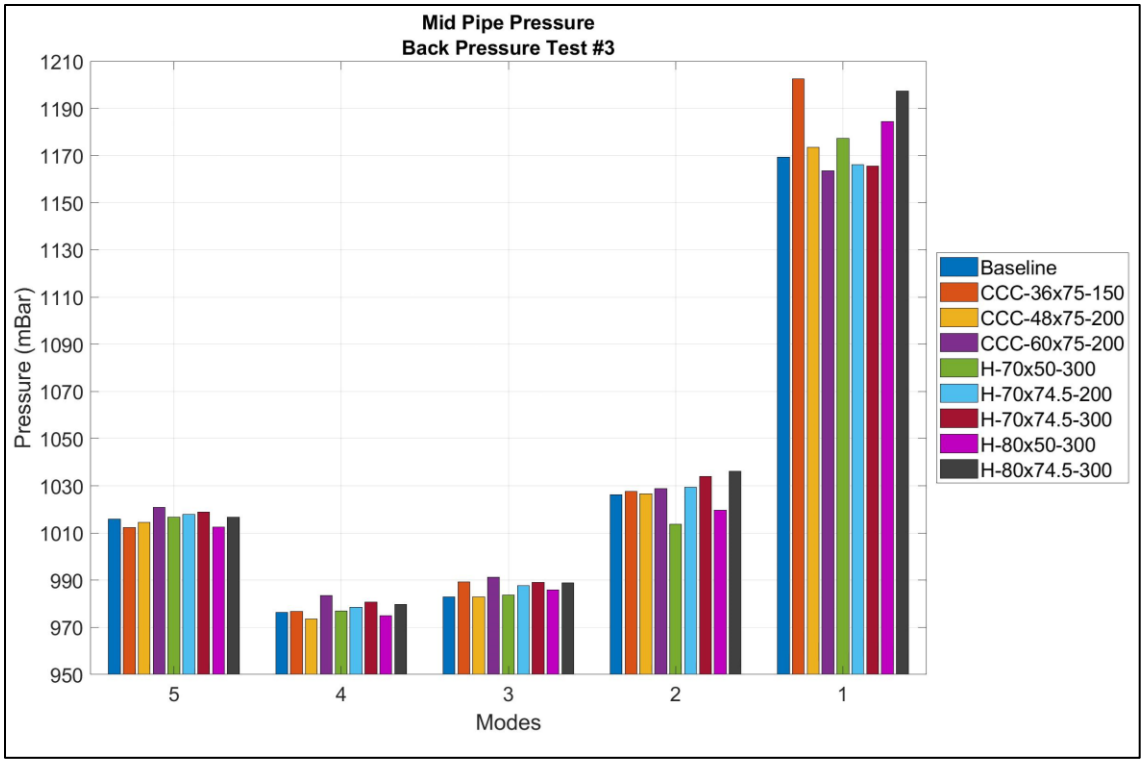

Figure 6.26 - Mid-pipe Pressure - Back Pressure Test #3

The key features in Figure 6.26 are mainly found in mode 1 where several samples caused significant increase in mid-pipe pressure. The CCC-36-75-150 and H-80x74.5-300 samples caused an increase of greater than 20 $mBar$ in pipe pressure which would be considered significant enough to affect the gas dynamics within the mid-pipe.

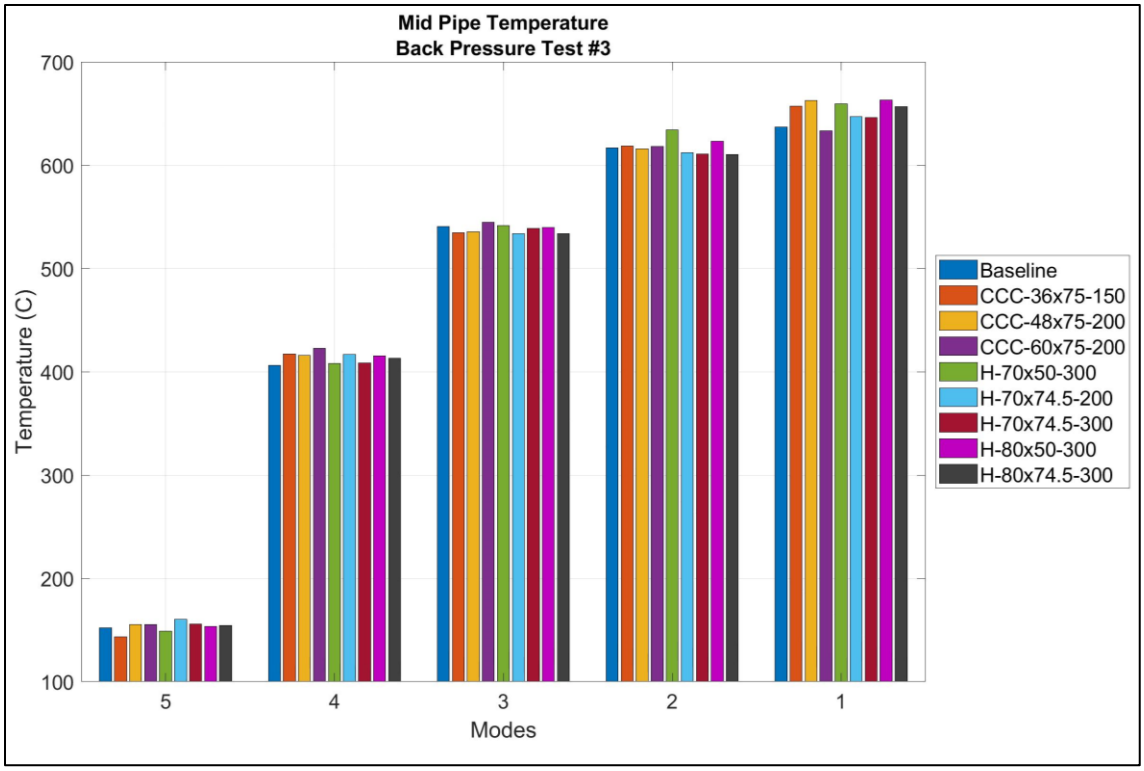

Figure 6.27 - Mid-pipe Temperature - Back Pressure Test #3

Figure 6.27 shows that mid-pipe temperature was constant, within 25℃, for all tests and did not show any outstanding trends.

6.2.6 Reaction Phenomenon Investigation

As previously mentioned, a very interesting and unexpected phenomenon occurs with the Heraeus catalyst samples. The temperature differential across the catalyst was much higher than anticipated. When testing, upon initial startup no significant temperature differential exists, and warmup behavior is normal. Moving into mode 4 normal behavior and temperature differentials across the catalyst continue. Yet when the outlet temperature reaches approximately 375℃ outlet temperatures begin to climb at a faster rate than inlet temperatures, eventually surpassing the inlet temperature. Outlet temperature eventually plateaus at a relatively stable temperature well above the inlet temperature. The temperature at which this plateau occurs is dependent upon the engine operating point. This behavior is similar to normal catalyst operation once the activation temperature is reached. However, activation temperatures are often on the order of 500 to 600 ℃ not 375 ℃. Yet upon returning from this elevated outlet temperature state back to mode 5 an even more interesting behavior is observed. Catalyst inlet temperatures fall gradually, like other exhaust temperature measurements as the thermal energy in each mass is transferred out to the surroundings. However, the outlet temperature, initially dips, but almost immediately rises again and approaches another plateau anywhere from

500℃ to 600℃ and will sustain this temperature for an extended period of time. During testing the longest duration exceeded 8 minutes and showed no signs of the outlet temperature falling back to normal levels. Finally, when exiting this abnormal mode 5 state into mode 4 outlet temperatures spike quickly to anywhere from 700℃ to 800℃ and then drop just as quickly and approach the temperature of the catalyst inlet similar to the state observed when entering mode 4 after initial warmup. This behavior was repeatable between all samples and on various testing dates.

To further investigate the behavior being observed emissions data was collected pre and post catalyst for two samples, one from each supplier. Testing was conducted using H-80x50-300 and CCC-48-75-200 samples from Heraeus and CCC respectively. It should be noted that the emissions bench utilized for testing can only sample one stream at a time. So, to gather pre and post catalyst measurements, two separate 5 modes tests were performed for each sample. Since these results were collected as part of an investigation the possible engine operating point variation between tests was not of concern. Finally, the Heraeus sample used in this investigation was not initially tested at mode 1 due to concerns in exceeding safe outlet temperatures and potentially damaging the substrate. The results of this emissions test are shown below in Figure 6.28 through Figure 6.31.

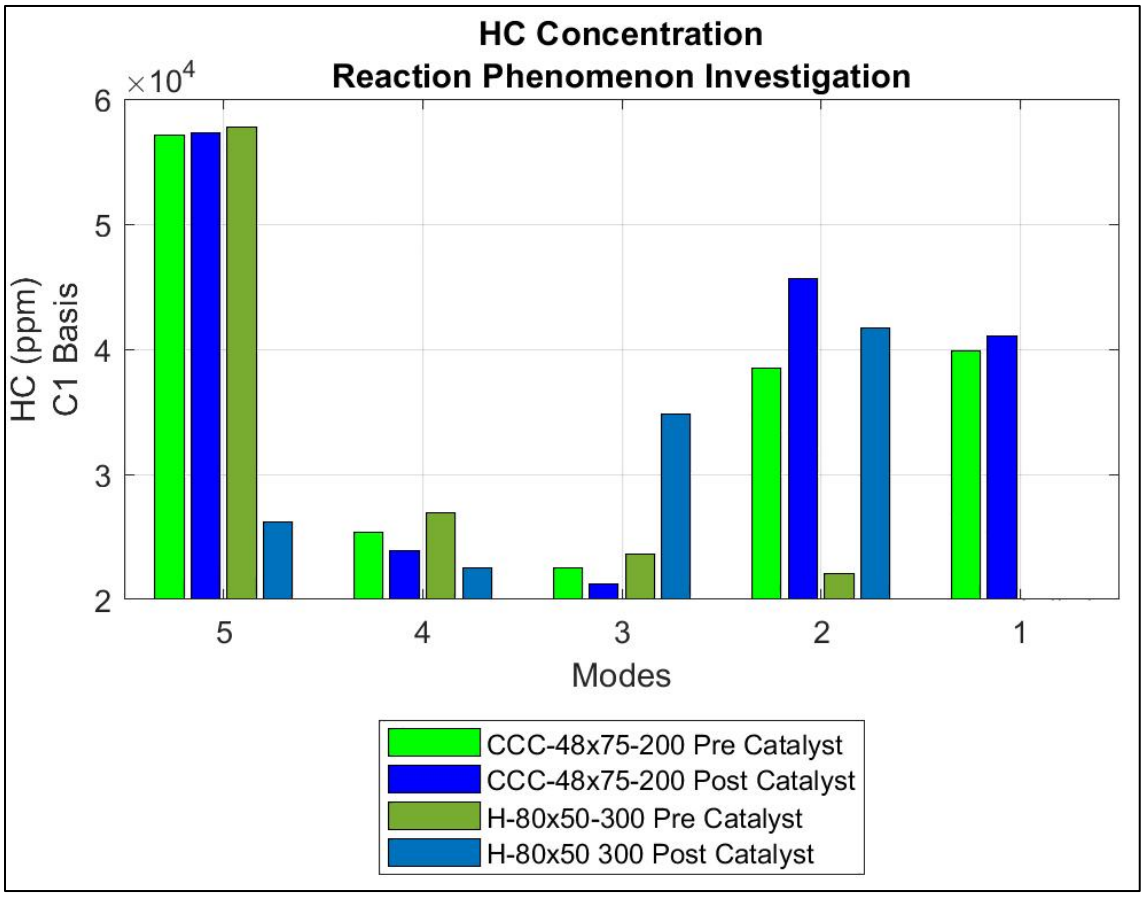

Figure 6.28 - HC Concentration - Reaction Phenomenon Investigation

The Heraeus sample shows a very significant reduction in HC at mode 5, on the order of $95{,}000\ ppm$. Recall that the AVL SESAM's FID saturates at approximately $57{,}000\ ppm$, but historical data from Arctic Cat shows HC concentrations of approximately $120{,}000\ ppm$. Overall, the CCC sample exhibited a much more typical behavior of a catalyst with no precious metals in the wash-coat. It should be noted that the increase in HC concentrations observed at modes 1 and 2 for the CCC sample is linked to the decrease in global lambda previously observed in back pressure test #3.

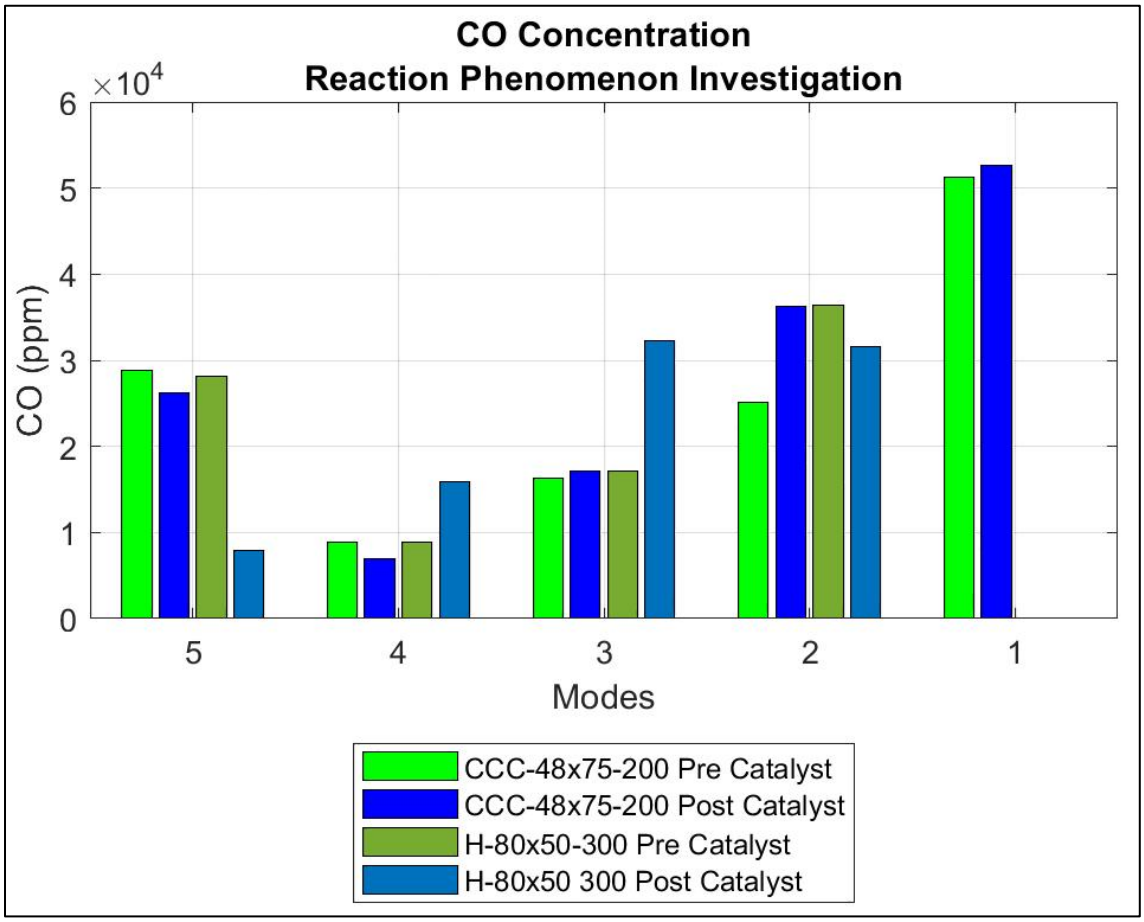

Figure 6.29 - CO Concentration - Reaction Phenomenon Investigation

CO concentrations also show abnormal behavior of the Heraeus sample at modes 3 through 5. A significant reduction in CO of nearly $20{,}000\ ppm$ occurs at mode 5, where modes 3 and 4 show increases of $5{,}000\ ppm$ and $10{,}000\ ppm$ respectively. Again, the CCC sample exhibits a more normal behavior in terms of its effect on CO concentrations.

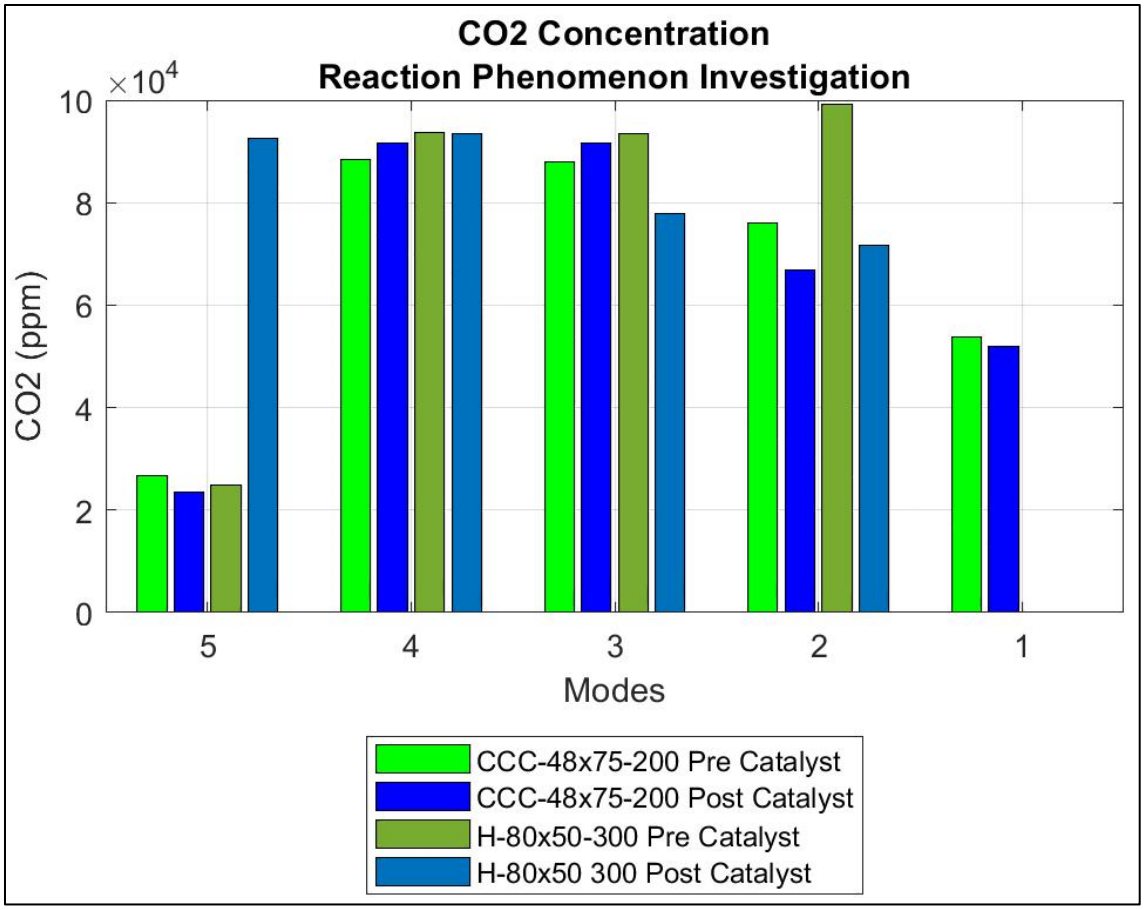

Figure 6.30 - CO2 Concentration - Reaction Phenomenon Investigation

Looking at CO2 concentrations again we see a massive increase at mode 5 of nearly $70{,}000\ ppm$ paired with a $15{,}000\ ppm$ and $30{,}000\ ppm$ decrease in CO2 at modes 3 and 2 respectively. The CCC sample is again exhibited a more normal behavior in terms of its effect on CO2 concentrations.

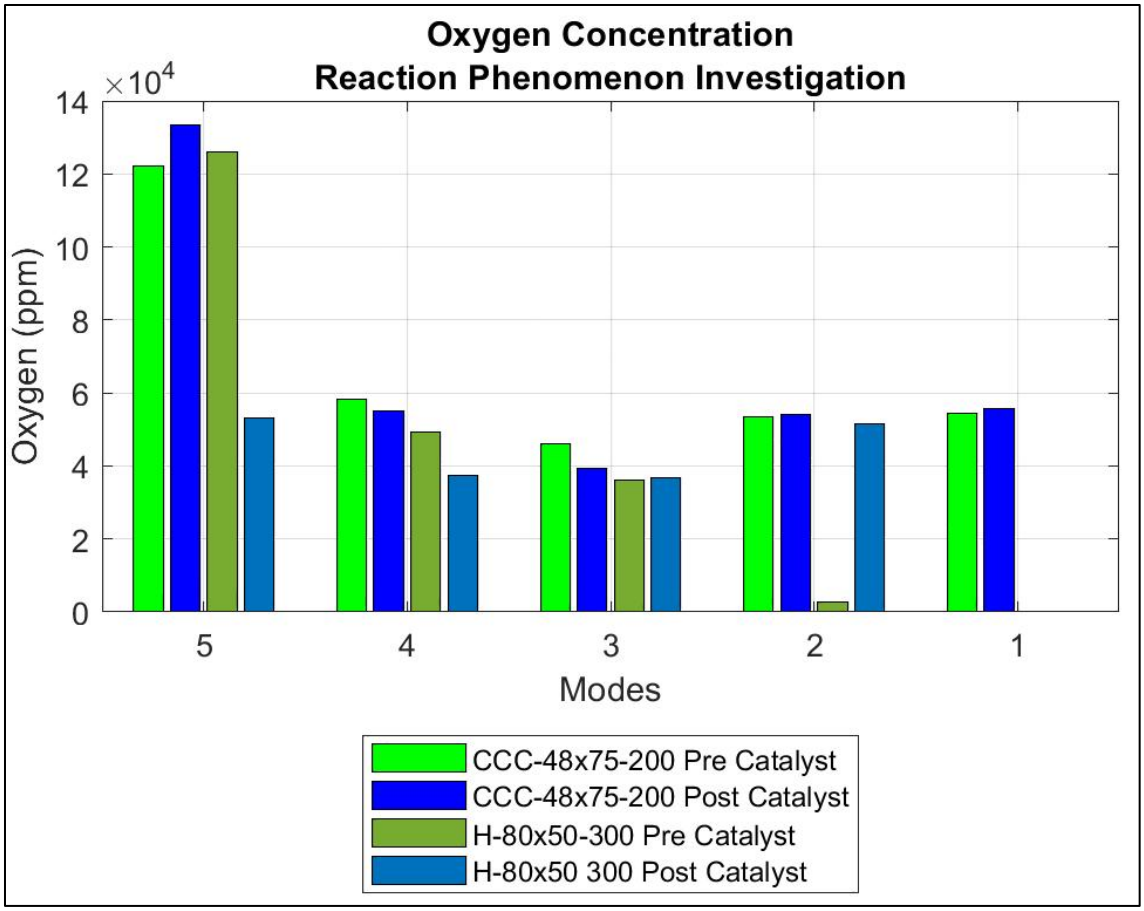

Figure 6.31 - Oxygen Concentration - Reaction Phenomenon Investigation

Oxygen concentrations show a reduction at mode 5 of approximately $75{,}000\ ppm$ with the Heraeus sample. The Heraeus sample only observed small changes in O2 concentration at the remaining modes. The CCC sample O2 concentrations were consistent across the test as expected. Another thing to observe is that the mode 2 pre-catalyst data for the H-80x50-300 sample is an outlier, likely because two separatee 5 mode tests were collected, one for pre-catalyst and the other for post-catalyst measurements. Additionally, mode 2 is the least stable in terms of maintaining torque and could cause varying emissions results. Despite this outlier, the significant changes observed in mode 5 are enough to conclude that some sort of reaction is occurring due to the addition of the Heraeus samples. In general, this reaction is causing major reductions in HC, CO, and oxygen as well as an increase in CO2 at mode 5. This supports the increased outlet temperatures being observed at this mode during testing.

To capture and better understand this phenomenon a typical start of day test sequence was performed. This includes a warmup period, heat soak at mode 4, control point, and start of a 5 mode test working from mode 5 up to mode 4 and so on. Both dyno and emissions data were sampled continuously throughout this test so that results could be directly compared. The tests sequence is laid out below in Table 6.6.

Table 6.6 – Typical Start Up Test Sequence

Mode	Engine Speed (RPM)	Torque (Nm)	Approx. Duration (seconds)
Warmup	1750	0.0	180
Mode 4	5360	16.5	120
Control	6300	35.5	240
Mode 5	1750	0.0	180
Mode 4	5360	16.5	180

The results of this test sequence are shown below in Figure 6.32. This figure shows relevant dyno data on the top plot and emissions data on the bottom plot. These subplots are separated by a test timeline showing the approximate duration of each operating point. Several colored ovals are added to aid in discussion of the results following the figure. It should be noted that the engine had been run prior to this test, so entering the warmup period the outlet temperature of the catalyst slightly exceeded that of the catalyst inlet due to the thermal mass of the catalyst retaining additional heat from the previous testing. This is not a normal observation during initial engine warmup but does not have significant impact on the results presented for this test.

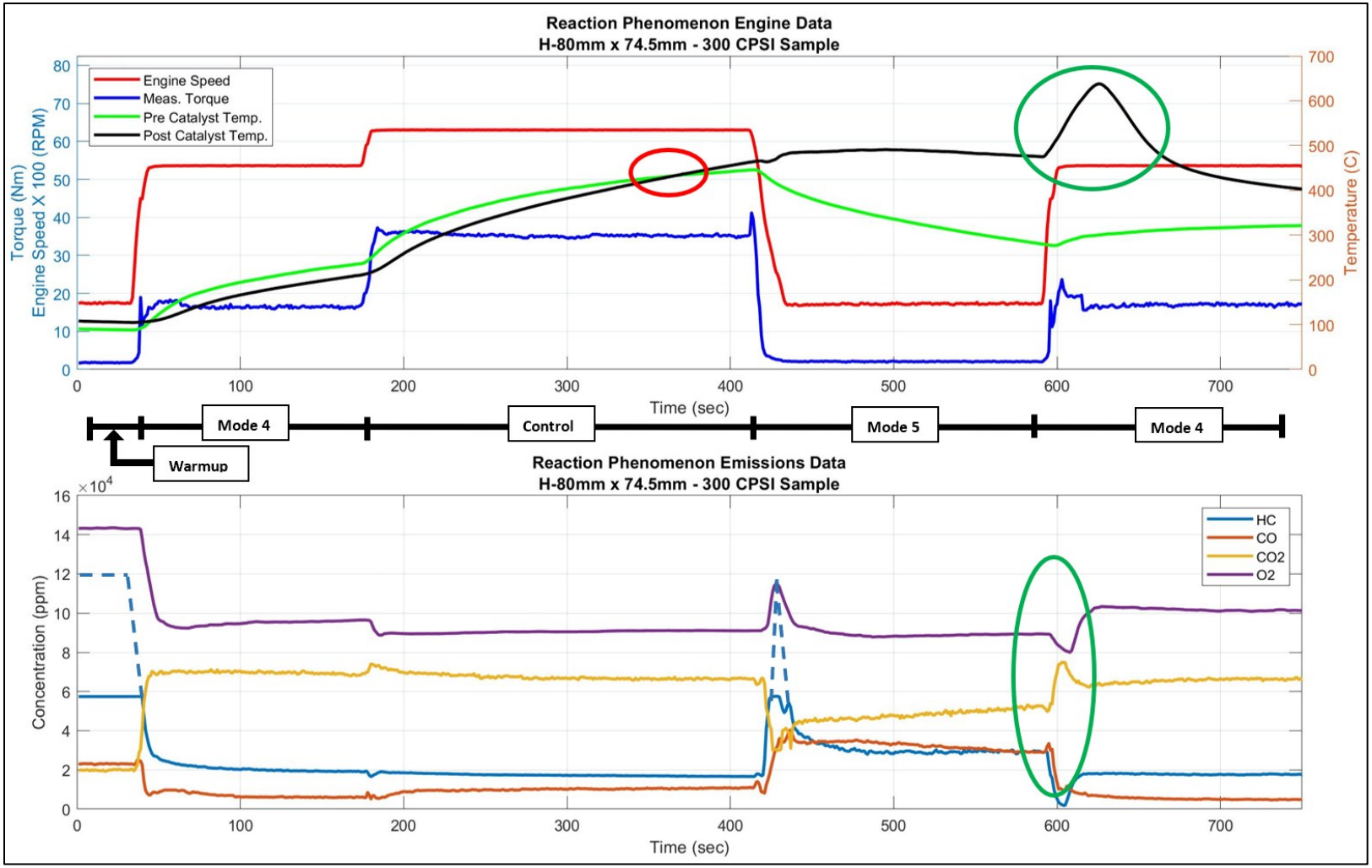

Figure 6.32 – Typical Start of Day Test Results

There are three main observations to be made from Figure 6.32. The first of which is that catalyst temperatures and emissions concentrations change dramatically between the warmup and mode 5 phases of the test despite the engine operating point being the same. Starting with the temperatures, the outlet temperature tracks closely with the inlet temperature in the warmup phase, however at the mode 5 phase the outlet temperature is approximately 200 ℃ higher than the inlet by the end of that portion of the test despite the engine operating point being the same. It can also be observed that the outlet temperature is plateaued at this temperature of approximately 475 ℃ whereas the inlet temperature exhibits normal cooling behavior for a significant thermal mass. Looking at the emissions levels, warmup shows high concentrations of HC and oxygen with moderate levels of CO and CO2. Keep in mind that the FID measurement is saturated at warmup. The engine is actually producing approximately $120{,}000\ ppm$ of HC at idle as shown by the dashed blue lines. Distinct changes occur in all constituents in the mode 5 phase while the catalyst outlet temperature is at an elevated state. HC and O2 concentrations have dropped by approximately $90{,}000$ and $55{,}000\ ppm$ respectively. CO and CO2 show increases of approximately $5{,}000$ and $23{,}000\ ppm$ respectively by the end of the mode 5 phase. This all indicates that an exothermic reaction is occurring in which HC and O2 are being consumed and to a lesser degree CO2 and CO formation is occurring.

The second key observation is that the temperature differential across the catalyst reverses during the control point portion of the test. Throughout the first mode 4 operating point the outlet temperature maintains a temperature of approximately 30 ℃ less than the inlet. This temperature differential makes sense for catalyst samples with a non-active wash-coat. However, as indicated by the red circle on Figure 6.32, at a temperature of approximately 430 ℃ the outlet temperature surpasses that of the inlet, reversing the temperature differential. Based on my observations, this is indicative of the reaction phenomenon starting and from this point onward returning to idle will exhibit the abnormal elevated catalyst temperature state previously discussed. This indicates that there is a specific state of the catalyst, most likely linked primarily to temperature, that initiates the reactive state being observed.

The final key observation occurs when transitioning from idle at the elevated catalyst outlet temperature state into mode 4. Upon initial entrance into mode 4 a spike in outlet temperature is observed as well as distinct changes in emissions concentrations. This region of Figure 6.32 is detailed by the green ovals. It is suspected that the increased exhaust flow is the primary difference causing this abrupt change in the data. When in mode 5 exhaust gas flow is very low and when at the elevated outlet temperature state there is a large amount of heat within the substrate. Transitioning to mode 4 increases exhaust flow, causing two distinct changes. One is the heat within the catalyst is pushed out of the outlet accounting for some of the temperature spike and the second is that HC

and O2 rich exhaust gas is moved past the reacting catalyst at an increased rate. The increased flow rate of exhaust gasses across the reacting catalyst likely increases the reaction rate temporarily. This can be observed by the drop in HC and O2 as well as the increase in CO and CO2 aligned with the outlet temperature spike observed upon entry into mode 4. This presumed increase in the reaction rate would account for a portion of the temperature spike and the associated changes in emissions concentrations. It should also be observed that after these initial transient events in temperature and exhaust concentration relatively stable concentration levels are achieved and outlet temperature is steadily approaching inlet temperature. The HC, O2, and CO2 concentrations of the second mode 4 phase were within 5% of the first mode 4 phase results and CO is within 18% by the end of the test. It is presumed that if the final mode 4 phase test duration were increased to allow the outlet temperature to reach steady state these concentrations would align with the first mode 4 phase results. This indicates that mode 4 will cause this reaction phenomenon being observed at idle to stop. This is expected to be due to the increased exhaust gas flow rate, lower HC and O2 concentrations, and a catalyst inlet temperature below the previously mentioned transition point at approximately 430 ℃.

Based on observations made during the testing of the Heraeus samples a trend was noted that appears to be linked to surface area of the catalyst substrate. As surface area increased the steady state outlet temperature in the elevated outlet temperature state was increased. To a lesser degree the peak temperature of any spikes as well as the rate at which temperatures changed during such transients were also increased as surface area increased. After observing this trend, the surface areas of each of the 8 samples were compared. The resulting estimated surface areas are tabulated below in Table 6.7. Please note this does not consider the microstructure surface area, but instead treats each wall surface of the substrate as a flat plane.

Table 6.7 - Catalyst Sample Surface Area Comparison

Catalyst Sample	Approx. Surface Area (mm^2)	Percent Increase in Surface Area[9] (%)
CCC-36-75-150	145.7	0.0
CCC-48-75-200	298.6	105.0
CCC-60-75-200	466.5	220.2
H-70x50-300	517.0	254.9
H-74.5x50-200	630.7	332.9
H-80x50-300	675.3	363.5
H-70x74.5-300	770.3	428.8
H-80x74.5-300	1006.1	590.6

Table 6.7 shows that there is a significant variation in surface area across the test samples. The CCC samples make up the lower three values of this range and the closest surface areas between the two suppliers are still separated by approximately 35%.

When discussing these results with Heraeus many potential causes of this non-active catalyst reaction phenomenon were discussed. It was concluded that it is most likely related to the high ceria content of the wash coat that Heraeus utilized on the samples tested in back pressure test #3. Ceria is added for its oxygen storage capabilities. This stored oxygen in conjunction with the hot surfaces in the substrate initiate what can be referred to as a hot surface reaction which oxidizes HC. Heraeus has experienced similar reactions in diesel particulate filter projects, however typically occurring at higher temperatures. This hot surface reaction is similar to what is referred to as a base metal catalyst. In general, base metal catalysts incorporate a non-coated substrate made from a material with oxygen storage capabilities. While conversion efficiencies of base metal catalyst are much lower than precious metal catalysts, it does provide a possible explanation to the phenomenon observed in back pressure test #3.

[9] The CCC-36-75-150 sample was used as the reference surface area for all percent increase calculations.

Seeing as any knowledge about what was in the Heraeus wash coat could be advantageous in analyzing the samples performance the wash coat was analyzed at Michigan Tech's Material Science Department. Utilizing an Energy Dispersive Spectroscopy (EDS) type X-Ray Fluorescence (XRF) machine details about the composition of the wash coat were revealed. The XRF gives a bulk analysis, giving the weight percent of each element present in the sample. In summary the test revealed that the wash coat did in fact have high ceria content at approximately 82 weight percent as well as about 12.5 weight percent Zirconia, both of which promote oxygen storage. This supports the hypothesis that oxygen storage is a contributing factor to the reaction phenomenon being observed with the Heraeus samples. The complete results of the XRF measurement on the non-active Heraeus wash coat can be found in Appendix 9.2.

6.2.7 Selecting Samples to be Coated

Through the results of back pressure test #3 and the investigation of the reaction phenomenon observed with the Heraeus samples a total of 4 samples were selected to be coated. The CCC-48-75-200 and CCC-60-75-200 samples from CCC were selected because they offered the lowest pressure drop of the three samples provided by CCC. The H-74.5x50-200 and H-80x50-300 samples were selected to be coated by Heraeus for several reasons. Namely the H-74.5x50-200 offered the lowest pressure drop. However, the surface area of each part was a significant consideration because it was uncertain whether the reaction phenomenon effects on outlet temperature would be compounded by the addition of an active wash-coat. Therefore, these two samples were also selected based on having significantly different surface areas. Ultimately Heraeus did not actively coat the H-74.5x50-200 and H-80x50-300 samples, but instead recommended an H-80x30-100 sample. This change came about due to concerns with how the reaction phenomenon observed with the high ceria content wash coat could have a compounding effect on outlet temperatures once an actively coated sample begins a catalytic reaction. The H-80x30-100 sample also has a very low cell density, equating to a high open frontal area, which will minimize pressure contributions. Due to this late change in substrate geometry, back pressure test #3 was not able to include the H-80x30-100 sample. However, its pressure contributions were evaluated in the conversion efficiency test outlined in Section 6.3.4.

6.3 Coated Catalyst Testing

The final testing phase of the project includes running the actively coated samples each through a 5 mode test and characterizing their performance from conversion efficiency and engine performance impact standpoints. Due to time constraints, as well as the lack of a drive cycle dyno program and proper engine drive cycle test setup, durability testing

was not conducted as a part of this project. The following sections outline how wash-coat formulas were developed with each supplier, catalyst de-greening procedure, and the catalyst samples performance results. The final portion of this section addresses validating the usefulness of the EES conversion efficiency and Hagen Poiseuilli pressure drop models using data collected in back pressure test #3 and conversion efficiency testing.

6.3.1 Wash-coat Development

Catalyst wash-coat development requires significant experience and resources as well as extensive testing. Therefore, the approach for this project was to rely upon each supplier to recommend the best coating formula for this specific application. As previously mentioned the suppliers required some engine, emissions, and durability data to select a wash-coat. The data utilized in the wash-coat formulation process and how each parameter was used in the development process will be covered in this section. With increased experience it is likely supplier knowledge would be less critical and wash-coat formulas could be co-designed by the supplier and an OEM then applied to samples by each supplier.

The main data sets required by CCC and Heraeus included expected inlet temperatures, emissions concentrations, target conversion efficiencies, exhaust flow rate, and durability information. The inlet conditions were defined by inlet temperatures gathered from the baseline established in back pressure test #3 and emissions concentrations from the original engine baseline data. Exhaust flow rate was approximated using fuel flow data collected at each mode and a variation of the AFR equation previously introduced in detail in Equation 5.3. A slight change to this variation is shown again in Equation 6.5.

$$\dot{m}_{Air} = AFR_s * \lambda * \dot{m}_{Fuel} \tag{6.5}$$

Using the sum of the calculated intake air mass flow rate and the measured fuel mass flow rate the exhaust mass flow rate can be determined. The final step is to convert this mass flow into a volume flow rate for use in the GHSV calculation. For this step the exhaust density is approximated as an ideal gas with air properties relative to the mid-pipe temperature of each mode. The data provided to each supplier for use in wash-coat formulation is shown in Table 6.8 below.

Table 6.8 – Wash-coat Formulation Data

Mode	HC Concentration (ppm)	CO Concentration (ppm)	O2 Concentration (ppm)	Inlet Temperature (℃)	Exhaust Flow Rate (kg/s)
5	120000	33142	113929	150	0.0083
4	24027	8167	49058	280	0.0353
3	21046	14152	36699	405	0.0628
2	42795	39261	55690	515	0.1097
1	32560	59521	46617	590	0.2837

Additionally, as previously discussed, an EES simulation built around the combustion reactions shown previously in Equations 5.7 through 5.9 was used to approximate conversion efficiency targets that remained below a safe outlet temperature. A conversion efficiency of 30% was recommended for both HC and CO based on the results of this simulation.

Finally, the required lifespan and necessary thermal durability of the catalyst was considered. In general, it is helpful to know how many engine hours the catalyst is expected to survive. Additionally, it is helpful to break these hours down into durations at specific inlet temperatures to fully understand the thermal load the catalyst will experience. For this project the lifespan of a typical 600cc two stroke snowmobile engine has already been well established to be about 120 hours within the snowmobile industry. Using this with some generalized RPM and duration histogram data from a colleague in the powersports industry, the durability requirements for the catalysts were determined below in Table 6.9.

Table 6.9 - Durability Requirements

Engine Speed (RPM)	Portion of Lifespan (%)	Portion of Lifespan (hrs)	Associated Mode	Expected Inlet Temp. (℃)
8000-8250	1	1.2	1	590
7000-8000	20	24	2	515
4000-6000	50	60	3-4	280-405
1750-4000	35	36	5	150

Based on these results it was determined the catalyst will spend half of its lifespan in the 280℃ to 405℃ inlet temperature range, about a fifth of its lifetime at inlet temperatures in excess of 500℃ and the remaining time at very low inlet temperatures.

This data is then utilized by the supplier to determine catalyst material selection, geometry, and the wash-coat formula. Because extensive back pressure testing was conducted prior to wash-coat development the catalyst geometry and substrate material were already well defined. Therefore, the key targets the suppliers worked to achieve was the target conversion efficiency levels and the durability requirements. Although the exact process used to design a catalyst to meet these requirements is proprietary information, the basic workflow was apparent. Suppliers utilize the exhaust flow rate, emissions concentrations, and expected inlet temperatures to select the wash-coat formula from a library of formulas their company has developed. Based on the constituents being targeted and to some degree the application, the type of PM used can be selected. Then flow rate in conjunction with the substrate volume is used to determine the GHSV. The GHSV, paired with an inlet temperature, defines a specific catalyst operating point. Each wash-coat formula then has a unique reaction rate constant that is temperature and GHSV dependent. So, a supplier aims to select the wash-coat that has a reaction rate that will achieve the conversion efficiency target at each critical operating point. This concept can be a bit abstract to understand. To aid in visualizing how these parameters interact and how their interaction influences wash-coat selection Figure 6.33 was created. This is a simple representation of the process; no values correlate to any specific catalyst operating points or wash-coat formulas.

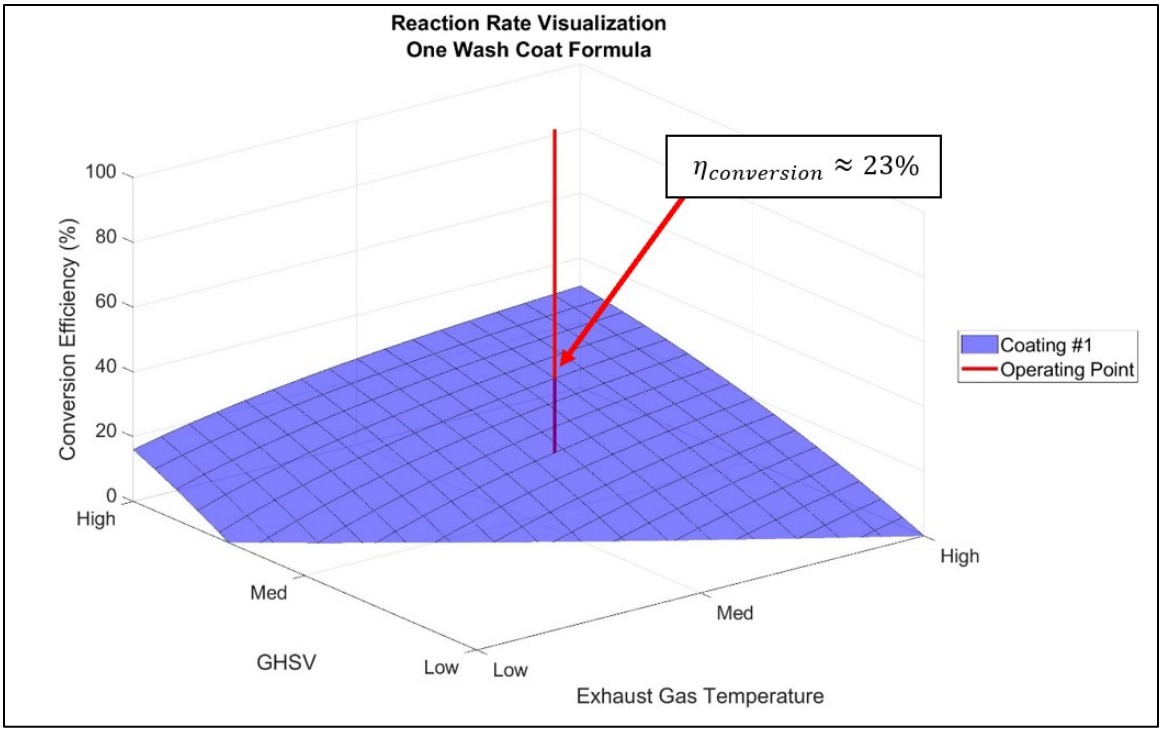

Figure 6.33 - Reaction Rate Visualization Graphic – Coating 1

Figure 6.33 shows an XY coordinate system that consists of catalyst inlet temperature vs GHSV. These coordinates define the catalyst operating point, as shown by the vertical red line. The blue surface displayed represents the conversion efficiency surface for a given coating across the operating range. As a catalyst supplier, given your customers operating points and conversion efficiency targets, a particular wash-coat formula can be selected. In the case of this example, coating #1 would achieve a 23% conversion efficiency at the given operating point. This may or may not be sufficient to meet design requirements. Each wash-coat formula that is available to the supplier has a unique reaction rate constant and therefore will have a unique conversion efficiency at any given operating point. The visual representation of this can be seen below in Figure 6.34 where an additional surface has been added to the previous figure. This green surface represents a wash-coat with a higher rate constant, translating to a higher conversion efficiency surface across the operating range.

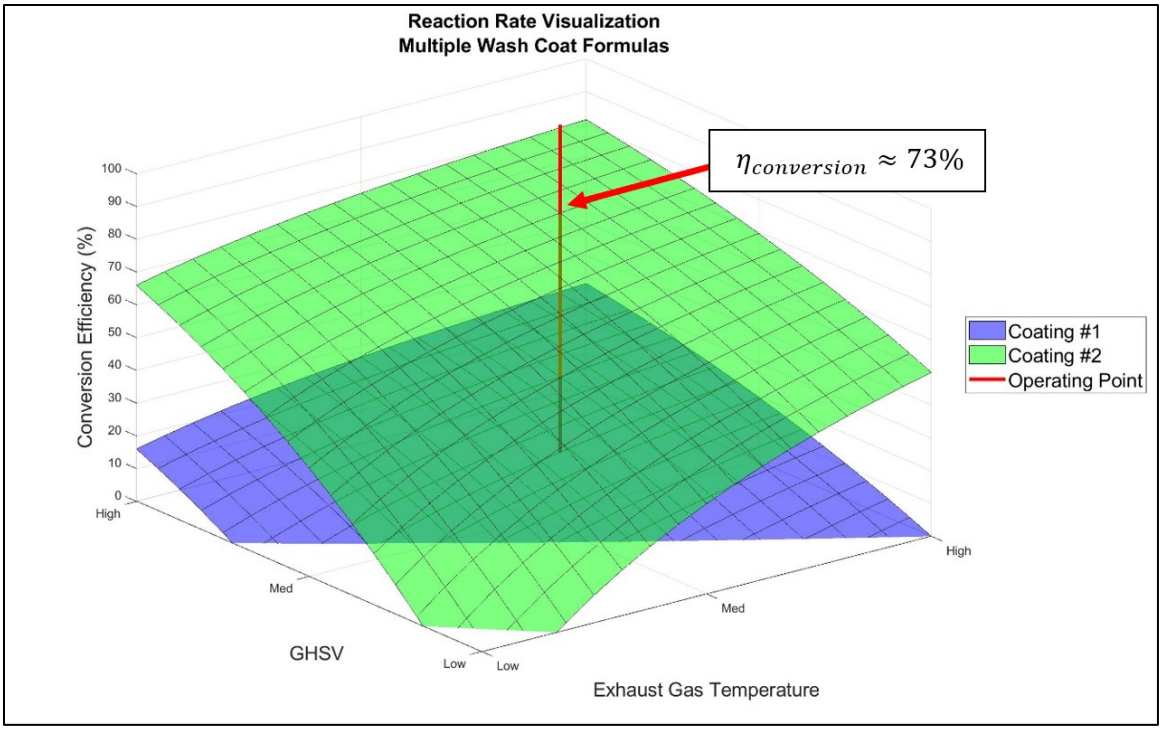

Figure 6.34 - Reaction Rate Visualization Graphic – Coatings 1 & 2

Coating #2 in this example offers a conversion efficiency of 73% at the same operating point, which may be closer to meeting the conversion efficiency target of the customer. While this is a greatly simplified explanation of how wash-coat formulas are selected, one can quickly understand the complexities involved. The catalyst experiences a wide range of operating points each of which has a unique reaction rate associated with it. Therefore, achieving a constant conversion efficiency across a broad operating range is very rarely feasible. In addition to selecting a wash-coat formula based on the expected operating points and target conversion efficiencies, durability also must be a key consideration.

When considering catalyst durability, the primary concern is keeping the catalyst under a temperature threshold to prevent accelerated rates of thermal aging. The expected inlet temperatures are likely used in conjunction with conversion efficiency targets and emissions concentration levels to approximate the outlet temperature of the catalyst, like the EES simulation developed for this project to approximate conversion efficiency targets. In addition to this, poisoning is a valid concern to durability in two stroke applications. However, since modern injection oils are regulated on both phosphorus and ash content and the lifespan of these engines is drastically less than automotive applications, poisoning due to injection oil can be thought of as a minor threat to durability in comparison to thermal ageing. Finally, suppliers have an arsenal of additives that can be used to prolong durability as well as promote certain desirable effects in the

catalytic reaction process. Based on the experience gained in this project, additives to promote durability typically aim to give the wash-coat microstructure improved thermal stability so that surface area remains high and reaction sites remain open and well dispersed throughout the lifespan of the catalyst. Whereas additives to enhance the catalytic reaction aim to promote oxidation or facilitate oxygen storage. Use of these additives can potentially be advantageous in a two stroke application due to the wide range of inlet emissions concentrations and temperatures the catalyst experiences.

Using their own processes CCC and Heraeus both selected wash coat formulas that should meet the given design requirements. CCC was willing to share significant details about their wash coat formula , whereas Heraeus did not wish to disclose this information. CCC recommended a PM package of Pt and Rh at a 1:1 ratio and a total PM loading of $33\,\frac{g}{ft^3}$ with a wash coat that was a mixture of Lanthanum stabilized Gamma Aluminum and both Cerium and Zirconium oxide. The majority of the wash coat was Cerium and Zirconium oxide to promote oxygen storage and the oxidation process. Gamma Aluminum is known for its inherently high surface area. Lanthanum was utilized to dope the base material to provide better thermal stability properties. This was a key addition to maintain the high surface area and meet durability requirements.

The XRF was again used to determine the contents of the active wash coat from Heraeus. However, this particular XRF utilized a Rhodium detection surface. This is significant because this machine then cannot detect Rh or determine its weight percent accurately. Therefore, a Scanning Electron Microscopy (SEM) machine with Energy Dispersive X-Ray Spectroscopy (EDS) was also used to give a micro analysis, showing which elements are present in the sample, but not the relative quantities. The XRF results are presented below in Table 6.10. The complete analysis results can be found in Appendix 9.2.

Table 6.10 - XRF Results - Heraeus Wash Coat Formula

Elements	**Weight Percent (%)**
Aluminum	6.416
Iron	0.120
Ceria	92.131
Zirconia	0.066
Platinum	0.638

As the XRF results show the Heraeus wash coat appears to utilize a high ceria content aluminum based wash coat with some zirconia. The XRF also detected a small amount of platinum in the sample, however the SEM showed a small amount of palladium. Based on the literature review information stating that platinum can lead to massive CO formation under fuel rich exhaust conditions it is believed that palladium is more likely to be the precious metal in the Heraeus wash coat. No rhodium was detected in the Heraeus wash coat when using the SEM. The SEM results can be found in Appendix 9.2.

6.3.2 Conversion Efficiency Testing Setup

To collect more consistent conversion efficiency data, the emissions sampling setup required modification. As previously mentioned in Section 4.2.2 the AVL SESAM can only sample one exhaust gas stream at a time. To determine conversion efficiency, the difference in emissions constituent concentrations must be measured across the catalyst. To achieve this a set of pneumatically actuated valves was configured to allow the sample stream measurement location to be changed mid test from the test cell control room. The system utilizes two solenoids that control supply air to the pneumatically actuated valves. This sample stream switching setup is display below in Figure 6.35. It should be noted that the stainless lines used in the sample switching setup were wrapped in fiberglass insulation tape to ensure the sample gasses remained hot until reaching the heated sample line.

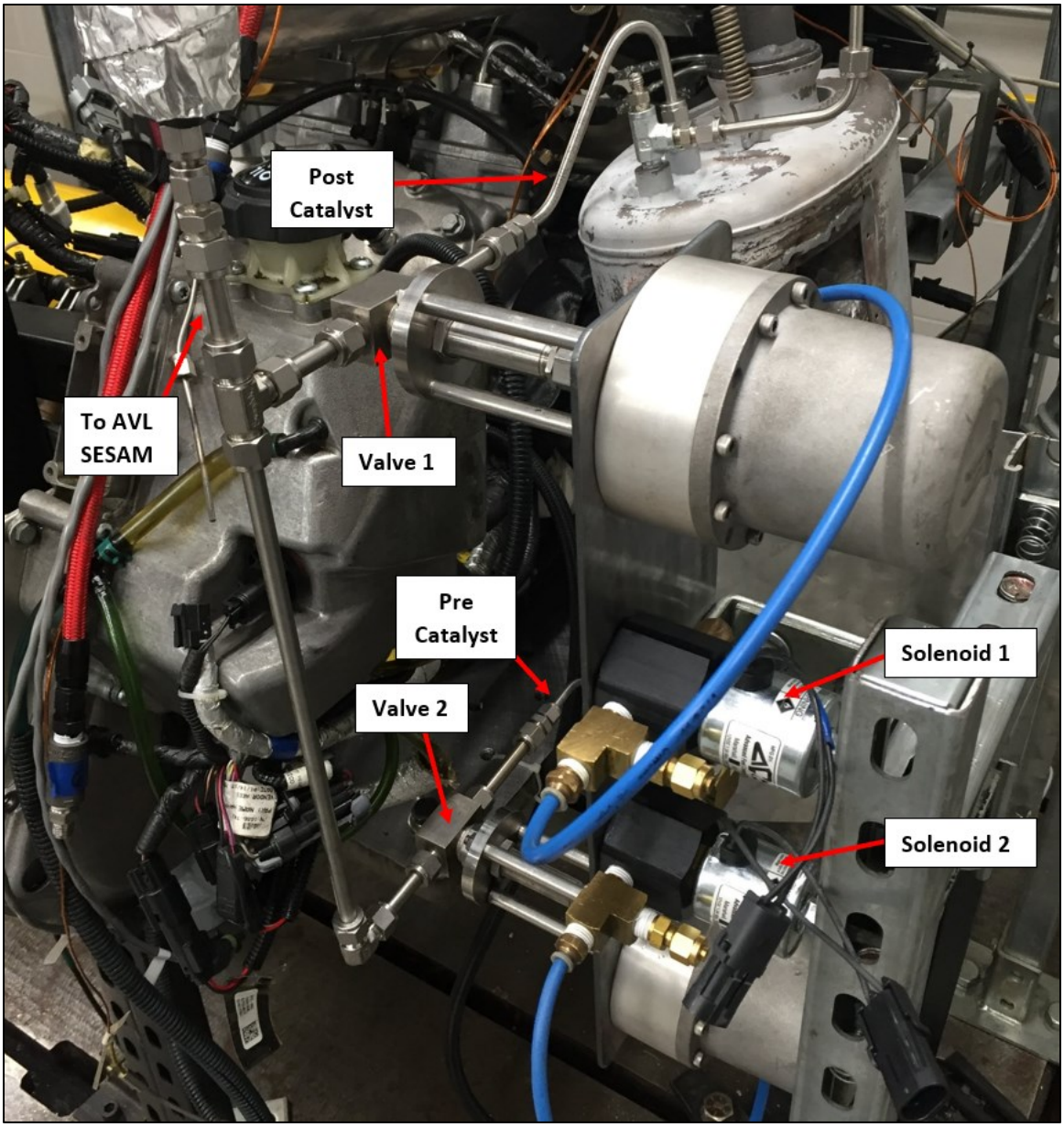

Figure 6.35 - Sample Switching Setup

By activating solenoid one, valve one is opened, sampling emissions from the post catalyst location. Whereas activating solenoid two opens valve two, sampling from the pre catalyst location. This sample switching capability was critical to maintaining the same operating state for each emissions sample collected. To accommodate this setup the standard discrete 5 mode test procedure used throughout the project was slightly modified. When testing conversion efficiency, the standard 3 minute stability period was still achieved for each mode before sampling data. Dyno and engine data were sampled

continuously after the stability period was completed, whereas emissions data was sampled first from the pre catalyst location followed by the post catalyst location in two separate files. When switching sample streams the emissions bench was given one minute to stabilize readings between the sample stream switches before beginning to collect the next data set. The appropriate portions of dyno and engine data was then split into two files and trimmed accordingly to be time aligned with the corresponding emissions data. Using this sample switching setup and modified test procedure pre and post catalyst emissions measurements were collected at all 5 modes for each actively coated catalyst sample. Conversion efficiencies were then calculated using Equation 6.6 below. In this equation the letter c represents the concentration of a given emissions constituent.

$$\eta_{conversion} = \left(\frac{\left|c_{pre} - c_{post}\right|}{c_{pre}}\right) * 100 \qquad 6.6$$

6.3.3 Catalyst De-Greening Process

A de-greening procedure is commonly accepted as a very important step to incorporate when testing catalysts. However, there is no universally agreed upon method to de-green catalysts or for how long this process should be performed. It appears that incrementally increasing the temperature the catalyst is exposed to over a period of time is a generally accepted de-greening procedure. The goal of this process being to finish exposing the reaction sites that are blocked by the crystal structures of the wash coat. In general, the wash coat that carries the PM when coating the catalyst forms various crystal structures over and amongst the reactive sites. Breaking down the structures that cover reactive sites will increase conversion efficiency to the full potential of the catalyst. Extended periods of time at elevated temperatures break down these structures and expose the remaining reaction sites. Performing this step during the manufacturing process is not feasible, therefore, when testing catalysts, the de-greening process falls upon the consumer. It is very important to de-green samples before measurements are collected to ensure that results are reflective of how a catalyst will perform for most of its lifespan.

As previously mentioned there is no standard de-greening procedure. Common approaches include cycle and ramped type processes. Cycled approaches are often performed on the engine, where temperatures are increased to a given value for an amount of time and then returned to a lower temperature. This process is repeated for given number of cycles, typically with increasing temperature values until a maximum temperature or specific run time duration is reached. Ramped approaches are typically done in high temperature ovens, where samples can be held at a controlled temperature for specific periods of time. It appears that ramped processes typically start at a lower temperature step and work up to a peak temperature step over a given period of time at

each temperature step. The important things to keep in mind during the de-greening process is to slowly increase the temperature over a long period of time. Keeping in mind that during an in engine de-greening process the catalyst is active, and the catalytic reaction will increase the bed temperatures significantly above the measured inlet temperatures. Therefore, it is more controlled to perform de-greening in a high temperature oven than on engine if possible.

For this project the de-greening procedure consisted of an extended warm up period at idle, followed by approximately 5 minutes at the heat soak operating point previously outlined. Following this the control point was run, and finally a 5 mode test following the standard procedure used throughout this project. The entire de-greening process was approximately a half hour in duration. Typically, the de-greening process is longer in duration, however, it was felt that because the catalyst sizes were relatively small this de-greening duration was sufficient. After completion of this procedure each sample was ready for conversion efficiency testing.

6.3.4 Conversion Efficiency Testing Results

Using the modified 5 mode testing procedure outlined in section 6.3.2 each of the three samples were tested and conversion efficiencies were then calculated for each mode. Figure 6.36 shows the HC conversion efficiency results, followed by CO conversion efficiency results in Figure 6.37. It should be noted that any negative conversion efficiency represents a formation of the given emissions constituent.

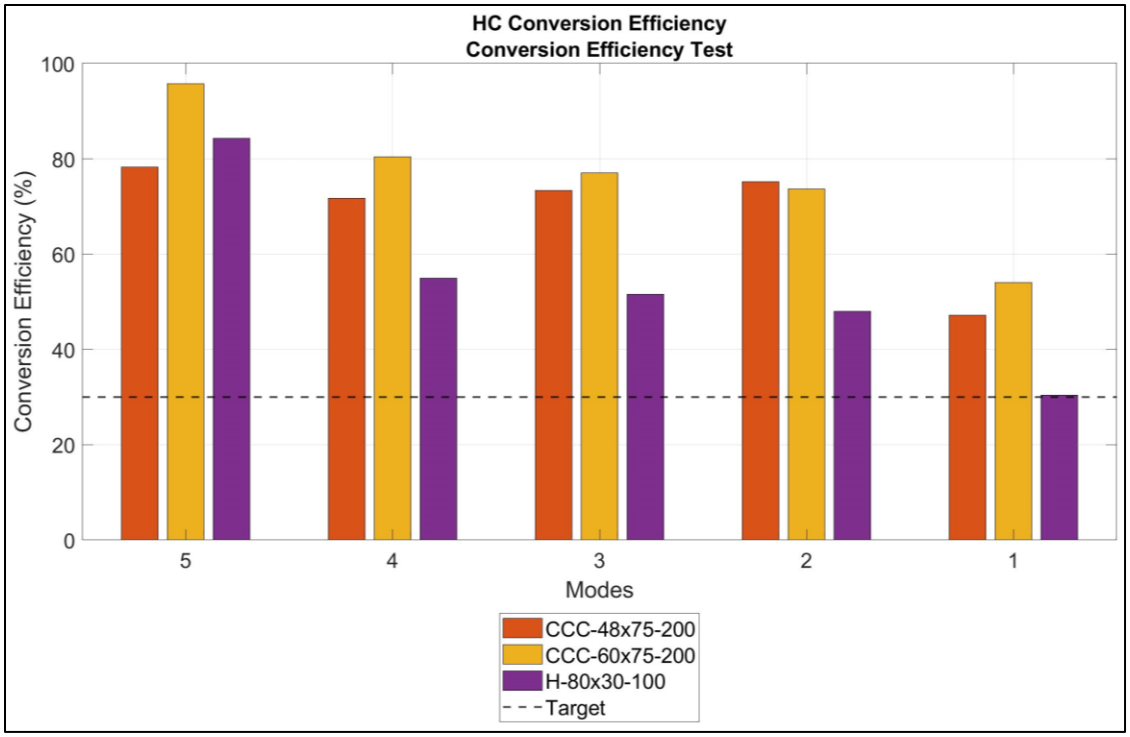

Figure 6.36 - HC Conversion Efficiency Results

As Figure 6.36 shows HC conversion efficiencies were higher than anticipated over all modes for each sample with the exception of the H-80x30-100 sample at mode 1. Several observations can be made from this data. When comparing the CCC samples the CCC-60-75-200 samples conversion efficiency is consistently higher than the CCC-48-75-200 sample. This trend holds true to the expected impact of increased surface area upon conversion efficiency. Another observation of the CCC samples is that the general trend of the conversion efficiency between modes varies between the two samples. The CCC-48-75-200 sample has a gradual ark shape to it where conversion efficiency is lower in modes 1 and 5 and peaks in modes 2 and 3. This is distinctly different than the CCC-60-75-200 sample, which shows a consistent decrease in conversion efficiency from mode 5 all the way to mode 1. This trend is also observed with the H-80x30-100 samples conversion efficiency.

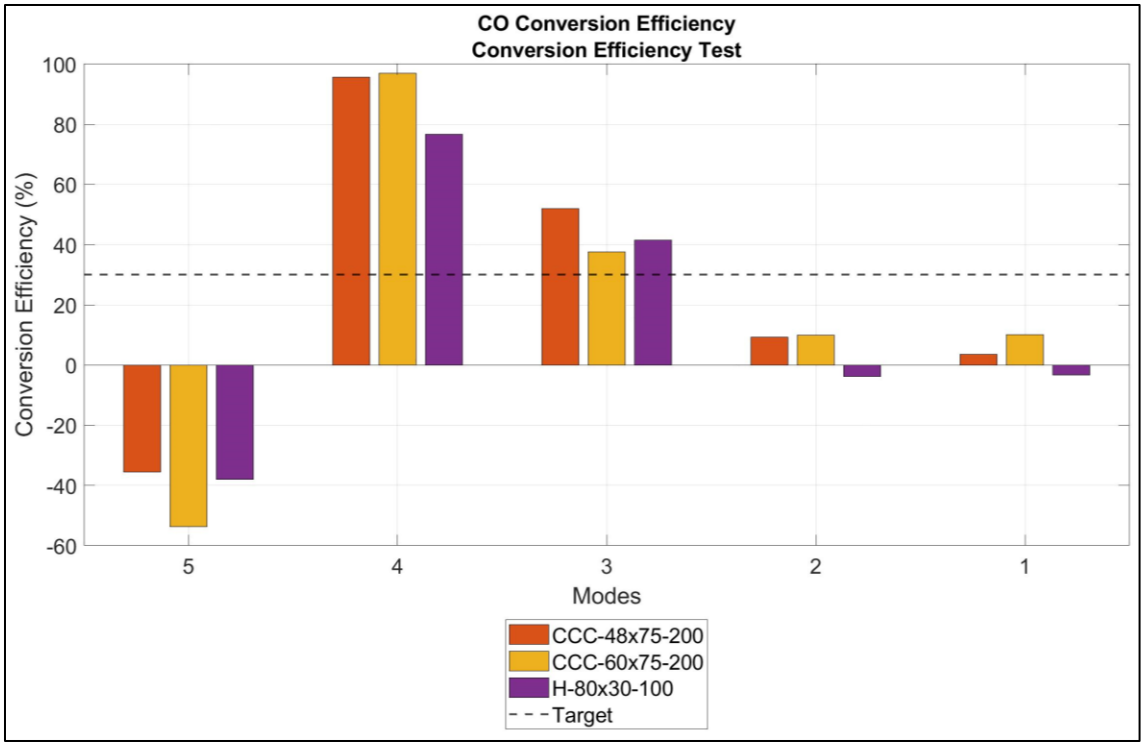

Figure 6.37 - CO Conversion Efficiency Results

Figure 6.37 shows some interesting results for CO conversion efficiencies. Most notable is the significant formation of CO in mode 5 by all three samples as well as slight formation in modes 1 and 2 for the H-80x30-100 sample. Additionally, the CCC-60-75-200 sample showed a lower conversion efficiency than the CCC-48-75-200 sample in mode 3. This is contrary to the expected impact of an increase in surface area on conversion efficiency.

The formation of CO in mode 5 was certainly unexpected and is not ideal. When discussing these results with suppliers it was concluded that the formation of CO at mode 5 was most likely due to incomplete oxidation of the HC. The primary cause of this incomplete oxidation is thought to be due to the low inlet temperatures observed in mode 5. In general, the reaction is at such a low temperature that HC are only being partially oxidated, and the product of this partial reaction is CO. It was expressed that HC oxidation typically begins to activate at a temperature of approximately 300 ℃. When in mode 5 the inlet temperatures are typically in the range of 200℃to 270 ℃. Based on this the HC reaction would not be activated. However, the 5 mode test format used in this project incorporates a heat soak and control point prior to mode 5. It is entirely possible that while the exhaust system cools the catalytic reaction started during the heat soak and control point is sustained at mode 5 by the exotherm caused by the catalytic reaction process. This reaction could easily give off a large enough exotherm to heat part of the

catalyst bed above the HC oxidation activation temperature, sustaining the reaction but not enough to promote full oxidation of the incoming HC to non-harmful constituents.

Conversion efficiency testing also provided another opportunity to collect pressure drop data across each sample and compare those measurements to the baseline used in back pressure test #3. Below in Figure 6.38 are the pressure drop results. It should be noted that ambient barometric pressure was approximately 10 mBar lower than the baseline data ambient barometric pressure when the results in Figure 6.38 were collected.

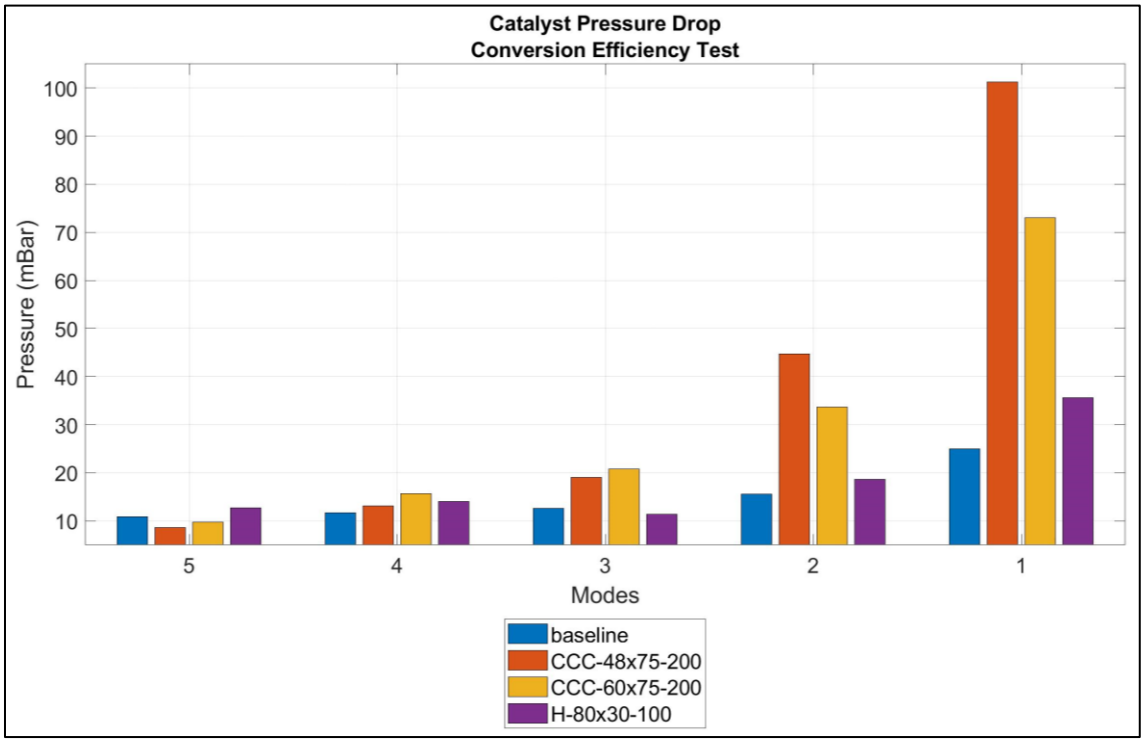

Figure 6.38 - Catalyst Pressure Drop - Conversion Efficiency Test

As Figure 6.38 shows the pressure drop results are consistent with previous findings in that as open frontal area decreased the pressure drop increases. This is especially apparent at modes 1 and 2. The H-80x30-100 sample performed very well in terms of pressure drop seeing only a 11 mBar increase over the baseline at mode 1.

Below, plots of trapped lambda, mid-pipe temperature, and mid-pipe pressure are shown in Figure 6.39 through Figure 6.41 to look at the engine performance impacts of the actively coated catalyst samples. The same baseline data used in back pressure test #3 was used for comparison in these figures.

Figure 6.39 shows trapped lambda values which were calculated from pre catalyst emissions data measured during each test using the Roy Douglas method. [17] Trapped

lambda was utilized in reporting this data because the global lambda measured by the wideband oxygen sensor showed significant variation from the baseline data. The variation was greatest in mode 5 where global lambda values were approximately 0.06 lower than the baseline data. This was seen as significant because in all previous tests global lambda values at mode 5 were very consistent. The reasons why this variation was observed during conversion efficiency testing are not apparent. However, it is almost certainly linked to the presence of the active catalyst in the system, as this was the only notable change from back pressure testing.

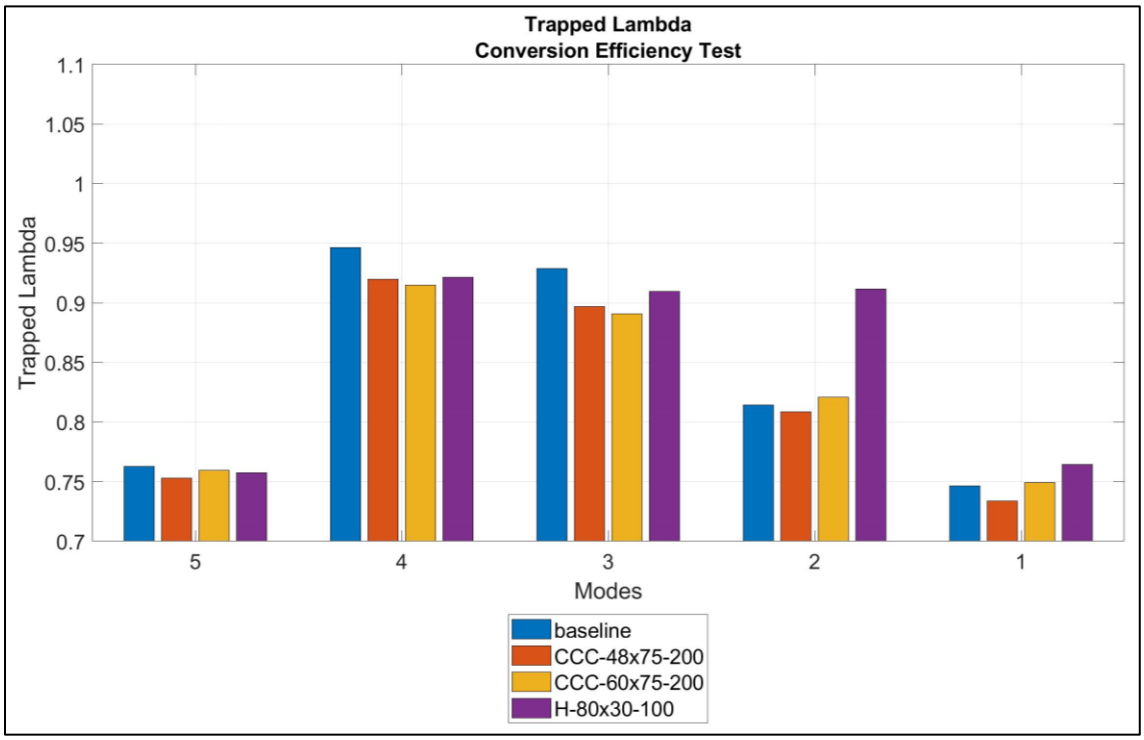

Figure 6.39 – Lambda – Conversion Efficiency Test

The data in Figure 6.39 shows that trapped lambda behavior is very similar to previous global lambda measurements in that as restriction levels increase lambda decreases. However, the magnitude of the trapped lambda values is lower in general than the results collected in back pressure test #3. This is not surprising as trapped and global lambda are known to vary significantly in spark ignited two stroke engines.

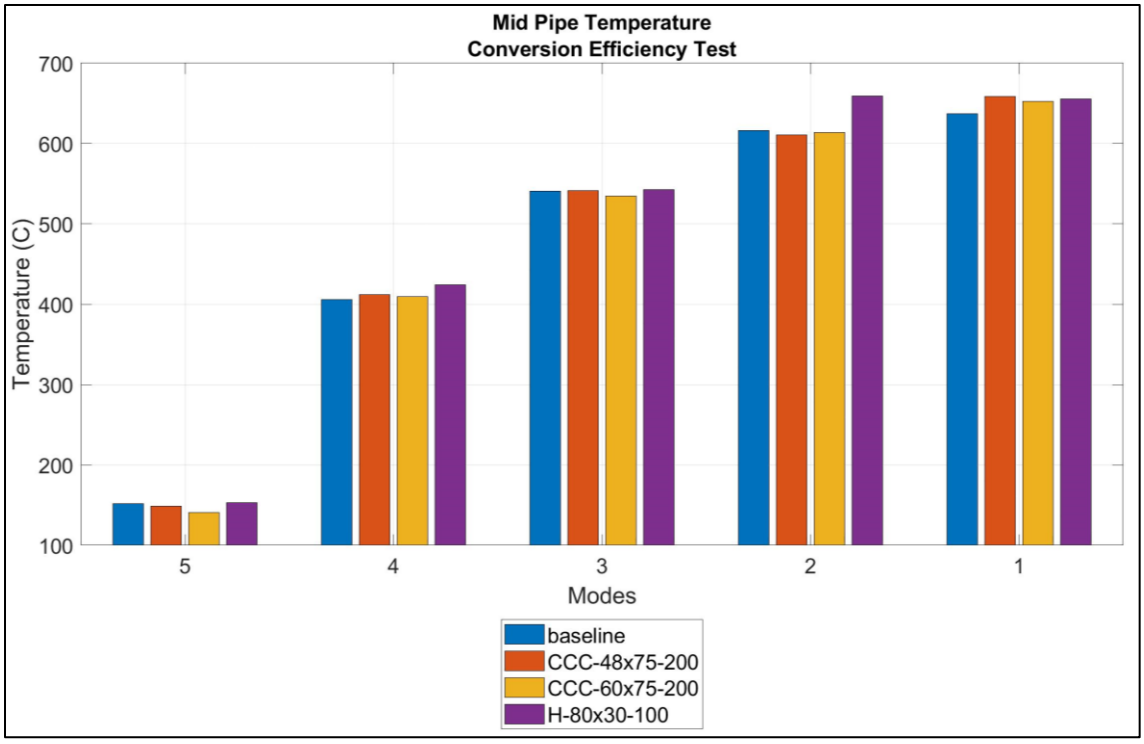

Figure 6.40 - Mid-Pipe Temperature – Conversion Efficiency Test

Figure 6.40 shows very consistent mid pipe temperatures for all samples at each mode except for the 80-30-100 sample at mode 2. In general exhaust temperatures were higher than baseline data at this mode with the H-80x30-100 sample installed. The only notable factor that may have contributed to this was mid-pipe pressure differences, which will be reviewed following Figure 6.41.

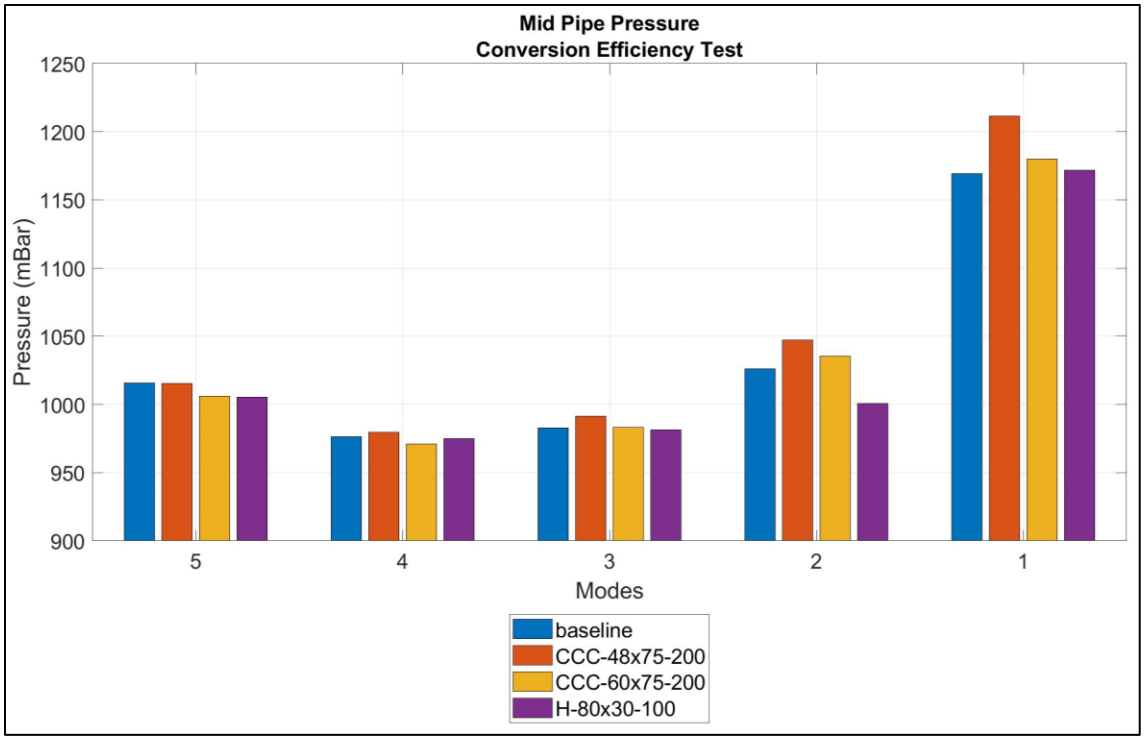

Figure 6.41 - Mid-Pipe Pressure – Conversion Efficiency Test

It should be noted that the ambient barometric pressure when testing the CCC-60-75-200 and H-80x30-100 samples was approximately 10 mBar lower than the baseline barometric pressure. This accounts for the slightly lower mid-pipe pressures in modes 2 through 5 for these samples. The mid-pipe pressure data from conversion efficiency testing was consistent with the observations in back pressure test #3 for the CCC-48-75-200 and CCC-60-75-200 samples. The H-80x30-100 samples effects on mid-pipe pressure were consistent with previous results in that the reduction in cell density and length of the substrate lowered the increase in mid-pipe pressure in comparison to the other 80mm diameter samples tested in back pressure test #3

Finally, circling back to the 4 Hp power loss limitation previously set, Table 6.11 outlines the average peak power output recorded with each sample during mode 1 of the 5 mode tests. The brake power loss column uses the baseline power output as a reference for power loss calculations.

Table 6.11 - Engine Power Loss Data

Test Case	Brake Torque (Nm)	Engine Speed (RPM)	Brake Power (Hp)	Brake Power Loss (Hp)
Baseline	86.5	8250	100.2	NA
CCC-48-75-200	85.4	8250	98.9	1.3
CCC-60-75-200	85.7	8250	99.3	0.9
H-80x30-100	86.0	8250	99.6	0.6

As Table 6.11 shows a maximum of a 1.8 Hp loss was observed with the most restrictive CCC-48-75-200 sample installed, whereas the least restrictive H-80x30-100 sample showed a mere 0.8 Hp loss. This shows that each of these samples meets the power loss requirement of no greater than 4 Hp. This also validates that samples with as minimal pressure drop as possible are ideal for these types of applications to have minimal impact on performance.

6.3.5 Durability

Due to equipment and time limitations durability testing was not able to be incorporated into this project. However, some suggestions can be made should durability testing be conducted in the future.

To perform a quality durability analysis several equipment modifications must be made. The most notable is to incorporate a portion of the snowmobile drive line into the engine and dyno system. This should include the CVT clutch and belt system as well as the OEM rubber engine mounts to ensure a realistic drive cycle performance can be achieved and longevity of the engine is also reflective of an in vehicle application. In addition to these hardware modifications a drive cycle must be developed that is reflective of typical snowmobile operation. This drive cycle will likely need to be co-developed with and OEM using historical driving data to produce a cycle reflective of typical snowmobile operation. Integration of these hardware and control changes are critical to executing a quality durability test that is reflective of the life cycle a catalyst will experience.

Durability testing should then be run out to the 120 engine hours lifespan previously outlined. Catalyst conversion efficiency and pressure drop should be measured at regular intervals throughout the test. Upon completion of the testing the degradation in conversion efficiency can then be plotted versus engine hours as well as any changes in pressure drop over the duration of the catalysts lifespan. It should also be noted that if an accurate curve can be fitted to conversion efficiency degradation it may be extended

beyond the tests duration to predict what conversion efficiencies would be at extended lifespans. This is not to act as a replacement for physical testing of catalyst durability but can offer a relatively accurate prediction. Lastly, it may be beneficial to have the catalyst sample wash coats analyzed after completing durability testing to gain further insight to the effects of thermal aging, poisoning, and other physical changes the catalyst may have undergone during its lifespan.

6.4 Model Validation

As previously stated two models were developed with the intent of simplifying the design process. These included an EES conversion efficiency model as well as pressure drop model built around the Hagen Poiseuilli equation. The usefulness of both these models in comparison to the experimental data collected during this project will be reviewed in this section.

The conversion efficiency model was used early in the design process to provide catalyst suppliers with a conversion efficiency target that should safely constrain the catalytic reaction temperature. This limit was set in an attempt to control the catalytic reaction and ultimately lessen the effects of thermal aging. The EES model was re-run with pre catalysts emissions, and both pre and post catalyst temperatures measured during the conversion efficiency testing. This produced a set of conversion efficiency estimations assuming that the catalytic reaction could be modeled as a combustion reaction under adiabatic conditions. These estimates are then compared with measured conversion efficiencies for each sample. Because the EES model has no way to incorporate the respective conversion rates of CO and HC it produces the same conversion efficiency estimation for both constituents. Therefore, the experimental HC and CO conversion efficiencies are individually compared to the same model results in Figure 6.42 and Figure 6.43 respectively.

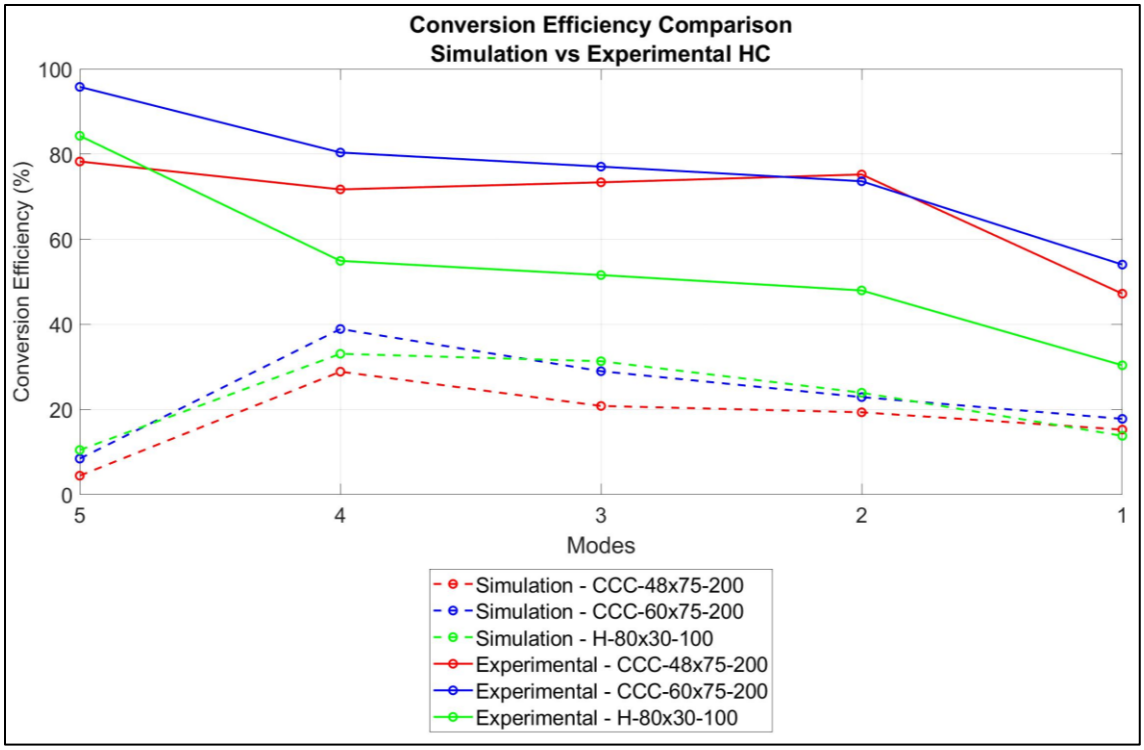

Figure 6.42 - EES Model Validation - HC Conversion Efficiency Comparison

In general, the EES model results for HC conversion efficiency showed very minimal correlation to the experimental conversion efficiency results. The trend from modes 4 to 2 was the closest portion of the model to experimental results, however the magnitudes are still far separated. In mode 5 the simulation produced the opposite trend to observations in the experimental data.

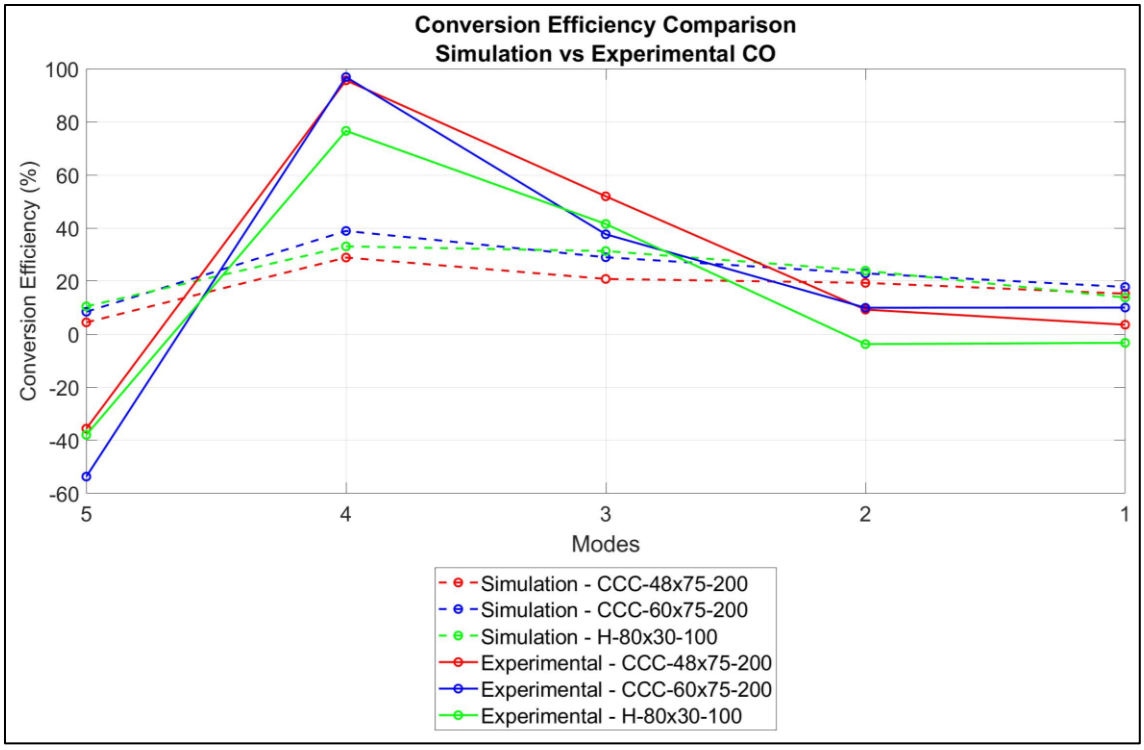

Figure 6.43 - EES Model Validation - CO Conversion Efficiency Comparison

The CO conversion efficiency simulation vs experimental results show even less correlation due to the production of CO observed in mode 5. The general trend of the simulation doesn't match experimental results. It appears that the EES model, while useful in understanding how limited conversion efficiency targets will be to keep catalyst temperatures in check, is not a good method to approximate conversion efficiency. Modelling the catalytic reaction as a simple adiabatic combustion reaction is too great of a simplification of the reaction occurring within an actual catalyst. To add to this, it became apparent that estimating a conversion efficiency target was not of particular value to the suppliers. Of greater value is understanding the inlet temperatures, exhaust concentrations, and durability requirements the catalyst will be subjected to in its given application. Having this information allowed suppliers to predict outlet temperatures and ensure that they remained in check in order to control the thermal ageing process.

The pressure drop model was not really utilized during the design process as intended for two main reasons. The first was substrate sample selection was limited for this project. If a wide range of samples were available this model certainly would have been further explored to narrow the test field. The second reason has to do with the GHSV constant of $200000\ hr^{-1}$ that was discovered through the literature review process. Using this GHSV constant produced impractically large substrate volumes, leading to unreasonable pressure drop estimations. It was determined that the GHSV parameter was the most

suspect cause to these unrealistic results, especially considering no documentation could be located on how this parameter had been previously determined. Therefore, three possible alterations the model could be made to bring the estimated pressure drops back to realistic values. These include using the physical substrate dimensions that were tested to define the part volume and then calculate and scale the resulting pressure drop estimations accordingly to match experimental results, utilize a small percentage of the substrate volume calculated using a GHSV of 200000 hr^{-1}, or use a different GHSV value altogether. Which method was the correct approach could only be determined by comparing the simulation to the experimental results. Back pressure test #3 provided the necessary experimental data to perform this validation. After modifying the model to explore these alterations it became apparent that utilizing actual part volume and then scaling the pressure drop estimation was the better method. These results are shown in Figure 6.44 below.

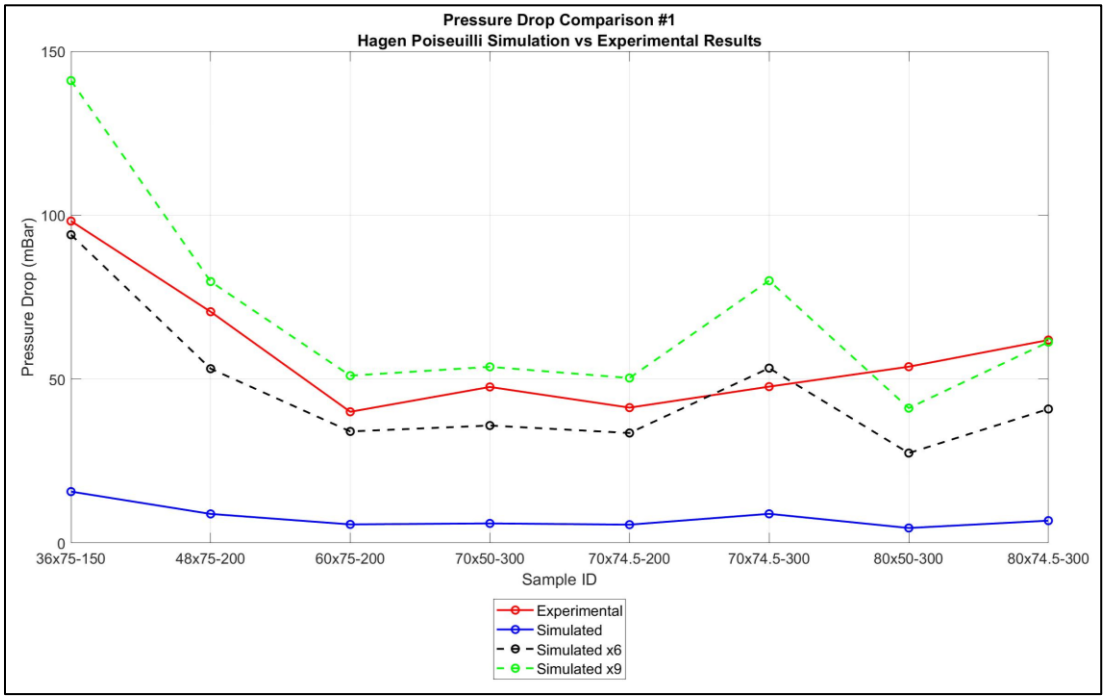

Figure 6.44 - Pressure Drop Model Validation

As Figure 6.44 shows the model results in blue were very low in comparison with the experimental results in red. However, by applying scaling factors of 6 and 9 the experimental results are bounded by the model results as shown by the black and green dashed lines respectively. The H-80x50-300 and H-80x74.5-300 experimental results are the only significant outliers to the scaled model results. As previously mentioned when discussing back pressure test #3 pressure drop results these points are thought to be outliers due to poor flow distribution in these largest diameter samples.

Based on these results it is assumed that model outputs, if scaled accordingly, could be used to approximate the pressure drop of samples prior to experiment testing. This has the potential to narrow the test field when selecting part geometry, saving time and cost. However, to further gain confidence in the models accuracy a larger sample size should be collected for experimental data and a flow bench should be utilized to better control inlet conditions and more accurately measure pressure drop across the samples.

7 Conclusions

The conclusions section includes a project outcome summary that reiterates the project goals and evaluates how well these goals were achieved as well as a section suggesting future work should this project be continued by another engineer in the future.

7.1 Project Outcome Summary

To reiterate the goals of this project recall that the main motivation was to explore catalyst design specific to spark ignited two stroke engines with the intent of starting to define a design process. Largely from the literature review process, several areas of consideration for the design process were defined. These areas included selecting a location for the catalyst, defining substrate geometry and materials, selecting conversion efficiency targets, developing a wash coat formula, and considering durability of the catalyst over its lifespan.

Staring with locating the catalyst, back pressure test #1 established that two stroke engines will be very sensitive to catalyst location. This led to back pressure test #2 which validated that locating the catalyst after the stinger offered significant freedom in terms of the restriction the catalyst could add without significantly impacting engine performance. Ultimately back pressure test #3 was the final validation of this hypothesis, and showed the muffler was a viable location to have minimal performance losses. Additionally, in back pressure test #3 the lower bound of the open frontal area was established as being no less than the cross sectional area of the stinger. If open frontal area is less than the stinger cross sectional area performance losses will ensue. Finally, back pressure test #3 provided experimental data to validate a substrate pressure drop model developed during this project. It was learned that when properly scaled the outputs of this model can roughly predict the pressure drop of a substrate with a given diameter, length, and cell density. This model could be used to narrow the test field when trying to experimentally determine an optimal substrate geometry, potentially saving time and cost in the design process.

Next a model developed to estimate conversion efficiency targets was able to be compared to experimental data form the conversion efficiency testing. This model proved to not be useful in predicting the conversion efficiencies of given samples based only on an adiabatic combustion reaction. Making a more accurate model will require better understanding of the catalytic reaction process and modelling how that relates to the exotherm of the reaction.

Finally, a great deal was learned about the wash coat development process, the catalytic reaction process, and catalyst durability. Most notably for wash coat development the information catalyst suppliers require to develop a wash coat was defined and some understanding of the development process suppliers use was gained. Both pieces of

information will certainly help a catalyst customer better understand what influences the wash coat development process and how they may have an influence on the resulting wash coat formula. Regarding the catalytic reaction process, the elements commonly used in wash coats as well as what aspect of the catalytic reaction they aim to influence were better understood. This information will also help catalyst customers to further influence the design process. Catalyst durability was also discussed at length in the literature review section. Although durability was not able to be tested, the consideration given to durability concerns was significant. Further testing is the only way to validate if these considerations would prove effective in influencing catalyst durability.

Recall that the high level motivation of this project was to address the emissions concerns that surround spark ignited two stroke engines through the design and implementation of a two way oxidation catalyst with the hope of preserving the use of these engines in the recreational powersports industry. With this overarching goal in mind, the results of the conversion efficiency testing are very promising and instill confidence that two stroke catalysis is a viable solution to the emissions concerns that threaten these engines. The project showed that a catalyst can successfully be integrated into a stock snowmobile engine without significantly affecting engine performance. It was also shown that a two stroke specific catalyst can be designed in such a manner as to control the reaction temperatures which will greatly increase the durability of the catalyst. Finally, significant emissions improvements were observed. Specifically, HC emissions were improved across the entire engine operating range and CO emissions were also significantly improved in modes 3 and 4, where snowmobiles typically spend nearly half of their lifespan operating. Table 7.1 shows a summary of the emissions improvements relative to the durability data previously presented. This information shows just how significant the improvements are in terms of the conversion efficiencies that were achieved and the net improvement this will provide relative to the vehicles lifespan.

Table 7.1 - Final Emissions Improvement Results

Engine Speed (RPM)	**Portion of Lifespan (hrs)**	**Portion of Lifespan (%)**	**Associated Mode**	**Reduction in HC Emissions** (%)	**Reduction in CO Emissions** (%)
8000-8250	1.2	0.8	1	30 to 54	-3 to 10
7000-8000	24	20	2	48 to 75	-4 to 10
4000-6000	60	50	3-4	52 to 80	38 to 97
1750-4000	36	30	5	78 to 96	-54 to -36

CO emissions in mode 5 and to a lesser degree in modes 1 and 2 could use improvement. It is believed that by increasing the inlet temperature of the catalyst at mode 5 CO conversion efficiencies could be greatly improved. One possible solution would be to implement a close coupled catalyst. Using this approach would increase inlet temperatures to the close coupled catalyst and would spread out the thermal load across two substrates spaced relatively far apart int eh exhaust system. The reduction in thermal load could also further relax the conversion efficiency limitations set to keep outlet temperatures in check.

In conclusion, this work was an excellent first step towards preserving the use of spark ignited two stroke engines in the recreational powersports industry. It was demonstrated that an oxidation catalyst can be designed to be integrated with a stock snowmobile engine and introduce minimal performance losses. The catalytic reaction was also able to be effectively controlled to promote catalyst durability. Most importantly, significant emissions improvements were also made despite the constraints durability and performance loss concerns introduce. Beyond the success of the catalysts tested during this project a design process was also defined. A better understanding of how to navigate the two stroke catalyst design process, how stages of the design process and specific design parameters are interconnected, and the sensitivity of these parameters relative to the challenges two stroke catalysis poses was gained through this work. Using this knowledge, the design process started here can continue to be improved and the possibilities of two stroke catalysis can continue to be explored.

7.2 Future Work

Through the duration of this project several areas for potential future work have become apparent. This section will review areas to improve and expand upon the results of this project with the aim of further developing the design process this project has started to define.

The first area that provides opportunity for improvement is when correlating back pressure to substrate geometries. While this project aimed to address this relationship through the substrate sample selection in back pressure test #3, it was difficult to isolate the pressure contributions of each geometric design parameter of the substrates. Running a substrate test matrix on an engine to explore this relationship adds unnecessary complexities. A better approach would be to utilize a flow bench to artificially induce conditions reflective of an engine exhaust environment. Using this testing approach, flow rate and gas temperature could more easily be controlled between tests to ensure that each sample experiences the same inlet conditions. This could make the sensitivity of pressure contributions to changes in substrate diameter, length, cell density, wall thickness, and cell shape more apparent than the methods used in this project. Understanding how individual geometric design parameters such as diameter, length, and cell density affect

pressure contributions will help the designer to better understand the tradeoffs associated with various substrate options.

The next area for future work focuses on improving the method to approximate conversion efficiency targets. For this project a simple adiabatic combustion reaction model was utilized that is undoubtably a great oversimplification of the catalytic reaction process due to several significant assumptions. However, it provided a starting point for conversion efficiency targets. This model may be able to be further improved to better predict the upper conversion efficiency limits of a given application. Areas to improve include better modelling the HC participating in the reaction, incorporating a method to weight the CO and HC reactions based on their associated reaction rates so that two separate conversion efficiency targets could be estimated, and finally, incorporating a heat transfer model would likely greatly improve the models predictions. There is also potential to take a completely different approach to approximating conversion efficiency by modelling the reaction as a catalytic reaction. This would likely be the best approach to refine the model, however, it will undoubtably require significant chemistry and catalytic reaction knowledge to develop.

On this note of chemistry and catalytic reaction knowledge, one of the simplest ways to continue to improve this design process will be to continue to gain knowledge about the catalytic reaction and associated wash coat development process. These areas are the most mysterious part of the entire catalyst design process, so any additional knowledge that can be gained from experimental testing, communication with suppliers, and reviewing catalyst literature will prove to be valuable. The reaction phenomenon observed with the non-actively coated Heraeus samples is one example from this project that comes to mind. Better understanding the reaction mechanism at work in those samples and what influences that reaction would be valuable knowledge to acquire as it may prove to be advantageous in future catalyst design projects.

The most significant addition to this project would certainly be extended durability testing to explore how well the final catalyst samples perform over their intended lifespan. As previously discussed, this step of the project will require some hardware and software changes, as well as a considerable amount of dyno time. However, beyond these investments durability testing would not be very difficult to perform and would provide valuable data.

The final area for improvement would be to fundamentally change the design approach to be more reflective of an OEM two stroke engine manufacturer by exploring engine architecture and calibration changes. The idea would be to modify an existing engine with the intent of a catalytic aftertreatment system in mind from the start. There is potential that the mid pipe could be designed around the anticipated pressure contributions of the catalyst, eliminating performance losses altogether. Further, the catalyst geometry and packaging could be optimized to be more seamlessly integrated into its location in the exhaust system. Finally, some aspects of calibration could be modified to either better control the catalyst under certain operating conditions or to further improve engine performance knowing that the catalyst will assist in keeping

engine emissions in check. This engine design with catalytic aftertreatment in mind approach would add significant complexity to the project but may produce even more viable catalyst solutions for the spark ignited two stroke engine industry.

In closing I sincerely hope that this project will continue to be developed in the future as this work is of significant value to the powersports and catalyst industries, as well as the engineering community. Spark ignited two stroke engines provide a fun an exciting way to explore the world, but their emissions are a real problem. It is my hope that others see the value in this work and pick up where I have left this project.

8 References

[1] W. J. Fiero, M. V. Ernest and K. Rajagopalan, "Design Considerations for Aftermarket Converte," SAE Technical Paper 852121, Davison Chemical Division, W.R. Grace & Co., 1985.

[2] B. P. Carberry, J. Magee and R. Douglas, "The Viability of Catalysing a Carburetted 50cc Two-Stroke Cycle Engine for Moped Applications," SAE Technical Paper 952136, The Queen's University of Belfast, 1995.

[3] G. Bickle, T. Yoshikawa, S. Sindlinger, R. Domesie and K. Fischer, "Emissions Control Systems for Two Stroke Engines - A Challenge for Catalysis," SAE Technical Paper 982710, ICT Co. Ltd., Degussa AG, 1998.

[4] R. Oswald, R. Kirchberger and S. Krimplstatter, "Technologies to Achieve Future Emissions legislations with Two stroke Motorcycles," SAE Technical Paper 2018-32-0042, Graz university of Technology, 2018.

[5] F. Jayat, S. Seifert, K. Babu and S. Waje, "Applications of a LS Metal Calatyst Substrate for BS IV Two and Three Wheelers," SAE Technical Paper 2015-26-0098, Continental Emitec GmbH, Emitec Emissions Control Tech. Ind., 2015.

[6] S. Seifert, F. Jayat, A. Reck and K. V. R. Babu, "Benefits of L-S Design, a Structured Metal Foil for Two and Three Wheelers Catalyst Substrates, to Minimize Catalyst Volumes, PGM loads, and the Route Towards Low NOx Emissions," SAE Technical Paper 2011-28-0042, Emitec GmbH and Emitec Emissions Control Technologies India, 2011.

[7] J. P. Day and L. S. Socha, "The Design of Automotive Catalyst Supports for Improved Pressure Drop and Converesion Efficiency," SAE Technical Paper 910371, Coming Inc., 1991.

[8] E. Szczepanski, A. Koda, D. Sweeney and N. Polcyn, "Impact of Substrate Geometry on Automotive TWC Gasoline (Three Way Catalyst) Performance," SAE Technical Paper 2017-01-0923, DENSO International America Inc. and DENSO Corporation, 2017.

[9] E. Bardasz, E. Schiferl, T. Curtis, F. E. Lockwood, T. Smith and T. Caudill, "Controlling Lubricant Derived Phosphorous Deactivation of the Three Way

Catalyst Part 1: Assesment of Various Testing Methodologies," SAE Technical Paper 2010-01-1544, The Lubrizol Corp. and Valvoline, 2010.

[10] B. Dohner, E. Bardasz and M. Brenner, "Development of Catalyst-Friendly FC-W Certified Marine Oils Utilizing Novel ZDP Technology," SAE Technical Paper 2009-32-0075, Lubrizol Corporation Wickliffe, Ohio USA, 2009.

[11] J. B. Heywood, Internal Combustion Engine Fundamentals 2nd Edition, New York: McGraw-Hill Education, 2018.

[12] G. P. Blair, Design and Simulation of Two-Stroke Engines, Society of Automotive Engineers Inc., 1996.

[13] G. Jennings, Two-Stroke Tuners Handbook, HP Trade, 1987.

[14] A. Insider, "Everything You Wanted to Know About the Arctic Cat CTEC-2 8000 Engine," 2017.

[15] E. P. Agency, "40 CFR 1051.505 Control of Emissions from Recreational Engines and Vehicles - Test Procedures," EPA.

[16] Technologies, Gamma, "GT-SUITE Exhaust Aftertreatment Application Manual," Gamma Technologies, 2020.

[17] R. Douglas, "AFR and Emissions Calculations for Two-Stroke Cycle Engines," SAE Technical Paper 901599, Department of Mechanical and Manufacturing Engineering Queen's University of Belfast, 1990.

[18] E. P. Agency, "40 CFR 1065.230 Raw Exhaust Flow Meter," EPA.

[19] S. T. Gulati, J. D. TenEyck and A. R. Lebold, "Durable Packaging Design for Corderite Ceramic Catalysts for Motorcycle Application," SAE Technical Paper 930161, Coming Inc. and The Carborundum Co., 1993.

[20] A. Schafer-Sindlinger, T. Yoshikawa, G. Bickle, R. Domesle and K. Fischer, "Emissions Control Sysems for Two Stroke Engines - A Challenge for Catalysis," SAE Technical Paper 982710, ICT Co. and Degussa AG, 1998.

[21] K. Babu, K. Fischer, B. Kang, K. Ostgathe and R. Sesseimann, "Advanced Catalyst Technologies with low Precious Metals for Indian Two Wheeler Applications," SAE Technical Paper 2003-26-022, Degussa India Pvt. and OMG AG, 2003.

[22] L. F. Jones, S. T. Gulati, R. Baker, M. J. Brady, S. Rajadurai and B. Snider, "Advanced Three-Way Converter System for High Temperature Exhaust Aftertreatment," SAE Technical Paper 970265, Coming Inc., Chrysler Corp, Johnson Matthey CSD-NA, and Walker Manufacturing, 1997.

[23] J. Broman, "Development and Demonstration of a Low Emissions Four-Stroke Outboard Marine Engine Utilizing Catalyst Technology," SAE Teechnical Paper 2012-01-1243, Mercury Marine, 2012.

[24] A. Reck, A. Bergmann, F. W. Kaiser and C. Dias, "Metallic Substrates and Hot Tubes for Catalytic Converters in Passenger Cars, Two- and Three Wheelers," SAE Technical Paper 962474, EMITEC GmbH, Germany and EMITEC Emissions Controls Pvt. Ltd., India, 1996.

9 Appendices

9.1 Engine Control Charts

A few notes regarding the control charts located below. First the fuel pressure was adjusted from 58 psi_g to 60 psi_g between test 5 and test 6 per Arctic Cat's recommendation. This can be distinctly seen in Figure 9.5. Second, variation can be seen in several control charts starting with test 14 and continuing through test 24. This is due to the fact that control points were collected with non-active and active catalysts installed in the muffler as a part of back pressure test #3 and conversion efficiency testing. While relative values for each control parameter remained close to the accepted control values, it wasn't expected that there would be no change to these measurements due to the addition of the catalysts. Third, there are a few outlying coolant in and intake air temperature points for test 11 and 12, this was due to some building water and air supply issues that were resolved starting with test 13. As you can see coolant out temperature was still well regulated during the building water and air supply issues. Lastly, the MAG EGT measurement is consistently higher than the PTO EGT because a cooling fan is set up on the PTO side of the engine to provide an air wash to the engine, cooling the PTO side more effectively than the MAG side.

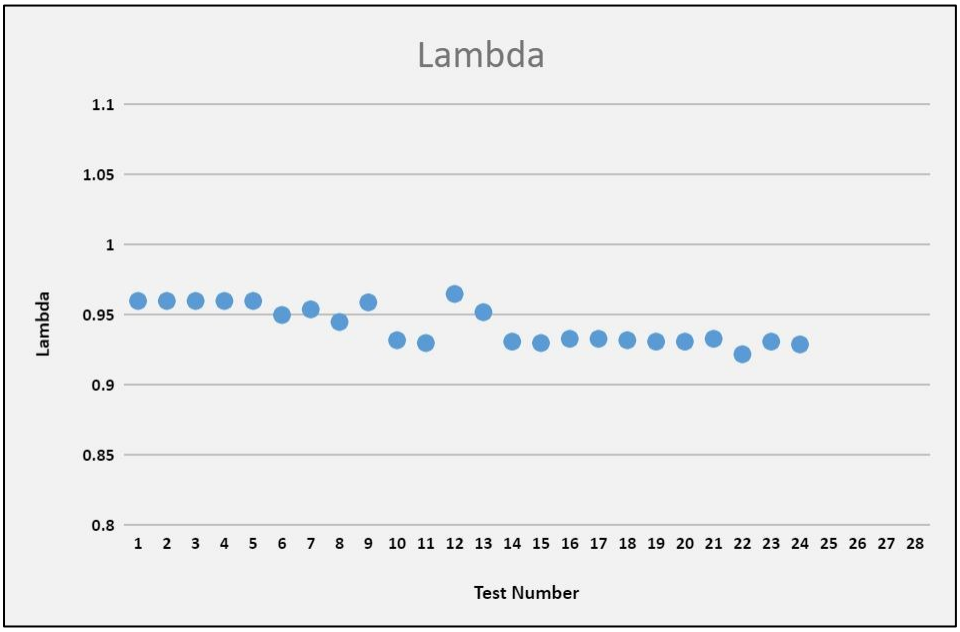

Figure 9.1 – Wide Band Lambda Control Chart

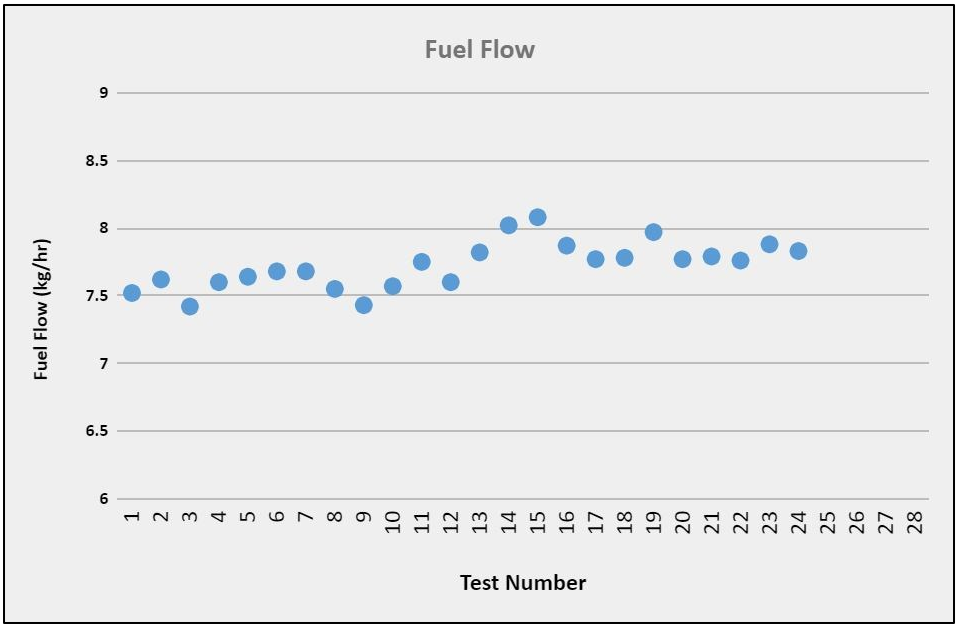

Figure 9.2 – Fuel Flow Control Chart

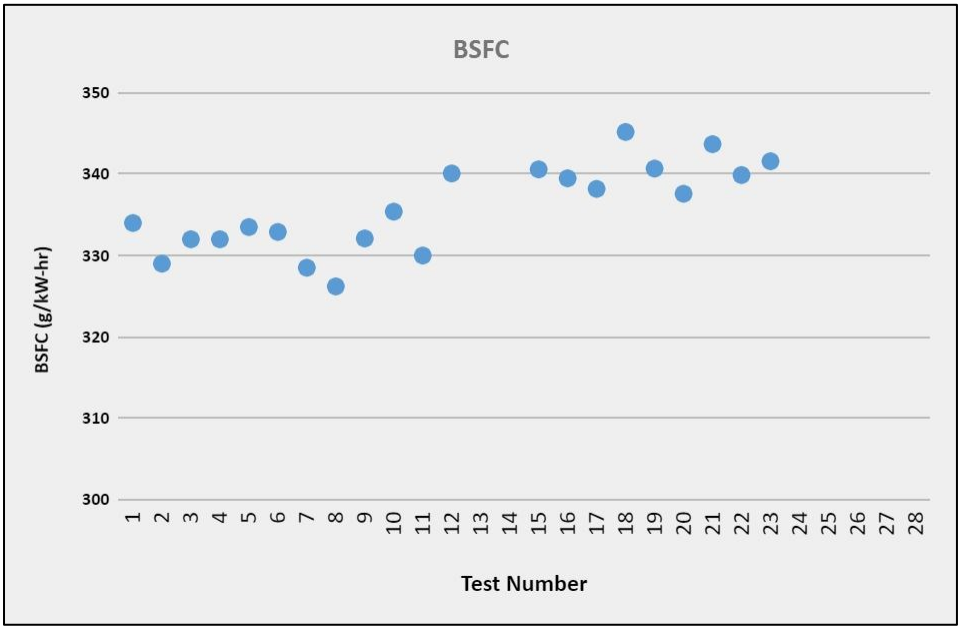

Figure 9.3 – BSFC Control Chart

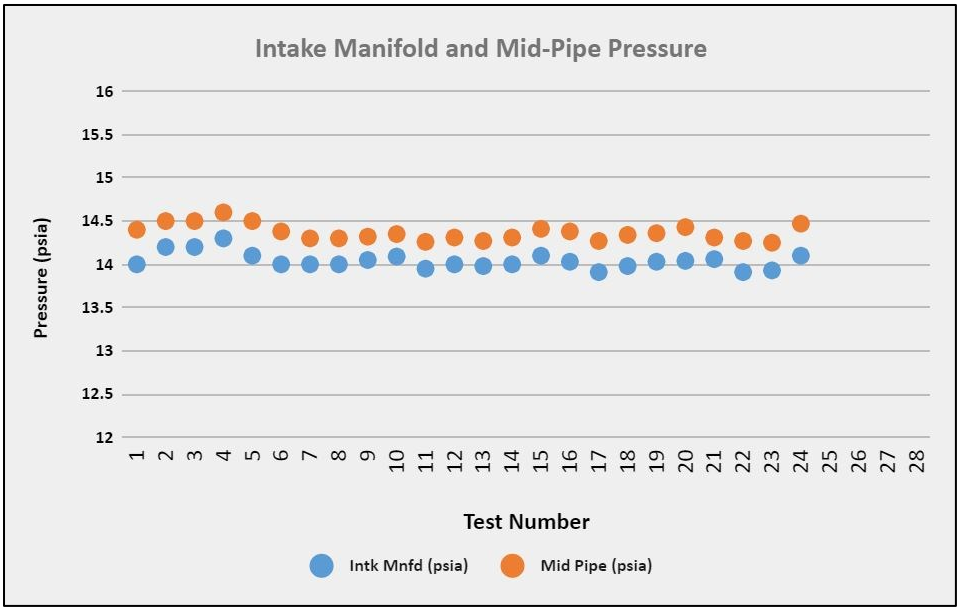

Figure 9.4 – Intake Manifold and Mid-Pipe Pressures Control Chart

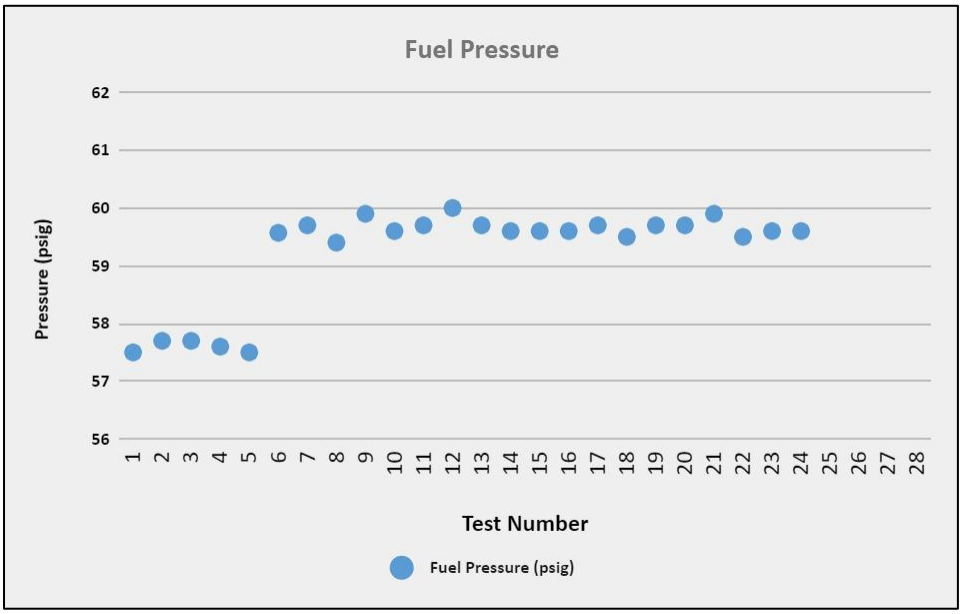

Figure 9.5 – Fuel Pressure Control Chart

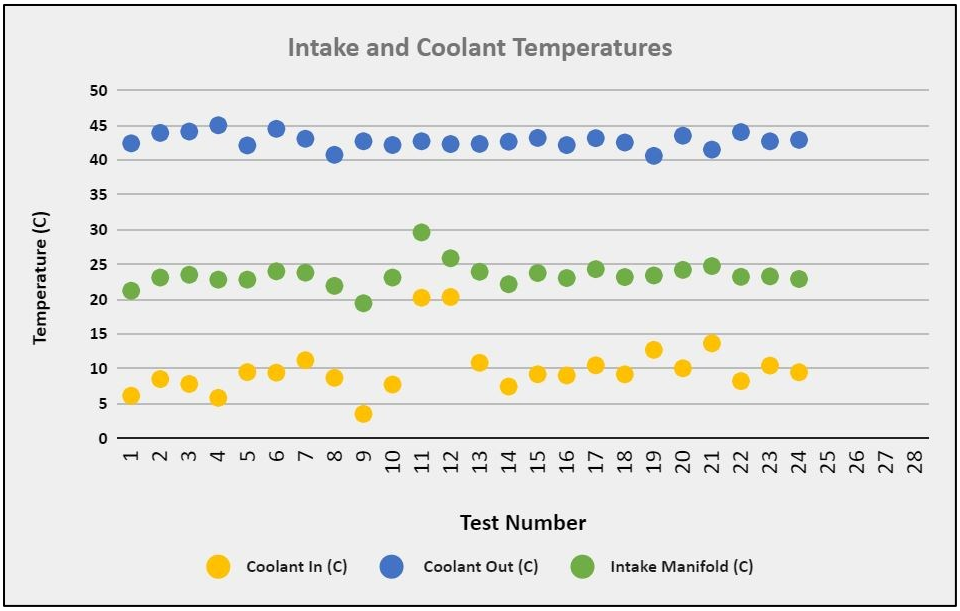

Figure 9.6 – Intake and Coolant Temperatures Control Chart

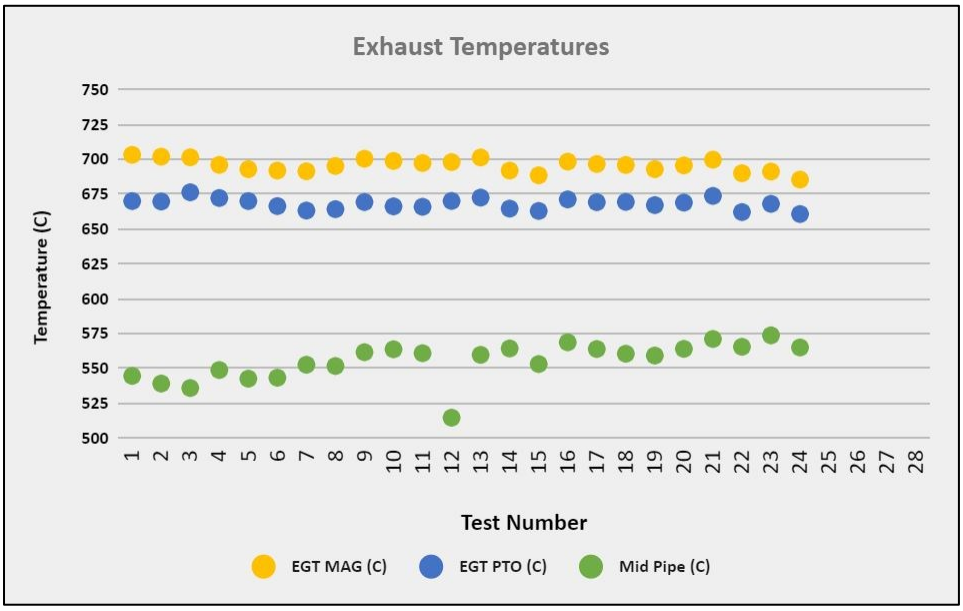

Figure 9.7 – Exhaust Temperatures Control Chart

9.2 XRF and SEM Results

CrossRoads Scientific XRF Analysis Report

File: D:\Results\MEEM\Noah_Squires_non_active.str

10:53:26 AM 05-Nov-21

Comment line

Layer Table

#	Thick	Type	Error	Units	Density	Norm.	Total
1	0.00	Bulk	0.00	mg/cm2	0.00	On	100.00

Sample Table

Layer	Component	Type	Concn.	Error	Units	Mole%	Error
1	Fe	Calc	1.872	0.028	wt.%	4.245	0.063
1	Ni	Calc	0.434	0.012	wt.%	0.937	0.026
1	Ce	Calc	82.089	2.464	wt.%	74.188	2.227
1	Cu	Calc	0.039	0.005	wt.%	0.078	0.011
1	Zr	Calc	12.483	0.040	wt.%	17.328	0.055
1	Y	Calc	0.024	0.004	wt.%	0.034	0.005
1	Nb	Calc	0.080	0.005	wt.%	0.109	0.007
1	Rh	Calc	1.126	0.030	wt.%	1.385	0.037
1	Pd	Calc	0.022	0.022	wt.%	0.027	0.027
1	La	Calc	1.831	0.396	wt.%	1.669	0.361

Element Table

Elmt	Line Code	Cond Code	Ratio Method	Intensity (c/s)	Error (c/s)	Intensity Method	Conc.	Conc Method	Calibration Coefficient
Fe	Ka	1	None	351.521	5.2117	Gaussian	1.872	FP	0.000
Ni	Ka	1	None	110.078	3.0483	Gaussian	0.434	FP	0.000
Cu	Ka	1	None	11.739	1.6050	Gaussian	0.039	FP	0.000
Y	Ka	1	None	13.194	2.0848	Gaussian	0.024	FP	0.000
Zr	Ka	1	None	6626.135	21.1301	Gaussian	12.483	FP	0.000
Nb	Ka	1	None	41.273	2.7710	Gaussian	0.080	FP	0.000
Rh	Ka	1	None	153.100	4.0519	Gaussian	1.126	FP	0.000
Pd	Ka	1	None	2.636	2.6205	Gaussian	0.022	FP	0.000
La	Ka	1	None	11.818	2.5550	Gaussian	1.831	FP	0.000
Ce	Ka	1	None	119.319	3.5822	Gaussian	82.089	FP	0.000

Analysis Conditions

#	Target	Filter	Thick. (um)	kV	uA	---Detector--- Type	Filter	Thick. (um)	Atmos	Preset Time(s)	Actual Time(s)
1	Rh	None	0.0	45.00	55.0	Si drift	None	0.0	Air	20.0	60.0

Processing Conditions

#	No. Smths	Escape Peaks	Sum Peaks	Back Type	C/R Ratio	Blank Rem.	----Blank---- ----File-----
1	2	Yes	Yes	Auto	No	No	

Figure 9.8 – Non-Active Heraeus Wash Coat XRF Tabulated Data

CrossRoads Scientific XRF Analysis Report

File: D:\Results\MEEM\Noah_Squires_active.str

11:00:49 AM 05-Nov-21

Comment line

Layer Table

#	Thick	Type	Error	Units	Density	Norm.	Total
1	0.00	Bulk	0.00	mg/cm2	0.00	On	100.00

Sample Table

Layer	Component	Type	Concn.	Error	Units	Mole%	Error
1	Al	Calc	6.146	0.478	wt.%	25.292	1.969
1	Fe	Calc	0.120	0.005	wt.%	0.240	0.009
1	Ni	Calc	0.046	0.003	wt.%	0.088	0.005
1	Zr	Calc	0.066	0.002	wt.%	0.081	0.002
1	Nb	Calc	0.021	0.002	wt.%	0.025	0.002
1	Ce	Calc	92.131	1.218	wt.%	73.014	0.966
1	Pt	Calc	0.638	0.011	wt.%	0.363	0.006
1	Rh	Calc	0.832	0.012	wt.%	0.897	0.013

Element Table

Elmt	Line Code	Cond Code	Ratio Method	Intensity (c/s)	Error (c/s)	Intensity Method	Conc.	Conc Method	Calibration Coefficient
Al	Ka	1	None	29.359	2.2851	Gaussian	6.146	FP	0.000
Fe	Ka	1	None	80.114	3.1430	Gaussian	0.120	FP	0.000
Ni	Ka	1	None	41.822	2.3672	Gaussian	0.046	FP	0.000
Zr	Ka	1	None	133.024	3.7502	Gaussian	0.066	FP	0.000
Nb	Ka	1	None	40.814	2.9842	Gaussian	0.021	FP	0.000
Rh	Ka	1	None	504.157	7.2104	Gaussian	0.832	FP	0.000
Ce	Ka	1	None	514.661	6.8065	Gaussian	92.131	FP	0.000
Pt	La	1	None	285.797	4.8497	Gaussian	0.638	FP	0.000

Analysis Conditions

#	Target	Filter	Thick. (um)	kV	uA	---Detector--- Type	Filter	Thick. (um)	Atmos	Preset Time(s)	Actual Time(s)
1	Rh	None	0.0	45.00	100.0	Si drift	None	0.0	Air	20.0	60.0

Processing Conditions

#	No. Smths	Escape Peaks	Sum Peaks	Back Type	C/R Ratio	Blank Rem.	----Blank---- ----File-----
1	2	Yes	Yes	Auto	No	No	

Figure 9.9 – Active Heraeus Wash Coat XRF Tabulated Data

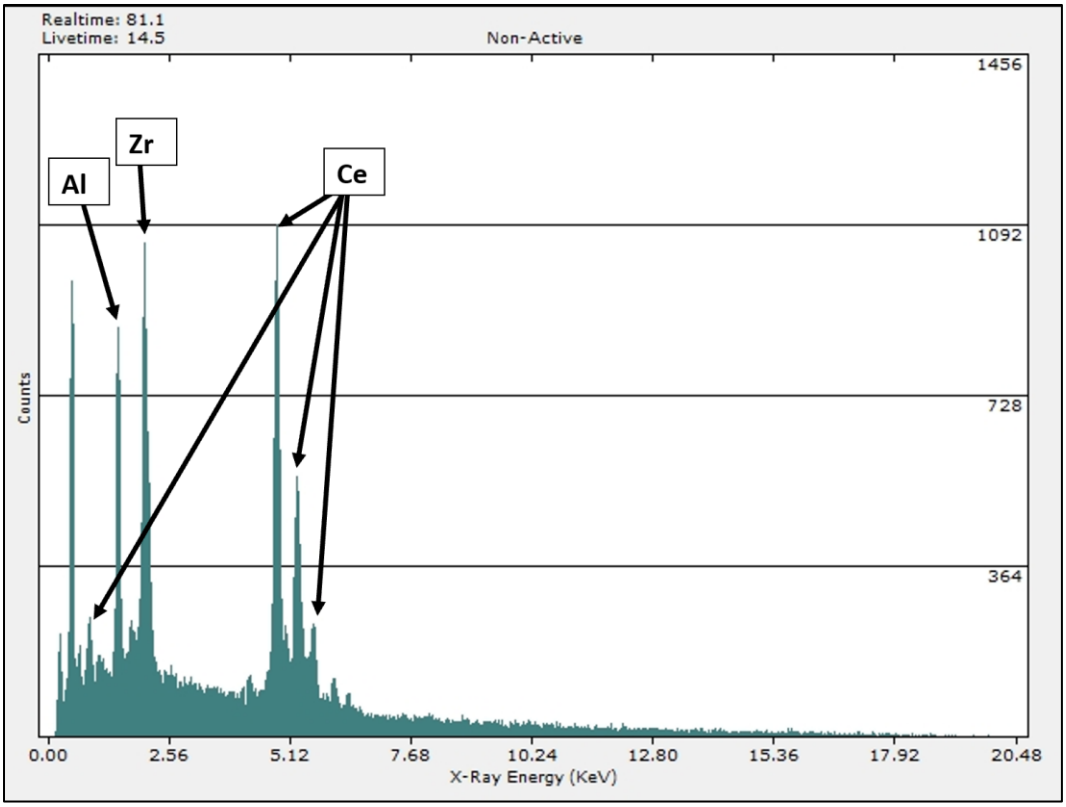

Figure 9.10 - Non-Active Heraeus Wash Coat SEM Results

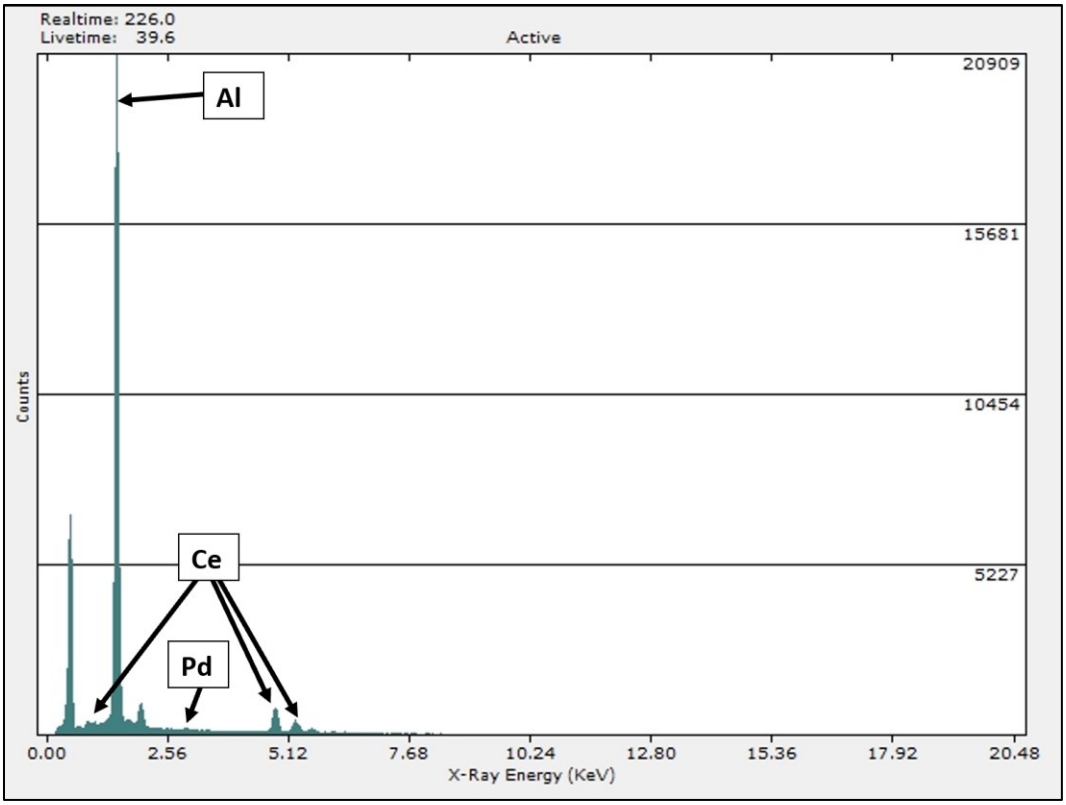

Figure 9.11 - Active Heraeus Wash Coat SEM Results

9.3 EES Catalytic Reaction Simulation Code

```
"!Two-stroke Catalyst Project - N. Squires" "Remember to set units system to SI/C/kPa/kJ/molar/deg"

"!Adiabatic Combustion of HC and CO to determine conversion efficiency that will keep outlet temperature in check"
"aCO2 + bCO + cH2O + dO2 + e(x_fast*C3H6 + x_slow*C3H8) + fN2 = gCO2 + hCO + cH2O + iO2 + j(x_fast*C3H6 +
x_slow*C3H8) + fN2"

"HC represented by ratio of fast (C3H6) and slow (C3H8) burning species based on GT-SUITE Exhaust Aftertreatment
Application Manual PDF"
"! Ratio of slow and fast HC's" " 80% C3H6 and 20% C8H18"
x_fast = 0.80
x_slow = 1.0 - x_fast

"! Mode 1 emissions for 600 DSI"
CO2 = 6.5 "%"
CO = 4.2 "%"
H2O = 11 "%"
O2 = 4.2 "%"
HC = 3.6 "%"
N2 = 70.5 "%"

"! Temperature Inputs"
T_cat_in = 600
T_cat_exit = 950
P_exh = 101.325

"mass balances"
"C" a + b + (3*x_fast + 3*x_slow)*e = g + h + (3*x_fast + 3*x_slow)*j
"H" "2*c + e = 2*c + e" "no new information"
"O" 2*a + b + c + 2*d = 2*g + h + c + 2*i
"N" "2*f = 2*f" "no new information"

"Using emissions"
CO2/100 = a/(a+b+c+d+e+f)
CO/100 = b/(a+b+c+d+e+f)
H2O/100 = c/(a+b+c+d+e+f)
O2/100 = d/(a+b+c+d+e+f)
HC/100 = e/(a+b+c+d+e+f)
N2/100 = f/(a+b+c+d+e+f)

"Degree of oxidation of CO and HC"
"solve" h = b/x
"solve" j=e/x

"enthalpy of the reactants"
H_r = a*enthalpy(CO2,T=T_cat_in) + b*enthalpy(CO,T=T_cat_in) + c*enthalpy(H2O,T=T_cat_in) + d*enthalpy(O2,T=
T_cat_in) + e*(x_fast*enthalpy(Propylene,T=T_cat_in,P=P_exh) + x_slow*enthalpy(C3H8,T=T_cat_in) ) + f*enthalpy(N2,
T=T_cat_in)

"Solving for T_cat_exit knowing the products"
H_p = g*enthalpy(CO2, T=T_cat_exit) + h*enthalpy(CO, T=T_cat_exit) + c*enthalpy(H2O, T=T_cat_exit) + i*enthalpy(O2,
T=T_cat_exit) + j*(x_fast*enthalpy(Propylene,T=T_cat_exit,P=P_exh) + x_slow*enthalpy(C3H8,T=T_cat_exit) )  + f*
enthalpy(N2,T=T_cat_exit)

"No Q_out of Catalyst outer surface"
H_p = H_r

"Conversion efficiency in catalyst"
eta_conv_CO = (1-h/b)*100
eta_conv_HC = (1-j/e)*100
```

9.4 Matlab Hagen Poiseuille Pressure Drop Code

Substrate Sizing - Hagen Poiseuille Method

Created by Noah Squires 03-29-2021

```
clc
close all
clear all
```

inputs

estimation method (2 = percentage of space velocity based volume, 1 = actual experimental part volume)

```
method = 2;
% engine inputs
T_exh = 590;            % exhaust temperature at mid pipe mode 1 [C]
P_exh = 17.0*6894.76;   % exhaust pressure at mid pipe mode 1 [Pa]
M_fuel = 31.0/3600;     % mass flow of fuel mode 1 (kg/s)
AFRs =  14.7;           % stoich AFR
Lambda = 0.8;           % lambda mode 1
% catalyst inputs
Dp = 0.08;              % substrate diameter [m]
L = 0.0745;             % substrate length [m]
N = 300/(0.0254^2);     % cell denisty [CPSm]
T = 0.02*0.0254;        % wall thickness [m]
Vsv = 200000;           % space velocity constant [hr^-1]
% constant
R_air = 287;            % gas constant air [J/kg-K]
```

calculated parameters

```
mu_exh = 1.716*10^-5*(((T_exh+273.15)/273.15)^(3/2))*((273.15+110.4)/(T_exh+273.15+110.4));     % Sutherland's formula dynamic viscosity of air [Pa-s]
rho_exh = P_exh/(R_air*(T_exh+273.15));                                                         % exhuast gas density [kg/m^3] assume ideal air
LL = (1-(sqrt(N)+1)*T)/sqrt(N);                                                                 % repeat distance [m]
```

Substrate Volume

```
M_air = AFRs*Lambda*M_fuel + M_fuel;    % mass flow rate air [kg/s]
M_exh = M_air + M_fuel;                 % mass flow rate exhuast [kg/s]
Q_exh = M_exh/rho_exh;                  % volume flow rate exhaust [m^3/s]
if method == 1
    % actual part volume method
    V_sub = (pi/4)*(Dp^2)*L;               % substrate volume [m^3]
    percent_SV = (V_sub*Vsv)/(Q_exh*3600);  % percentage of SV(@ 200000 hr-1) based part volume used [%]
elseif method == 2
    % calculated SV volume method
    percent_SV = 0.08; % percentage of space velocity based volume to be used in calculation
    V_sub = ((Q_exh*3600)/Vsv)*percent_SV;  % substrate volume [m^3]
    L = V_sub/((pi/4)*Dp^2);
end
Vsv_act = (Q_exh*3600)/V_sub;           % Actual Space Velocity required to get this part volume [hr^-1]
```

Pressure Drop

```
dP = (8*pi*(pi/4)^2)*(Q_exh*mu_exh)*(V_sub/(Dp^4))*(N./(1-(T./LL).^4)); % pressure drop across substrate [Pa]
```

Frontal Area/ Equivalent Restrictions

```
Ap = (pi/4)*Dp^2;                   % part cross sectional area [m^2]
n_cells = Ap*N;                     % number of cells
A_open = n_cells*LL^2;              % open cross sectional area on substrate face [m^2]
A_close = Ap - A_open;              % closed cross sectional area on substrate face [m^2]
D_Req = sqrt((A_open*4)/pi);        % equivalent restriction plate opening diameter [m]
TSA = n_cells*(LL/0.0254)*L*4;     % approximate total surface area [in^2]
```

Print results

```
formatSpec = 'Substrate Dimensions are %4.3f mm in length and %4.3f mm in diameter, for %4.2f percent of SV based volume\n';
fprintf(formatSpec,L*1000, Dp*1000, percent_SV*100) % print sizing information
% table of values of interest
T = table(Dp*1000,L*1000, N*0.0254^2, Vsv_act,dP*0.01,'VariableNames',...
    {'Part Diameter (mm)','Part Length (mm)','Cell Density (CPSI)', 'Total Surface Area (mm^2)','Pressure Drop (mBar)'})
```

9.5 Matlab Catalyst Geometry Calculations Code

Catalyst Geometry Calculations

created by Noah Squires 6/17/2021

```
clc
close all
clear all
```

Inputs

```
OD = 80;        % Part Diameter [mm]
Lp = 30;        % Part Length [mm]
N = 100;        % Cell density [CPSI]
T = 0.022;      % wall thickness [mm]
```

Convert Units

```
OD = OD/1000;   % convert mm to m
Lp = Lp/1000;   % convert mm to m
N = N/0.0254^2; % convert CPSI to CPSm
T = T/1000;     % convert mm to m
```

Caclulations

```
Ap = (pi()/4)*(OD^2);           % front cross sectional area [m^2]
n_cells = Ap*N;                 % number of cells in part
L = (1-sqrt(N+1)*T)/sqrt(N);    % cell width [m]
A_open = n_cells*(L^2);         % open frontal area [m^2]
A_close = Ap-A_open;            % closed frontal area [m^2]
D_Req = sqrt((A_open*4)/pi());  % diameter of equivalent orifice restriction [m]
TSA = n_cells*L*Lp*4;           % total geometric surface area [m^3]
```

Print Results

```
T = table(Ap*1000^2,n_cells,L*1000,A_open*1000^2,A_close*1000^2,D_Req*1000,TSA*1000,...
    'VariableNames',{'Ap (mm^2)','n_cells','L(mm)','A_open(mm^2)','A_close(mm^2)','D_Req(mm)','TSA(mm^3)'})
ratio = A_open/A_close
```